University of Stavanger

FACULTY OF SCIENCE AND TECHNOLOGY

MASTER'S THESIS

Study programme/specialisation: Petroleum Geosciences Engineering	Spring semester, 2020 Open
Author: Isabella Ghesla Rossetti	
Programme coordinator: Lisa Watson Supervisor(s): Nestor Cardozo	
Title of master's thesis: Predictive Dynamic Models of the Upper Jurassic Ula Fm Aquifer Between the Ula and Oda Fields, Norwegian Central Graben, North Sea	
Credits: 30	
Keywords: Ula Fm distribution Ula field Oda field Hydrodynamic aquifer Geological model History matching	Number of pages: 105 Stavanger, 15th July, 2020

Predictive Dynamic Models of the Upper Jurassic Ula Fm Aquifer Between the Ula and Oda Fields, Norwegian Central Graben, North Sea

by

Isabella Ghesla Rossetti

Master Thesis

Presented to the Department of Energy Resources

University of Stavanger

Stavanger

July 2020

Acknowledgements

Firstly, I would like to thank my supervisors Nestor Cardozo and Anders Sundgot Saunes for their guidance, continuous support and motivation throughout this project.

I would also like to thank the PL 405 (Spirit Energy Norway AS, Suncor Energy Norge AS, Aker BP ASA and DNO Norge AS) and PL 019 (Aker BP ASA and DNO Norge AS) licenses for allowing me to access and use their internal database during this study.

I am very grateful for all the help from the whole Spirit Energy Norway AS Subsurface Team, especially Espen Rørvik, Jessica Haege, Peter MacKintosh, Phil McCaffrey and Veronica Arrigoni.

Additionally, I am thankful to my family and friends for their continuous encouragement and care throughout my master studies.

I dedicate this thesis to my parents, Bernardete Soeli Ghesla Rossetti and Eugenio Rossetti, who are my foundation and biggest support in life. Muito obrigada!!

Abstract

Predictive Dynamic Models of the Upper Jurassic Ula Fm Aquifer Between the Ula and Oda Fields, Norwegian Central Graben, North Sea

Isabella Ghesla Rossetti

University of Stavanger, 2020

Supervisor: Nestor Cardozo

The Ula and Oda oil fields in the southern part of the Norwegian Central Graben have high quality Upper Jurassic sandstone reservoirs from the shallow marine Ula Fm. Pressure data from the Oda field indicates communication between the Ula and Oda fields through an aquifer in the Ula Fm. Through dynamic modelling of the Ula Fm aquifer, the communication between the Ula and Oda fields along this unit is evaluated. The models incorporate pressure and production data and are essential to understand reservoir depletion in the area.

The applied methodology integrates previous studies about the Ula Fm distribution, static and dynamic modelling of different scenarios, and history matching of the Ula field production and pressure data. Three scenarios for the Ula Fm fairway involve a possible communication between the Ula and Oda fields. Each scenario varies the size of the aquifer based on different hypothesis about the deposition and distribution of the Ula Fm. The most accepted scenario suggests that the Ula Fm was deposited in pod-shaped minibasins above salt walls and within the shoreface zone delimited by well data.

Dynamic modelling and history matching show that even in the scenario with the narrowest Ula Fm above the salt walls and sealing faults, there is still a channel communicating

the Ula and Oda fields, and the production effects of the Ula field are “felt” by the Oda field. Therefore, there is strong geological and reservoir modelling evidence of communication between the Ula and Oda fields through an aquifer in the Ula Fm.

A geological model for the communication between the Ula and Oda fields through the Ula Fm is proposed. This model can be used to evaluate the risks related to the presence of a hydrodynamic aquifer in the Ula Fm, indicate new prospects in the Central Graben area, and optimize the development of the Oda field.

Table of Contents

List of Figures

List of Tables

Abbreviations

Abbreviation	Explanation
API	American Petroleum Institute gravity
BCU	Base Cretaceous Unconformity
BHP	Bottom Hole Pressure
Bo	Oil Formation Volume Factor
cm	Centimeter
cP	Centipoise
CPOR	Core porosity
d	day(s)
DEN	Density
DT	Sonic
Fm	Formation
FWL	Free water level
GOR	Gas Oil Ratio
Gp	Group
GR	Gamma Ray
GRV	Gross Rock Volume
IFT	Interfacial Tension
K	Permeability
Kh	Horizontal permeability
Kr	Relative permeability
Krg	Gas relative permeability
Kro	Oil relative permeability

Krw	Water relative permeability
Kv	Vertical Permeability
Kx	Horizontal permeability
LSF	Lower Shoreface
MD	Measured Depth
mD	Milli Darcy
MSm^3	Million Standard Cubic Meter
NE	Northeast
NEU	Neutron
NPD	Norwegian Petroleum Directorate
NTG	Net to Gross
NW	Northwest
OWC	Oil Water Contact
Φ	Porosity
Pb	Bubble point pressure
Pc	Capillary pressure
PHI	Porosity
PHIT	Total porosity
PL	Production license
PVT	Pressure Volume Temperature properties
QC	Quality Check
RCAL	Routine Core Analysis
RES	Resistivity
RF	Recovery Factor
RT	Rock Type

SCAL	Special Core Analysis
SE	Southeast
Sgcr	Critical gas saturation
SGS	Sequential Gaussian Simulation
Sm^3	Standard Cubic Meter
Soi	Initial oil saturation
STOIIP	Stock Tank Oil Initially In-Place
Sw	Water Saturation
SW	Southwest
Swcr	Critical water saturation
Swi	Initial water saturation
Swirr	Irreducible water saturation
TD	Total Depth
TranZ	Vertical transmissibility
TVDSS	True Vertical Depth Subsea
TVT	True Vertical Thickness
TWT	Two WayTime
TZ	Transition Zone
USF	Upper Shoreface
VSH	Shale volume
WI	Water Injection
θ	Contact angle
γ	Surface tension
ρ_o	Oil density
υ_o	Oil viscosity

1. INTRODUCTION

The Oda and Ula fields are located in the southern part of the Norwegian Central Graben, in the North Sea (Figure 1). These fields are separated by a distance of 13 km between blocks 7/12 and 8/10, and are characterized by good quality Upper Jurassic reservoirs, salt structures and faults.

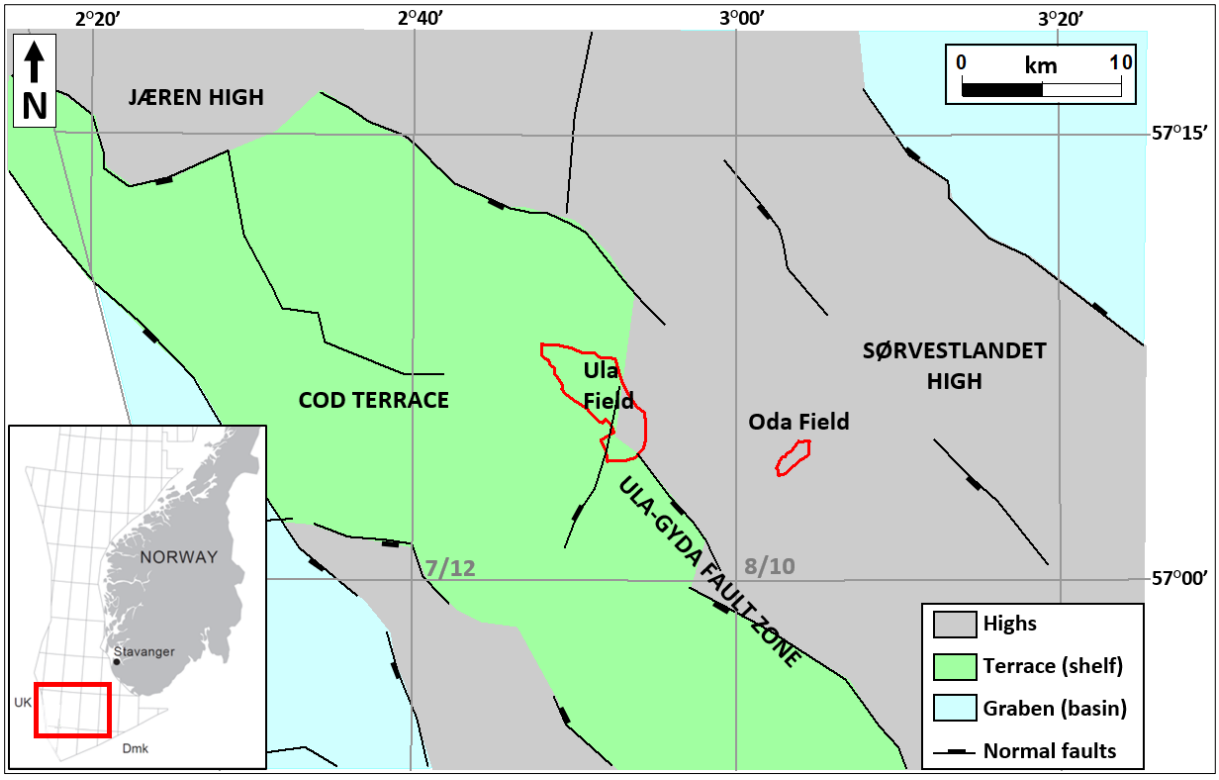

Figure 1. Inset: Location map of the Ula and Oda fields in the Norwegian Central Graben. The main regional provinces are highlighted. Modified after Ichron (2015) and NPD (2019).

The Ula field, which is located on the Cod Terrace, was discovered by well 7/12-2 in 1976 and its production started later in 1986 under the PL 019 license (NPD, 2019). The field produces from the prolific Ula Fm shallow marine, moderately to highly bioturbated sandstones (Upper Jurassic) (Baniak et al., 2015, 2014; Brown et al., 1992; Heum, 1996). Because the Ula field has been in production for more than 30 years, it has been extensively studied, and the

knowledge acquired about the Ula Fm reservoir has led to new discoveries in the area (e.g. the Oda field). The Oda field is located SE of the Ula field and its production started recently, in 2019, under the PL 405 license (NPD, 2019). The Oda field also produces from the Ula Fm, the reservoir is characterized by clean sandstones of high reservoir quality.

The deposition of the Ula Fm sandstones was controlled by halokinesis and faulting (Bailey et al., 1981; Bjørnseth and Gluyas, 1995; Mannie et al., 2014; O'Connor et al., 2011; Spencer et al., 1986; Stewart, 1993). Due to this complex structural evolution, there are several hypotheses for the distribution of the Ula Fm across the Ula and Oda fields, and some propose a connection or "fairway" between the fields along the Ula Fm (Armour et al., 2003; Hodgson et al., 1992; Ichron, 2015; Mannie et al., 2014; O'Connor et al., 2011). However, none of these hypotheses have been validated with dynamic models and history matching of pressure and production/injection data.

During the exploration and appraisal phases of the Oda field, pressure data from two nearby wells (8/10-4 S and 8/10-B-3 AH, Figure 2) showed potential depletion of the reservoir pressure before the production started. While well 8/10-4 S resulted in a reservoir pressure of 381.2 bar at -2515 m (TVDSS reference depth) in 2011, well 8/10-B-3 AH measured 380.2 bar at the same depth in 2018, which is ~1.5 bar lower than the expected pressure of 381.7 bar from the iso-thermal method, although within the ± 2 bar uncertainty of the oil gradient (Figure 3). Reservoir pressure history data from the wells in the Ula field (Figure 4) also indicated a considerable pressure decrease between 2009 and 2018 (Figure 5) of more than 20 bars in some wells. This could indicate communication between the Ula and Oda fields through a narrow channel such as an aquifer in the Ula Fm. This hypothesis could explain the reservoir depletion in the Oda field before production started.

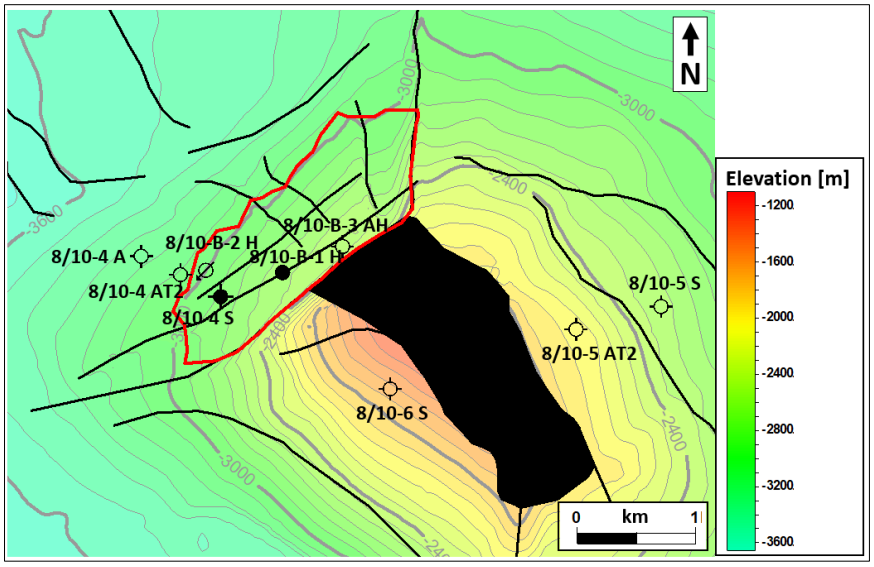

Figure 2. Structure map (depth) of the top Ula reservoir in the Oda field. The field boundary (red polygon) and wells are included. Well 8/10-B-3 AH is the location used for the "dummy" well in the history matching process. The location of the figure is displayed in Figure 1.

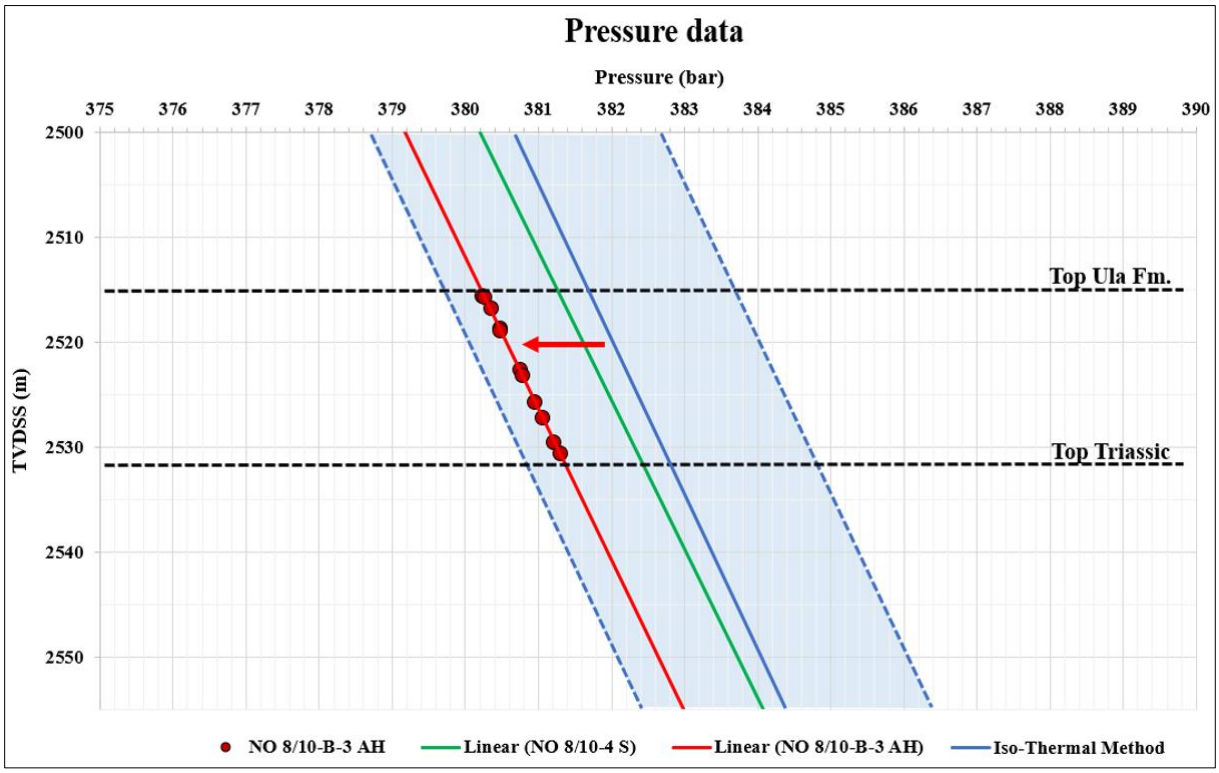

Figure 3. Reservoir pressure differences between the wells 8/10-4 S (green line) and 8/10-B-3 AH (red line) in the Oda field. While well 8/10-4 S shows 381.2 bar of reservoir pressure at -2515 m TVDSS (reference depth), well 8/10-B-3 AH shows 380.2 bar at the same datum, which is 1.5 bar lower than the 381.7 bar expected from the iso-thermal method (blue line), but within the ± 2 bar uncertainty (light blue). The red arrow indicates the depletion in well 8/10-B-3 AH. Source: Spirit Energy Norway AS Subsurface Team.

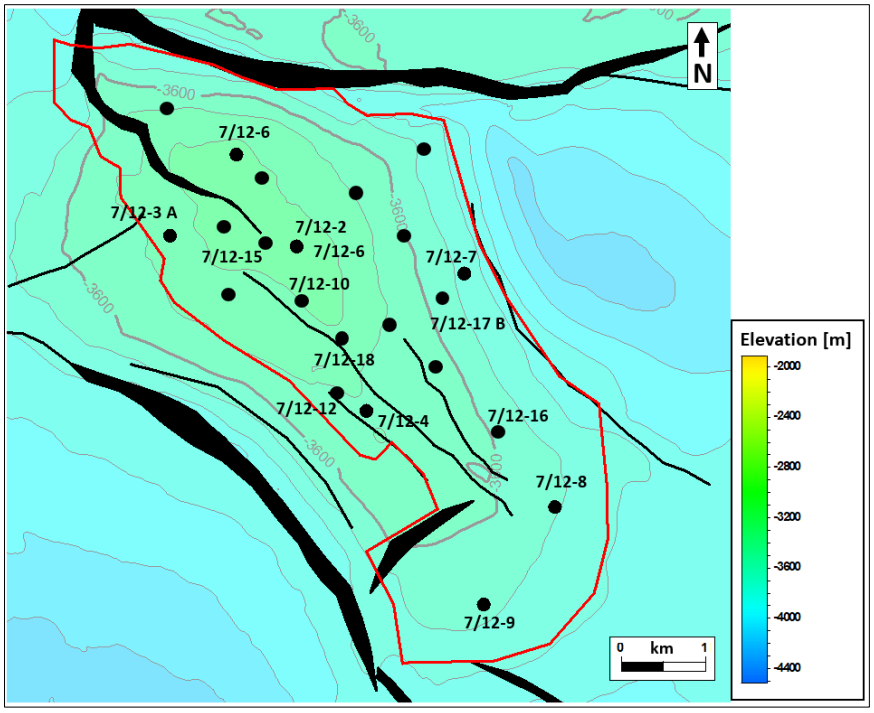

Figure 4. Structure map (depth) of the top Ula reservoir in the Ula field. The field boundary (red polygon) and wells are included. The location of the figure is displayed in Figure 1.

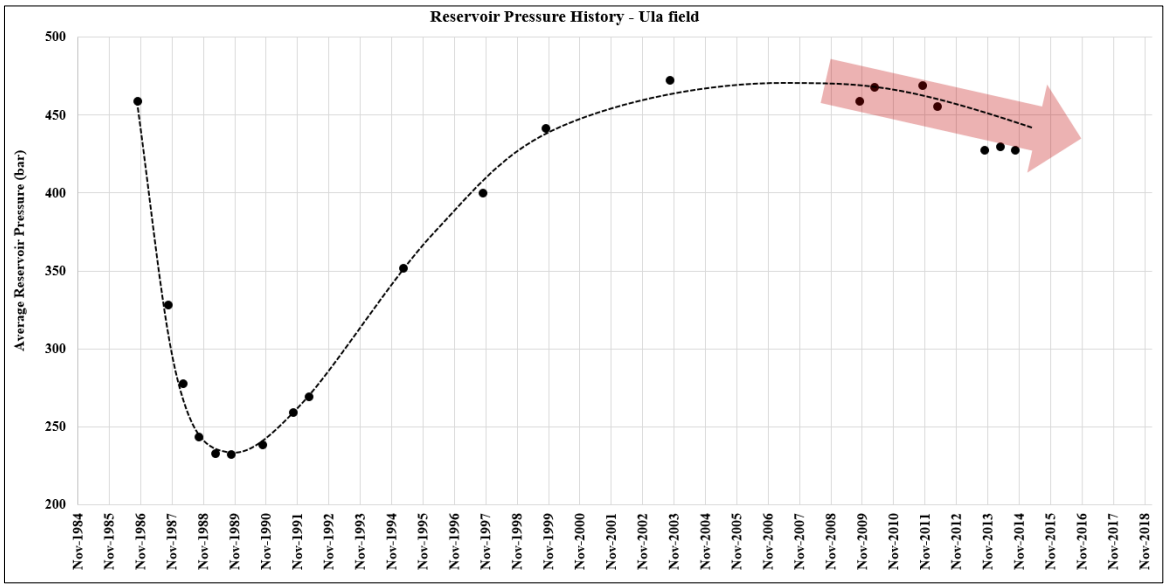

Figure 5. Reservoir pressure history overall trend through the production years of the Ula field. The red arrow shows a pressure decrease trend between 2009 and 2018. Source: Spirit Energy Norway AS Subsurface Team.

Many studies associate the Ula Fm reservoirs with hydrodynamic aquifers (Dennis et al., 2005; Green et al., 2014; Heum, 1996; O'Connor et al., 2011). Aquifers in hydrocarbon reservoirs can be characterized by static or hydrodynamic water flow (Green et al., 2014)

(Figure 6). According to Dennis et al. (2005, 2000), hydrodynamic conditions in aquifers lead to lateral variations in overpressure that are responsible for lateral flow of groundwater and, consequently, OWC tilting. In this situation, water from the aquifer flows from high pressure towards low pressure, but the trapped hydrocarbons are in static equilibrium. According to Heum (1996) and O'Connor et al. (2011), the Ula field has a depth difference in the OWC ranging between 150 m to 440 m from the west (shallower OWC) to the east (deeper OWC). Both studies interpreted this difference as a hydrodynamic effect, with oil being driven by overpressure into the Ula structure from the deeper North Central Graben in the west towards the graben flank and the Sørvestland High to the east. The hydrodynamic aquifer assumption in the Ula field and the water flow from the NW to the SE reinforce the hypothesis of communication between the Ula and Oda fields through an aquifer in the Ula Fm.

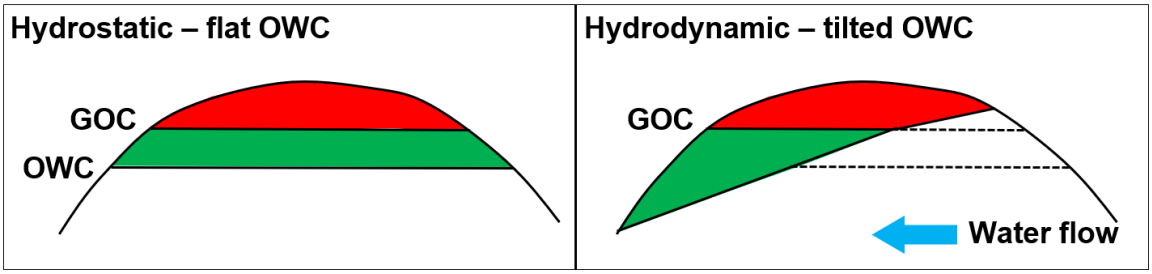

Figure 6. Schematic figures showing the differences in the OWC and GOC in a reservoir with hydrostatic and hydrodynamic water flow. Modified after Green et al. (2014).

1.1. **AIM OF THE STUDY**

Because the production of the Oda field started recently in March 2019 (NPD, 2019), there are few data and studies explaining the causes for the observed reservoir pressure depletion. Furthermore, the distribution of the Ula Fm in the study area is not certain and is a key risk element for new prospects, due to the complex distribution of this formation which is

controlled by the structural relief at the time of deposition (Bjørnseth and Gluyas, 1995; Mannie et al., 2014; O'Connor et al., 2011; Stewart, 1993).

Consequently, predictive dynamic models of a possible Ula Fm fairway between the Ula and Oda fields incorporating pressure and production data are essential to understand reservoir depletion in this area. This study could also help minimizing risks related to the reservoir presence and its properties, and indicate possible new prospects associated to a hydrodynamic trap. Therefore, the aim of this thesis is the dynamic modelling of the Ula Fm aquifer in order to evaluate the possible communication between the Ula and Oda fields along this formation.

1.2. **OBJECTIVES**

The main objective of this thesis is to implement static (steady state system) and dynamic (time-dependent system) models of a potential Ula Fm fairway between the Ula and Oda fields in order to answer the following questions:

- Are there geological evidences that prove communication between the Ula and Oda fields through an aquifer in the Ula Fm?
- What are the implications of communication between the Oda and Ula fields along the Ula Fm for both reservoir pressure and production?
- Is it possible to validate with dynamic models the hypothesis of a Ula Fm fairway between the Ula and Oda fields, using reservoir pressure and production history data?

2. LITERATURE REVIEW

2.1. GEOLOGICAL SETTING

2.1.1. Permo-Triassic

The area of interest is located on the eastern flank of the Central Graben within an Upper Jurassic extensional basin following the Cod Terrace and the Ula-Gyda fault zone (Ula field) in the west and the Sørvestlandet High (Oda field) to the east (Bjørnseth and Gluyas, 1995) (Figure 1). This Upper Jurassic basin developed on the western flank of a pre-existing Permo-Triassic basin (Rotliegend Gp) (Armour et al., 2003; Baniak et al., 2014; Bjørnseth and Gluyas, 1995).

The rift phase that generated the Permo-Triassic basin was followed by a glacio-eustatic sea level rise (Late Permian) caused by the Permo-Carboniferous melting of the Gondwana ice which resulted in a marine transgression from the north. This event caused the establishment of the Zechstein Sea covering large areas of northern and central Europe. Due to poor connection to the open ocean, thick successions of evaporites were deposited. Evaporite precipitation exceeded subsidence by the end of the Permian, and playa lakes were formed within gentle depressions between low-relief salt highs (Bjørnseth and Gluyas, 1995).

The presence of the Zechstein salt significantly influenced the subsequent evolution of the basin, with influenced both the Triassic and Jurassic sedimentation. Salt tectonics activated by sediment loading and fault activity caused the development of minibasins, separated by salt walls (or diapirs) of variable scales in which the Triassic sediments were deposited (Armour et al., 2003; Baniak et al., 2014; Bjørnseth and Gluyas, 1995; Hodgson et al., 1992). The accommodation space for thick Triassic successions in between the salt highs was generated by continuous salt withdrawal. Eventually, the Triassic minibasins formed welds and subsequently

deflation and dissolution of the salt walls created accommodation space for supra-salt pods filled by Triassic and Jurassic sediments. Figure 7 summarizes the generation of accommodation space for the Triassic and Jurassic sediments.

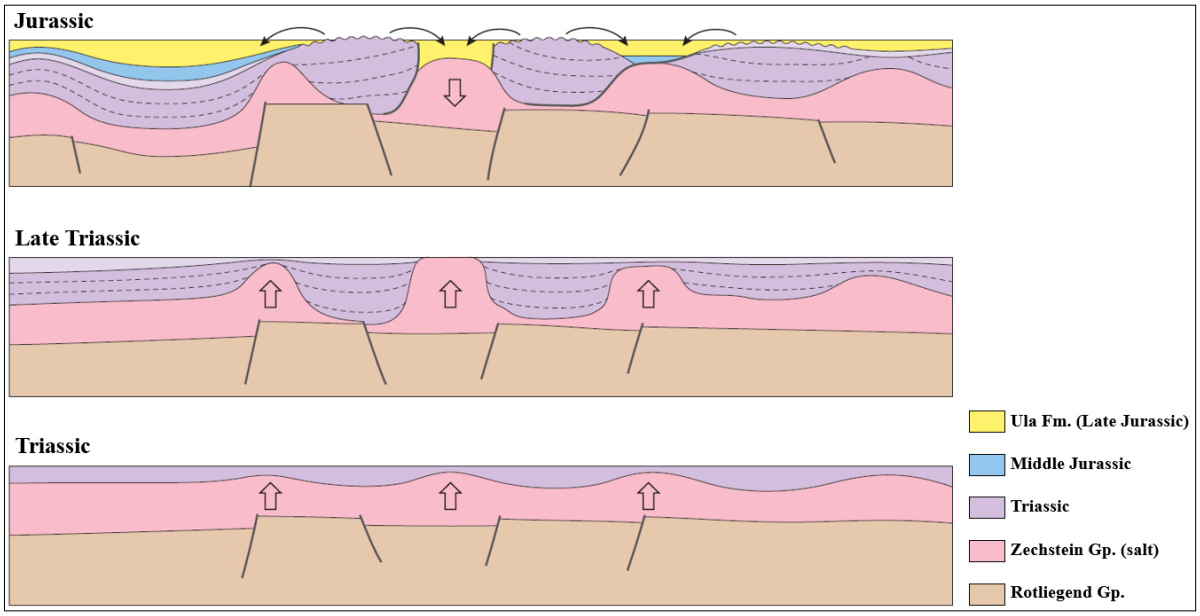

Figure 7. Structural development and generation of accommodation space for the Triassic and Jurassic (Ula Fm) sediments. Source: Mannie et al. (2014).

2.1.2. Upper Jurassic / Lower Cretaceous

During the Late Jurassic, a main rifting phase in the North Sea took place. This phase extended from the Barents Sea to the southern North Sea and generated a main NW-SE fault system trend (Armour et al., 2003). The Ula-Gyda fault zone represents the easternmost boundary of the rift, with rotated fault blocks containing Triassic deposits in the west (Cod Terrace) and the Sørvestlandet High in the east, which was a passive platform relatively unaffected by the Jurassic rifting (Bjørnseth and Gluyas, 1995).

The Late Jurassic was also characterized by a regional rise in sea level resulting from either eustasy, regional thermal subsidence, or rifting or a combination of all these three, which is still a subject of debate (Armour et al., 2003; Rattey and Hayward, 1993). The consequence

was the development of an extensive coastal-shelf depositional system characterized by shallow marine sands deposited in shoreline, shoreface and shelf environments.

The Ula Fm, which is the lateral equivalent of the Fulmar Fm in the UK Central Graben (Armour et al., 2003; Oda Subsurface Team, 2016), is the main reservoir of the Oda and Ula fields (Figure 8). The Ula Fm deposition was a consequence of the regional sea-level rise described previously. Salt movement and extensional faulting were the main factors for the generation of accommodation space for this formation. The rotated fault blocks containing Triassic sediments and the Jurassic fault system trending (NW-SE) controlled the shoreline orientation and shape of the Ula Fm deposition (Mannie et al., 2014). According to Mannie et al. (2014), the Ula Fm sediments were sourced from the Triassic and Permian rocks exposed on the Sørvestlandet, Jæren and Ringkøbing-Fyn highs (Figure 1) during the Late Jurassic, and possibly from emergent rotated fault block with poorly consolidated Triassic sediments (Bjørnseth and Gluyas, 1995; Mannie et al., 2014). The Ula Fm lithostratigraphy is characterized by upper shoreface (clean sand), lower shoreface (sandy to siltier), and transition zone (siltier to shelf mud) sediments (Ichron, 2015).

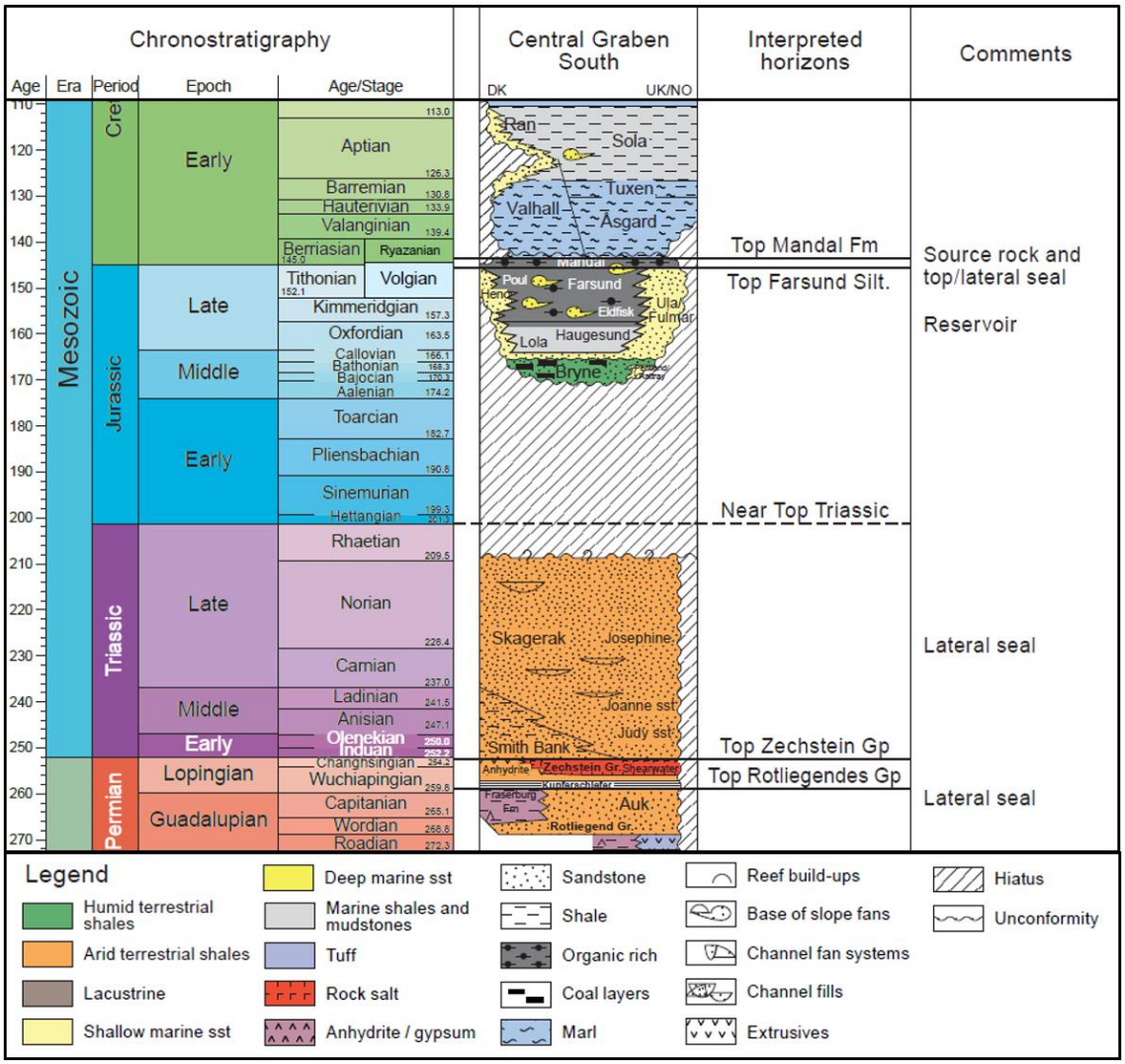

Figure 8. Lithostratigraphic column of the petroleum system components in the Ula and Oda fields. Modified after "Standard Lithostratigraphy of Offshore Norway" (2012) and nomenclature by Vollset and Doré (1984).

A flooding event marked the end of the Ula Fm which was conformably overlaid by the offshore shales of the Upper Jurassic Farsund Fm (Armour et al., 2003; Bjørnseth and Gluyas, 1995). The offshore shale deposition continued during the Early Cretaceous (Mandal Fm) when the rifting phase was followed by thermal subsidence (Armour et al., 2003). These organic rich shales from the Farsund and Mandal Fms are the top seal and source of the hydrocarbons in the Oda and Ula fields (Bjørnseth and Gluyas, 1995) (Figure 8). Afterwards, transgressive sediments covered the syn-rift topography forming the Base Cretaceous Unconformity (BCU) (Ziegler, 1975).

The Farsund and Mandal Fms in addition to the salt structures from the Zechstein Gp and the Triassic Fms provide top, lateral and bottom seals for the fault-bounded dip closure traps of the Ula and Oda fields (Hodgson et al., 1992) (Figure 8).

The Late Cretaceous was marked by post-rift thermal subsidence and the onset of active salt diapirism within the study area (Hodgson et al., 1992). The Oda field is located along the NW flank of a salt diapir developed from the Upper Cretaceous until the Miocene. The Ula field structure was also influenced by the Cenozoic diapiric movement of the Zechstein salt, as the field occurs above a NW-trending salt pillow formed during the Cenozoic (C&C Reservoirs, 2011).

The Zechstein active salt diapirism created fracture systems through which hydrocarbons migrated (Rattey and Hayward, 1993). In addition, the faults formed during the Upper Jurassic rifting phase and juxtaposing the Ula Fm reservoir and the Mandal and Farsund Fms source rocks were also important migration pathways for the hydrocarbons (Oda Subsurface Team, 2016).

2.2. **PREVIOUS STUDIES: UPPER JURASSIC DISTRIBUTION**

Many studies covering a potential Upper Jurassic fairway in the study area confirm that predicting the distribution of the Ula Fm is difficult since the deposition of this unit was controlled by halokinesis and extensional faulting (Bailey et al., 1981; Bjørnseth and Gluyas, 1995; Mannie et al., 2014; O'Connor et al., 2011; Spencer et al., 1986; Stewart, 1993).

The first publications to mention the issues related to the Ula Fm distribution were Bailey et al. (1981) and Spencer et al. (1986) during the beginning of the Ula field production. At that time, several models were suggested for the deposition of the reservoir. It was assumed that the Ula Fm was a continuous sand body though with high thickness variations controlled

by syn-sedimentary faulting in the Central Graben margins produced from movement of the underlying Zechstein salt.

Subsequently, new studies tried to explain the Late Jurassic tectono-stratigraphy of the Central North Sea, which is characterized by shallow-marine units deposited in supra-diapir depocenters (Mannie et al., 2014). The pod-interpod model proposed by Hodgson et al. (1992) suggests that passive diapirism and salt dissolution were caused by extension of the Rotliegend Gp and the differential loading of the Triassic sediments (Figure 9A and 9B) during the Early Triassic. Continued differential loading of the Zechstein salt by Triassic sediments resulted in deep depocenters (Triassic pods) surrounded by salt diapirs (Figure 9C). These salt structures were influenced by the Jurassic extension. The Jurassic rifting event lead to salt withdrawal and the widening of the diapirs, providing accommodation space for the Jurassic shallow-marine reservoirs to deposit in depocenters or interpods above the Zechstein salt walls (Figure 9D).

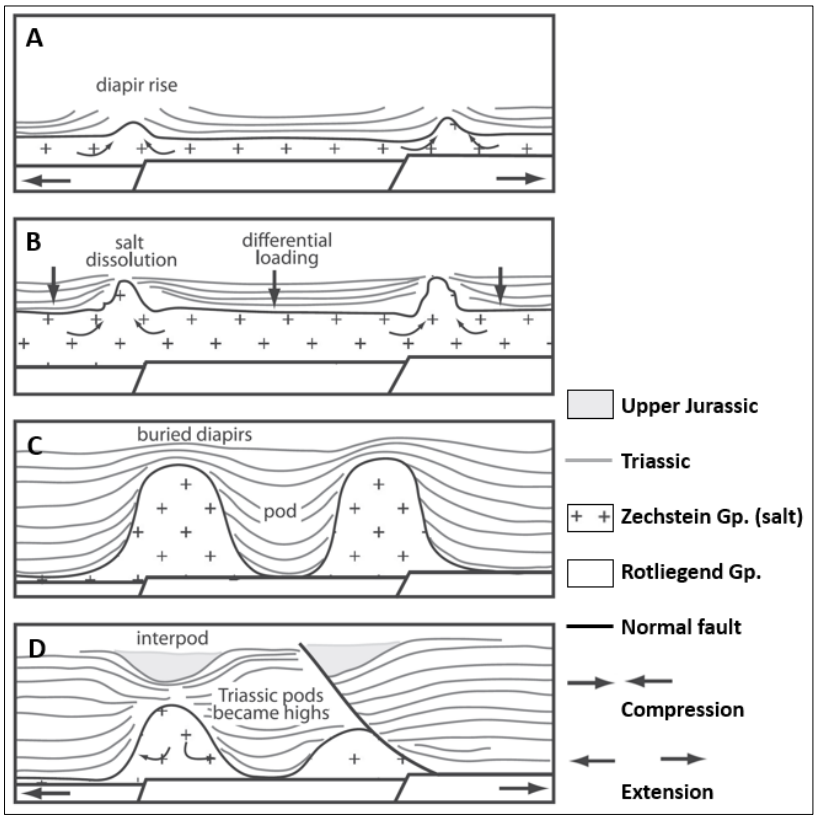

Figure 9. Pod-interpod conceptual model of extension over collapsing salt walls as described by Hodgson et al. (1992). Modified after Hodgson et al. (1992) and Mannie et al. (2014).

O’Connor et al. (2011) published a model to predict the presence of the Ula Fm sands in the Ula Trend (area between the Cod Terrace and the Ula-Gyda fault zone). The model suggests that the Ula Fm is laterally continuous over large areas of the Ula Trend, especially around the flanks of salt structures. From seismic amplitudes mapping, they located the salt highs in the study area (higher amplitudes) and used this information to make a correlation with the thickness of the Ula Fm from well data. This study showed that the top of the salt structures (highs, interpods) were associated to thicker Ula Fm sandstones and they coincide with the reservoir locations of the Ula, Tambar, Gyda and Oda fields (Figure 10). Furthermore, isochron maps of the Upper Jurassic and Lower Cretaceous showed a correlation between the thickness of these two sequences in the areas above the salt highs, compared to the Triassic pods, where the Ula Fm is absent or <20m thick with low reservoir quality and high muddy content. This correlation was proven by a cross-plot of the Upper Jurassic versus Lower Cretaceous thickness (Figure 11) from related wells in the vicinity. Figure 11 displays a linear trend (light gray) where thicker Lower Cretaceous correlates with thicker Upper Jurassic. Therefore, in Figure 10, thicker (green to blue) Lower Cretaceous areas represent thicker sections of the Upper Jurassic as well, indicating the presence of the Ula Fm to the east and SE of the Ula field and connecting to the Oda field.

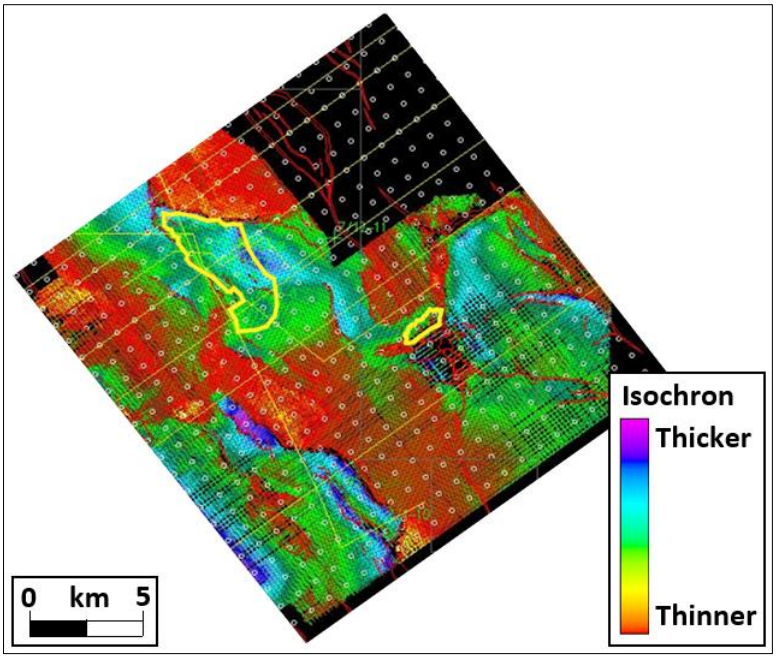

Figure 10. Lower Cretaceous isochron by O'Connor et al. (2011). Green to blue areas represent also thicker sections of the Upper Jurassic. Yellow polygons are the outlines of the Ula (NW) and Oda (SE) fields. Modified after O'Connor et al. (2011).

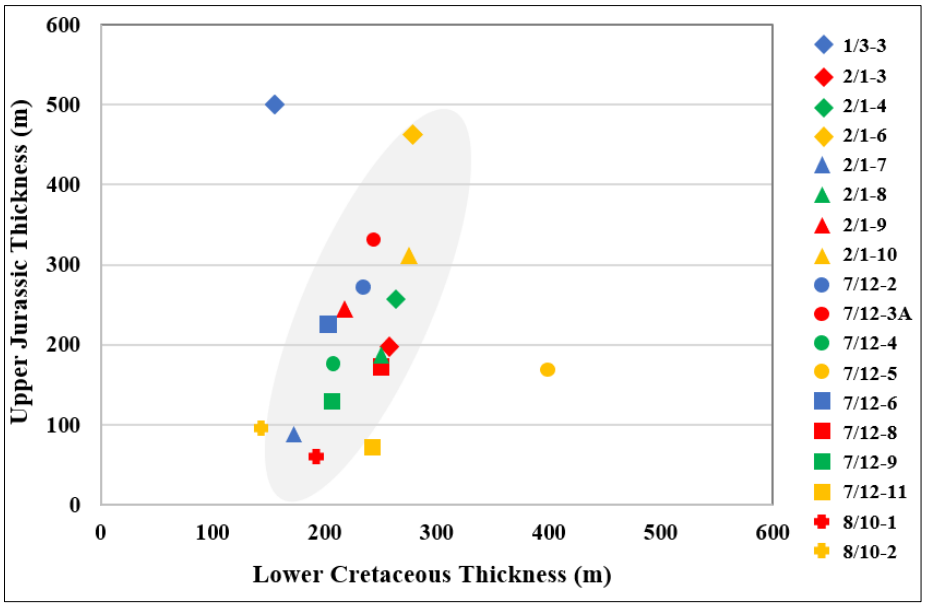

Figure 11. Cross-plot of the Upper Jurassic versus the Lower Cretaceous thickness. It is possible to observe a trend (light gray) where thicker Lower Cretaceous correlates with thicker Upper Jurassic. Modified after O'Connor et al. (2011).

The most recent model explaining the accommodation space for the deposition of the shallow marine sediments of the Ula Fm is attributed to Mannie et al. (2014). In this study, these authors concluded that the Upper Jurassic sands were deposited in pod-shaped minibasins

located above salt walls and they proposed a tectono-stratigraphic model to explain the evolution of the Jurassic supra-diapir minibasins. Mannie et al. (2014) observed that the Upper Jurassic strata onlap the margins of the supra-diapir minibasins, so the distribution of these strata is the result of syndepositional accommodation space within these minibasins, which was developed during the Late Jurassic. According to these authors, Early Triassic extension combined with Late Jurassic rifting were the responsible for the reactivation, rise and collapse of salt diapirs, providing accommodation space for the deposition of the Ula Fm minibasins above the collapsing salt walls as described by Figure 12 (Mannie et al., 2014). Figure 12 shows that the stretching of the supra-salt strata resulted in the generation of normal faults and the widening of the salt walls/diapirs. These led to subsidence above the salt structures forming the diapir-collapse minibasins bounded by normal faults, where the Ula Fm shallow marine sands deposited.

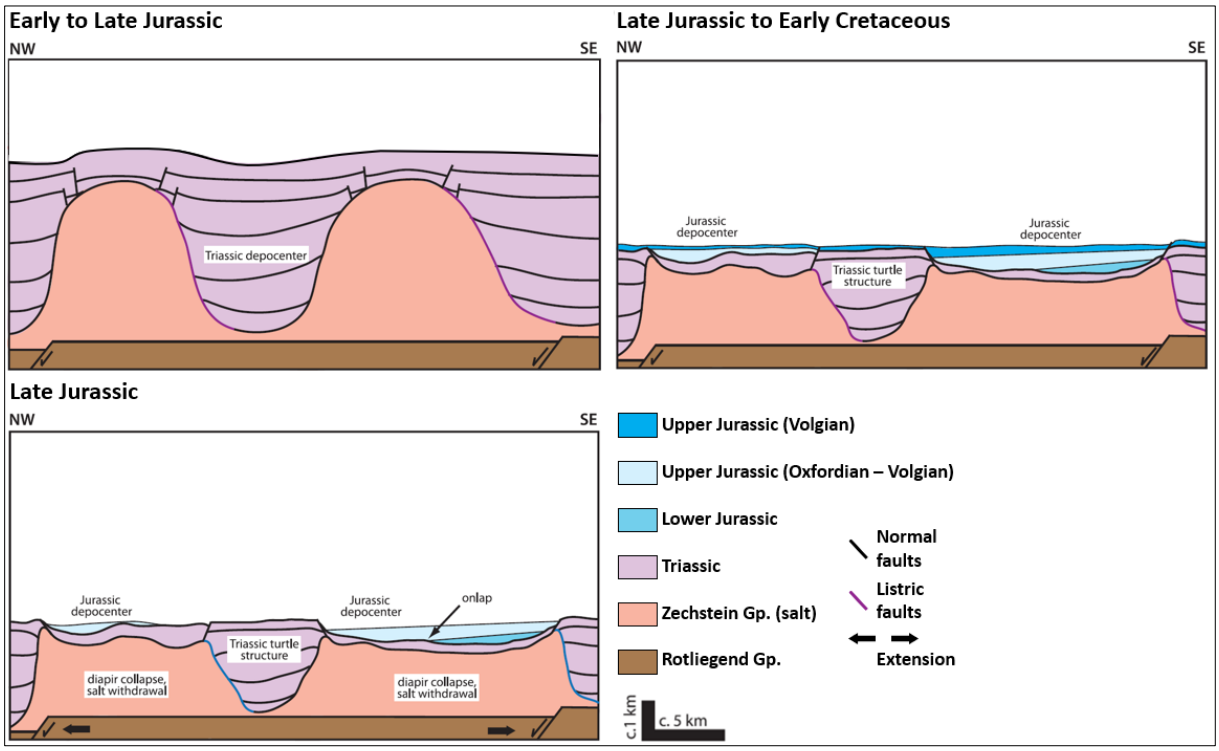

Figure 12. Conceptual model proposed by Mannie et al. (2014) to explain the creation of accommodation space for the Upper Jurassic Ula Fm. Modified after Mannie et al. (2014).

A core description and a depositional modelling study in the area between blocks 7/12 and 8/10 (Ichron, 2015) for the Oda development plan describes a potential Ula Fm fairway based only on well data (regional geology and geological settings were not considered in these interpretations). Wireline logs and core data from wells drilled in the area were correlated to generate depositional environment maps for each sequence in the Ula Fm. The stratigraphic sequences for this study were based on Partington et al. (1993) J-sequences in which sequences J62, J63, J64 and J66 are associated to the Ula Fm (Figure 13).

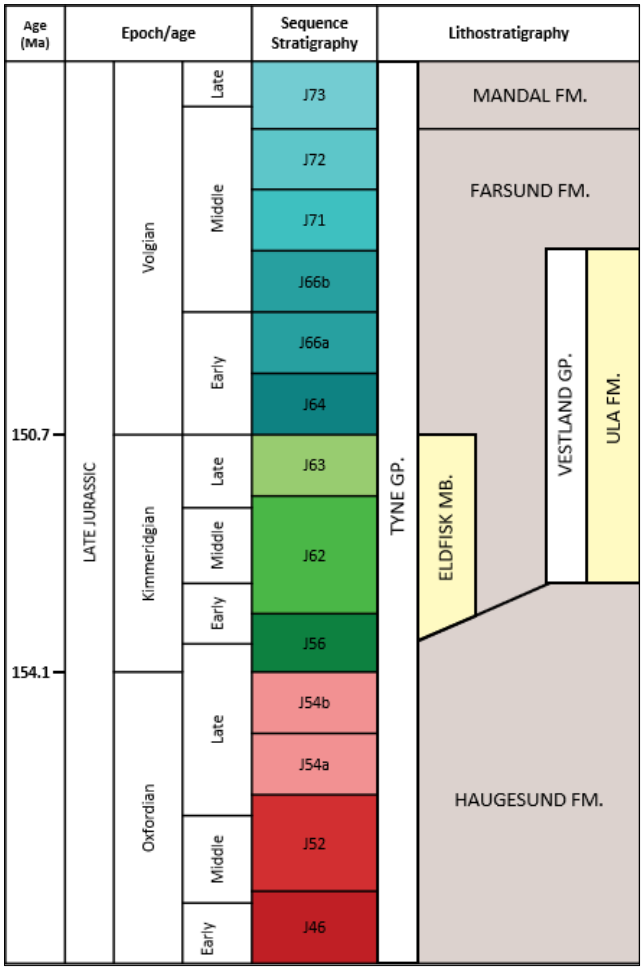

Figure 13. Sequence stratigraphic chart based on Partington et al. (1993). The J-sequences J62, J63, J64 and J66 are associated to the Ula Fm. Modified after Ichron (2015).

The maximum flooding surface of the Ula Fm is represented by the J63 sequence (Late Kimmeridgian). This sequence extends along the Cod Terrace, in the west, to the Sørvestlandet

High, in the east, as a wide belt of shoreface deposits. Figure 14 shows the depositional environment map from the Ichron's (2015) study for the J63 sequence. On this map a NW-SE trending shoreline marks the limit between the Upper and Lower shoreface sands (yellow area) and the non-deposition/non-preservation of the Ula Fm (NE – gray area). The Cod Terrace area is partially dominated by the transition zone (shelf mud facies – blue area). Since in this model rifting and salt tectonism were not considered, the deposition of the Ula Fm is assumed laterally continuous along the whole shoreface zone, which is of course an oversimplification.

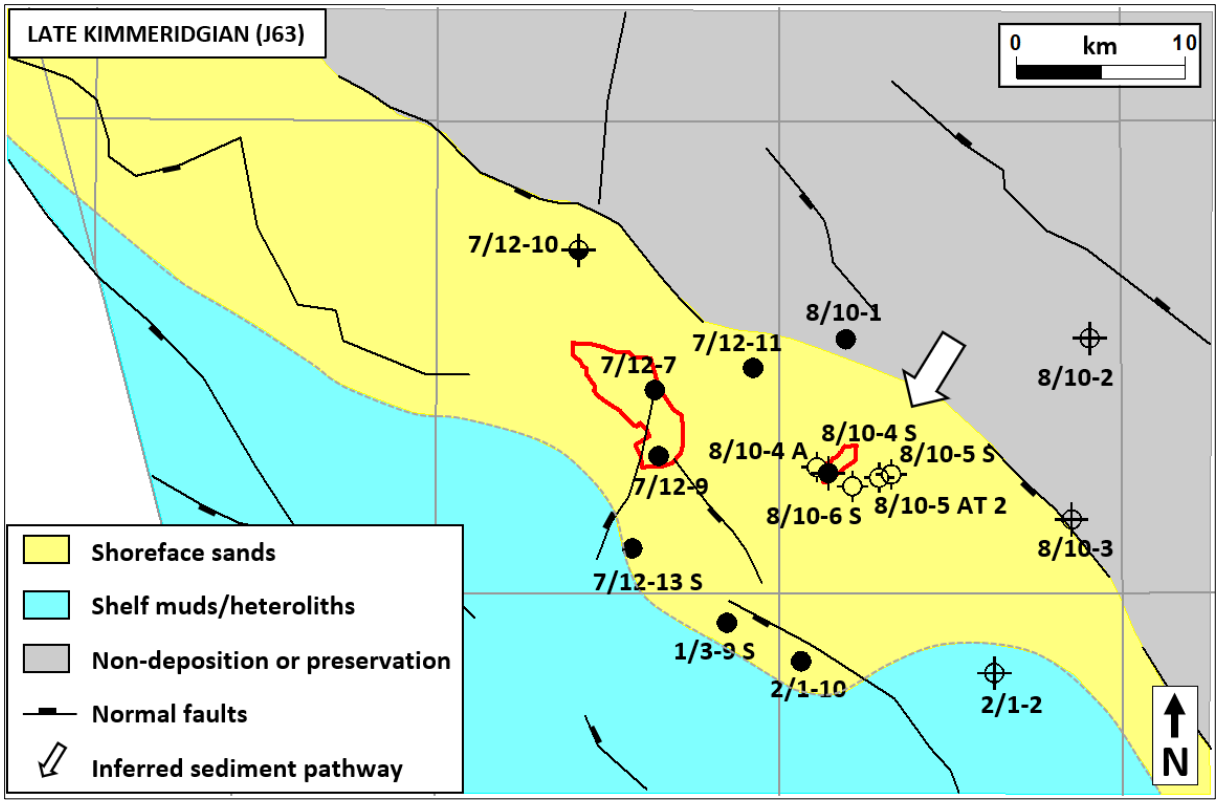

Figure 14. J63 Ula Fm depositional environment map proposed by the Ichron study. Modified after Ichron (2015).

3. DATA SET

The study area covers about 700.000 km^2, including both the Ula and Oda fields and part of the Ula Trend (western region) and the Sørvestlandet High (eastern region) (Figure15). Spirit Energy Norway AS Subsurface Team provided the regional structure maps in depth from previous interpretation studies of the top Farsund Fm (Figure 15), top Zechstein Gp (Figure 16) and the main faults in the area.

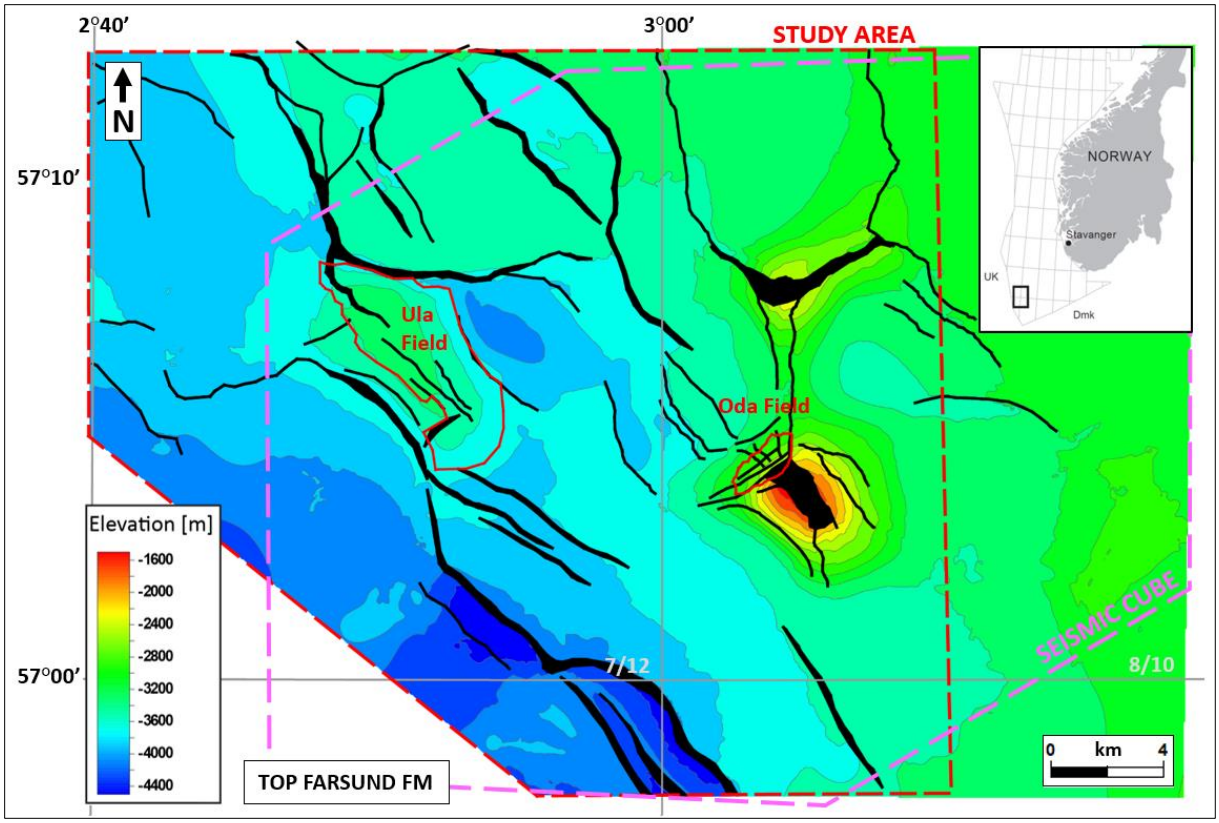

Figure 15. Top Farsund Fm structure map in depth showing the limits of the study area (red dashed line) including the Oda and Ula fields (red polygons). The pink dashed line shows the dimensions of the seismic cube used for QC of the input structure maps.

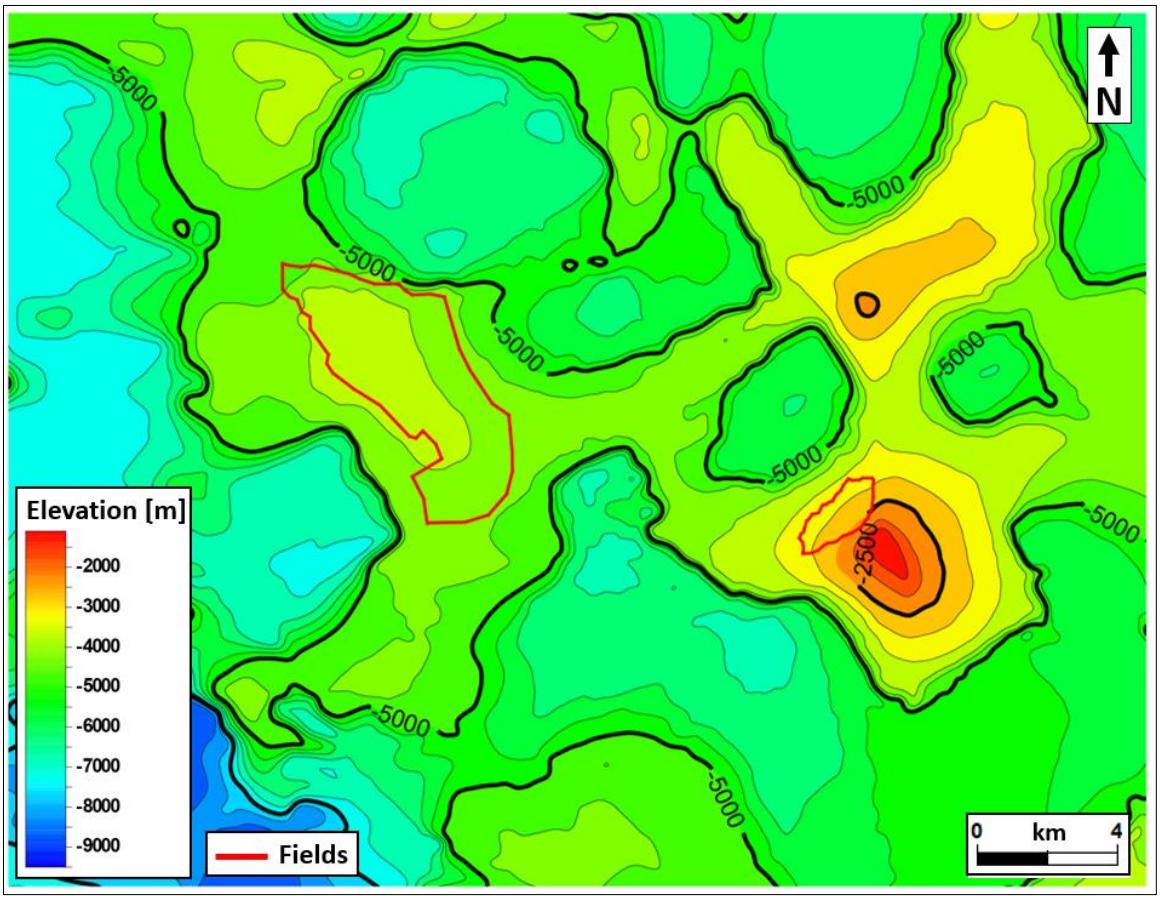

Figure 16. Top Zechstein Gp structure map in depth, including the Oda and Ula fields border lines (red polygons).

The top Farsund Fm was used to define the top Ula Fm (which is below seismic resolution) and the top Zechstein Gp represents the present-day salt structures, which can be used to understand the depositional regime of the Ula Fm

A 3D seismic survey (Figure 15) in depth domain (SEG normal polarity, i.e. increase in acoustic impedance is represented by a positive reflector, peak) covering the area of interest was used for quality control (QC) of the regional structure maps. The structure maps were compared against the seismic well tied reflectors interpreted as the top Farsund Fm (shale – increase in AI and strong peak) and the top Zechstein Gp (salt – increase in AI and strong peak) to ensure the surfaces were honoring the seismic data.

Data from 11 wells were obtained from a public database (DISKOS database) and from the PL 405 license internal database (Spirit Energy Norway AS, Suncor Energy Norge AS,

Aker BP ASA and DNO Norge AS) to build the geological model. The well data includes logs – Gamma Ray (GR), Resistivity (RES), Sonic (DT), Density (DEN), Neutron (NEU), Core Porosity (CPOR) – and computer processed interpretations (CPI) (Table 1). Well tops in depth (MD) from each lithostratigraphic unit were obtained from the NPD webpage (public access).

Table 1. Table of well log and CPI data for each well in the Ula (blue) and Oda (green) fields.

Well	Field	Well logs						CPI		
		GR	RES	DT	DEN	NEU	CPOR	Φ	NTG	Kh
7/12-5	Ula	x	x	x	x	x	x	-	-	-
7/12-6	Ula	x	x	x	x	x	x	-	-	-
7/12-7	Ula	x	x	x	x	x	x	-	-	-
7/12-8	Ula	x	x	x	x	x	x	-	-	-
7/12-9	Ula	x	x	x	x	x	x	-	-	-
8/10-4 S	Oda	x	x	x	x	x	x	x	x	-
8/10-4 A	Oda	x	x	x	x	x	-	x	x	-
8/10-4 AT2	Oda	x	x	x	x	x	-	x	x	-
8/10-5 S	Oda	x	x	x	x	x	x	x	x	-
8/10-5 AT2	Oda	x	x	x	x	x	-	x	x	-
8/10-6 S	Oda	x	x	x	x	x	x	x	x	-

Rock and fluid properties for the dynamic simulation were obtained from original well reports of special core analysis (SCAL) and pressure volume temperature properties (PVT) data, from the Plan for Development and Operation of the Oda field (Oda Subsurface Team, 2016) and from the DAKS database.

The historical production and injection data from each well and average reservoir pressure in the Ula field was obtained from the DISKOS NPD public portal and from the PL 019 license database (Aker BP ASA and DNO Norge AS).

4. METHODOLOGY

The research methods applied in this thesis are divided into four main groups: static model of the study area, conceptual model of the Ula Fm fairway, dynamic model of the hydrodynamic aquifer, and history matching.

4.1. STATIC MODEL

Geological models are static representations of the reservoir and adjacent aquifers. They contain structural features (faults), lithology characteristics and facies distributions (Batycky et al., 2007). In order to build a consistent geological model while acknowledging geological uncertainty, seismic interpretation and petrophysical data are combined with deterministic and stochastic techniques based on geostatistics.

For this part of the study, all processes were performed using the commercial software Petrel (Schlumberger). It is important to highlight that QC's of the grid cells and of the results obtained for static properties (porosity, permeability, net to gross, initial water saturation) and volumes (bulk volume, net volume, pore volume and oil in place) were applied to ensure the final static model honors the input data (well logs, structure maps and faults interpretation).

4.1.1. Geological Evaluation

From the analysis of synthetic seismograms of 5 wells in the Oda Field (8/10-4 S, 8/10-5 S, 8/10-5 AT2, 8/10-6 S and 7/12-11), it was established that neither the top nor the base of the Ula Fm correspond to clear acoustic impedance contrasts. The Ula Fm thickness, according to well data, can be thinner than 10 m, which is lower than the vertical seismic resolution of

~30 m at the Ula reservoir depth. Furthermore, tuning effects also affect the seismic definition of the Ula reservoir. Therefore, considering the difficulties in mapping the Ula Fm directly from seismic, the top Farsund Fm (strong seismic peak right above the Ula Fm with a similar structural setting) with a global adjustment (moving average) to the well tops of the top Ula Fm, and the top Triassic were used to generate the top and base of the Ula Fm, respectively (Figures 17 and 18).

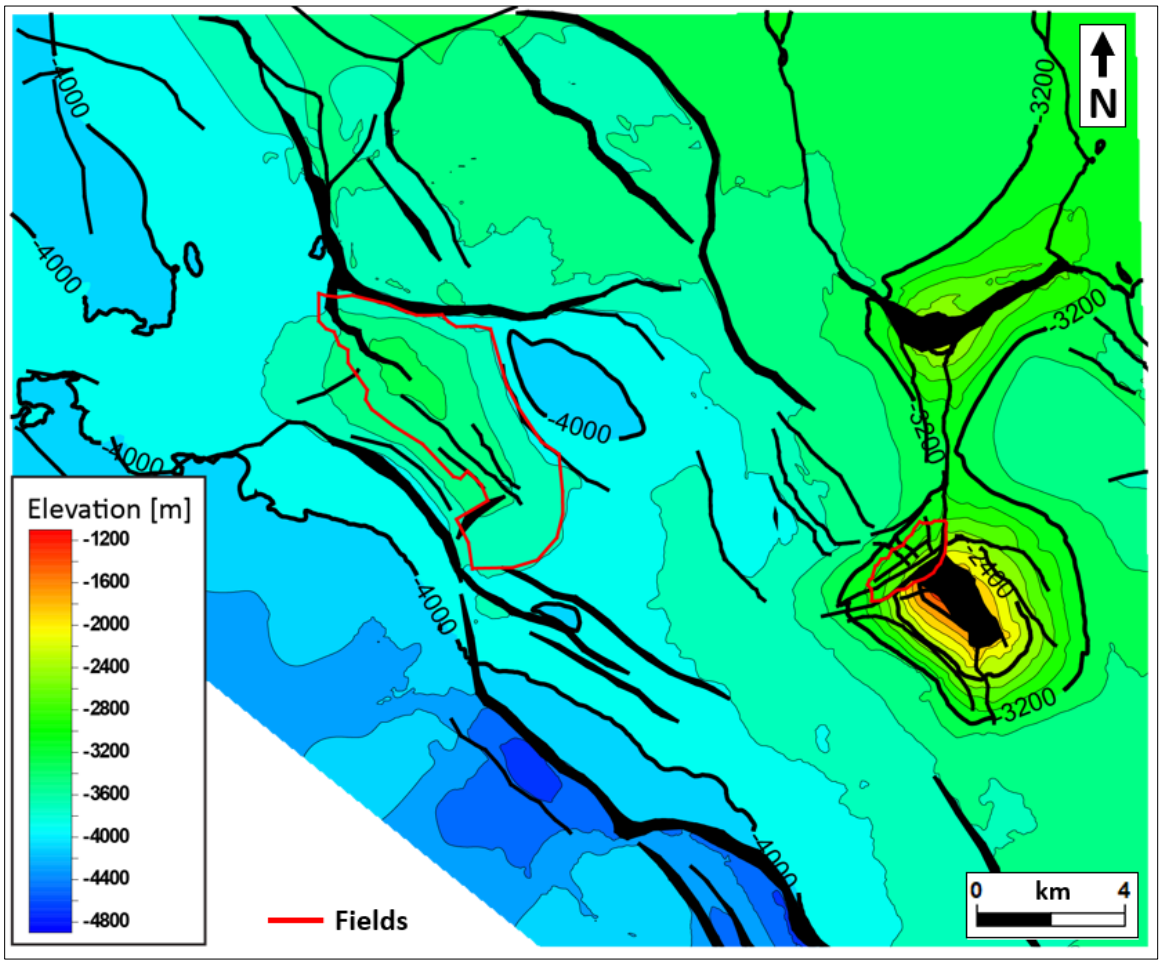

Figure 17. Top Ula Fm structure map in depth and main faults (black polygons), including the Oda and Ula fields border lines (red polygons).

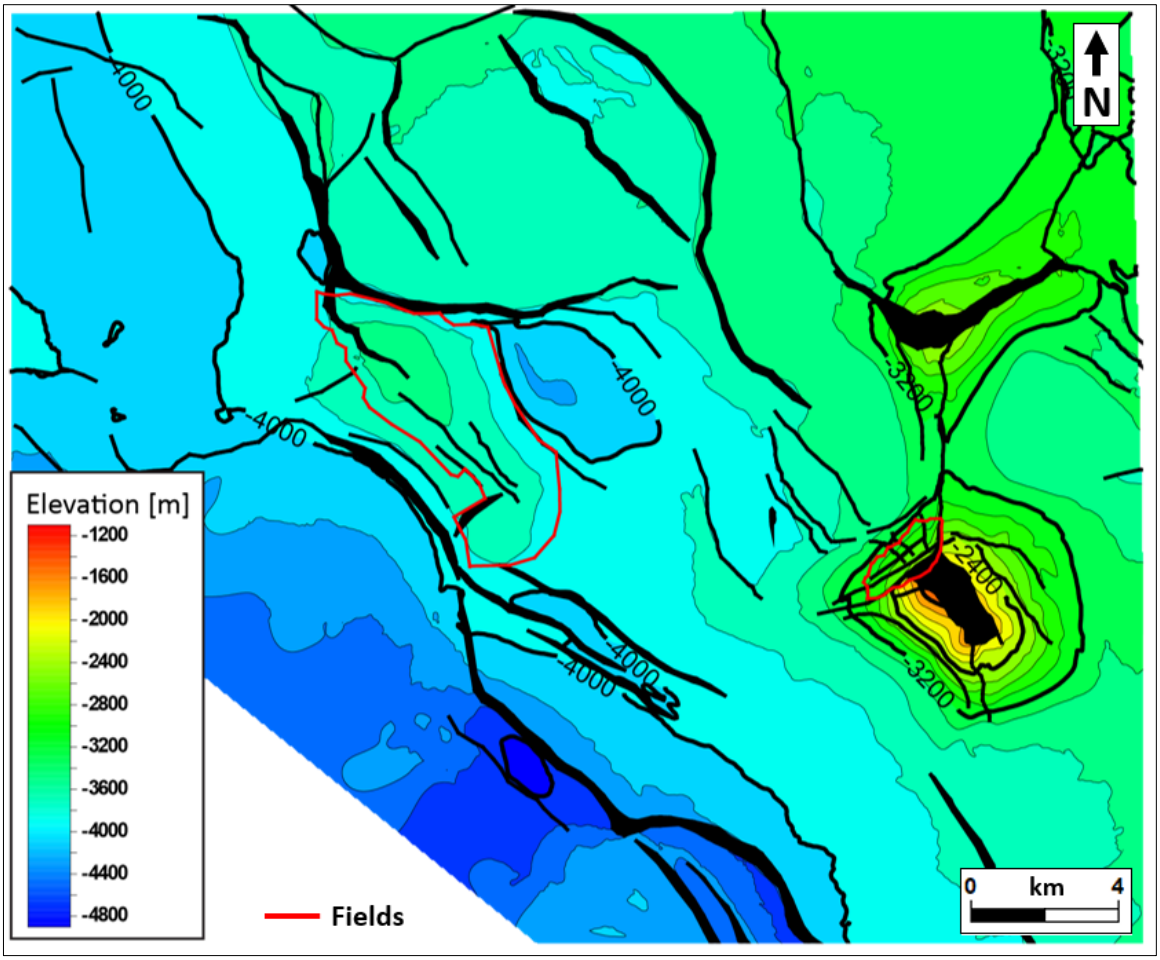

Figure 18. Base Ula Fm structure map in depth and main faults (black polygons), including the Oda and Ula fields border lines (red polygons).

4.1.2. Structural and Fault Modelling

The technique used to model the Ula Fm reservoir structure was Volume Based Modelling (VBM). This fully automated technique is recommended for complex structural models (salt diapirs, large structural relief, dense network of faults) by Souche et al. (2013). The main advantage of VBM is that it models directly volumes (geological layers) regardless of the geological setting and of the quality of the input data (sparse and noisy data).

The main faults interpretation (in depth), provided by the Spirit Energy Norway AS subsurface team, was converted to fault planes and the minor faults were truncated against the major faults. Figure 19 shows the fault framework used for the static model.

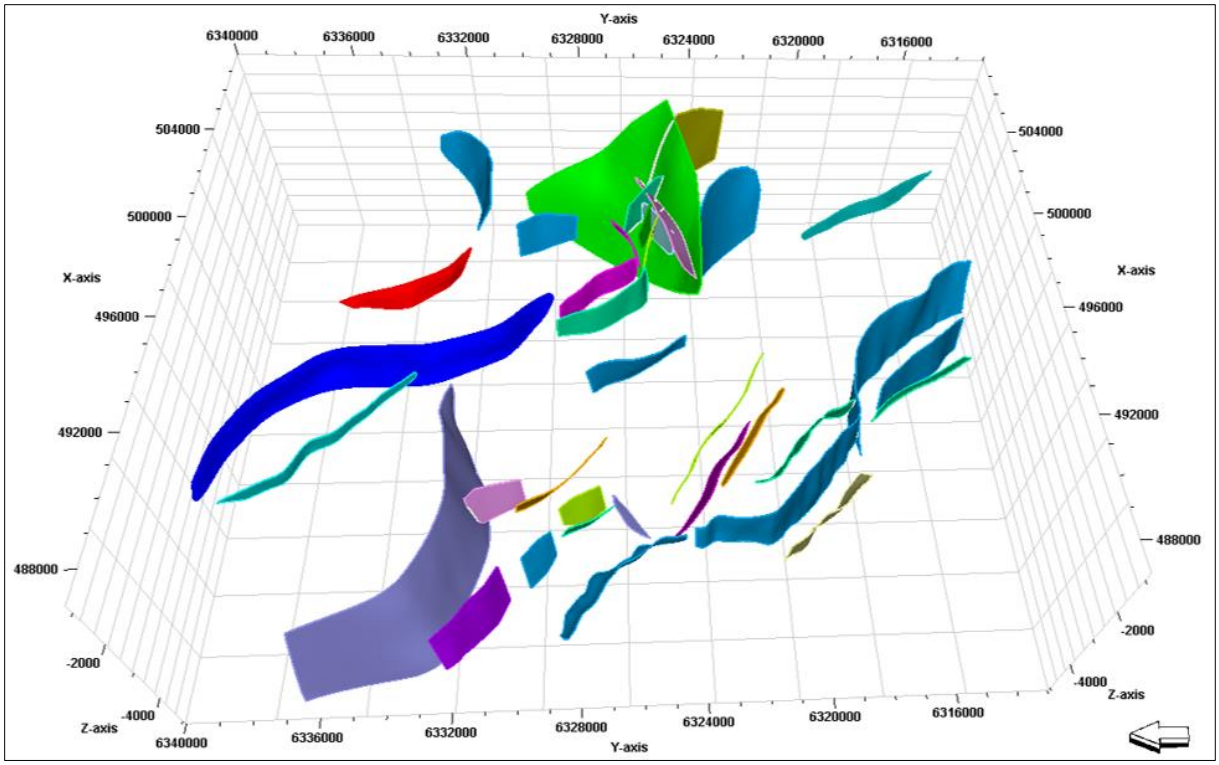

Figure 19. Fault framework with the interpreted faults converted to fault planes and the minor faults truncated against major faults (3D view).

4.1.3. Structural Gridding and Layering

Since the area of study is quite large (~700,000 km^2) and the aim is to model the Ula Fm aquifer, coarse grid cells of 100 by 100 m were used. These cells capture the main hydrodynamic processes while decreasing the time of computation. For the same reasons, the static model was divided in 10 layers of approximately 10 m thickness (Figure 20). The resulting grid contains a total of 1,256,100 cells.

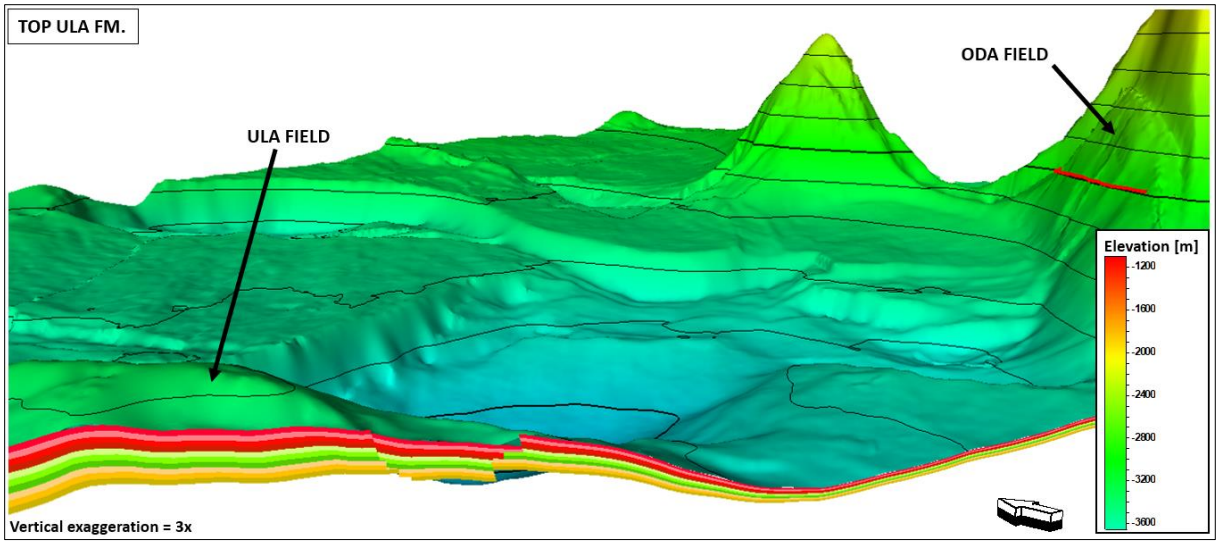

Figure 20. 3D view of the area between the Ula and Oda fields showing the layering division of the Ula Fm interval. The model has 10 layers in the vertical of approximately 10 m thickness. The red line in the Oda field indicates the OWC.

The model was constructed using the top and bottom horizons (in depth) of the Ula Fm (Figures 17 and 18). Well tops were used for global adjustment of the horizons. The faults were represented as stair-steps (Figure 21) and the grid orientation was rotated to 129° to follow the NWSE shoreline trend investigated by previous works (Figure 14, Ichron, 2015), aligning the grid with the direction of flow.

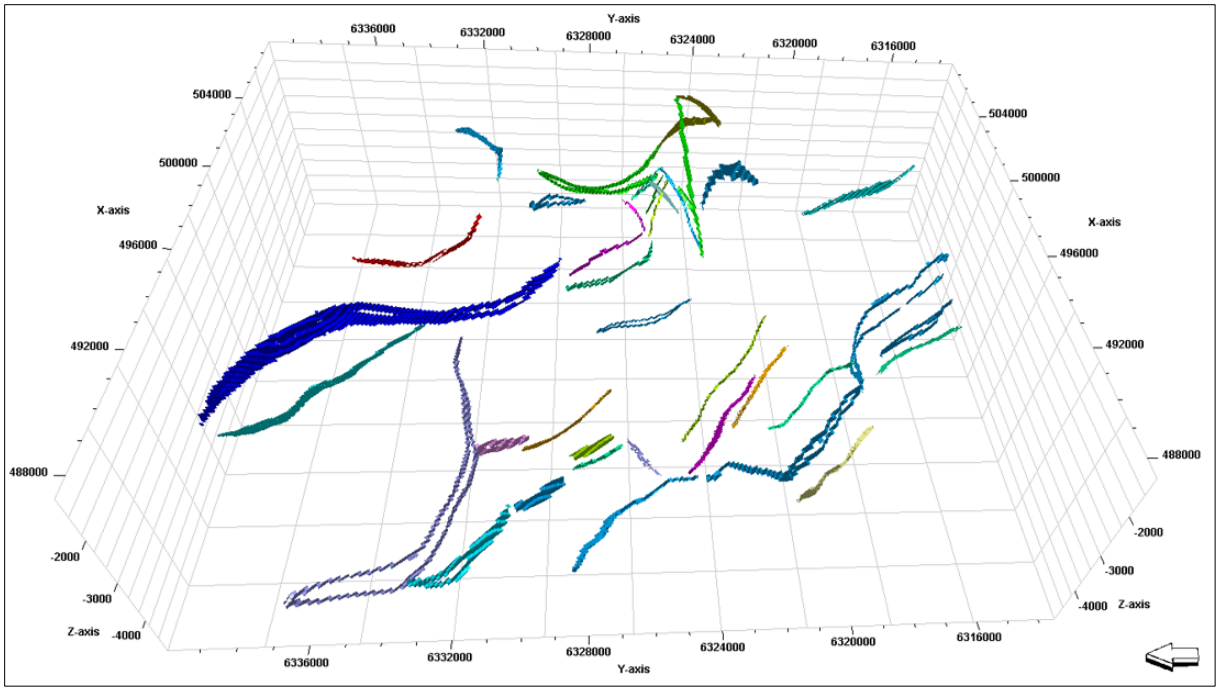

Figure 21. Stair-step representation of the faults in the static model (3D view).

The end grid model (Figure 22) was checked to ensure that the grid cells geometry was suitable for dynamic simulation. For this purpose, nine grid cells characteristics were evaluated: corners with negative thickness, corners with zero thickness, large dip, large twist, lateral aspect ratio, lateral concavity, maximum angle from vertical, twist angle and positive volumes. Table 2 shows the results and descriptions for each parameter. It can be seen that the grid cells geometry is appropriate for the dynamic simulation.

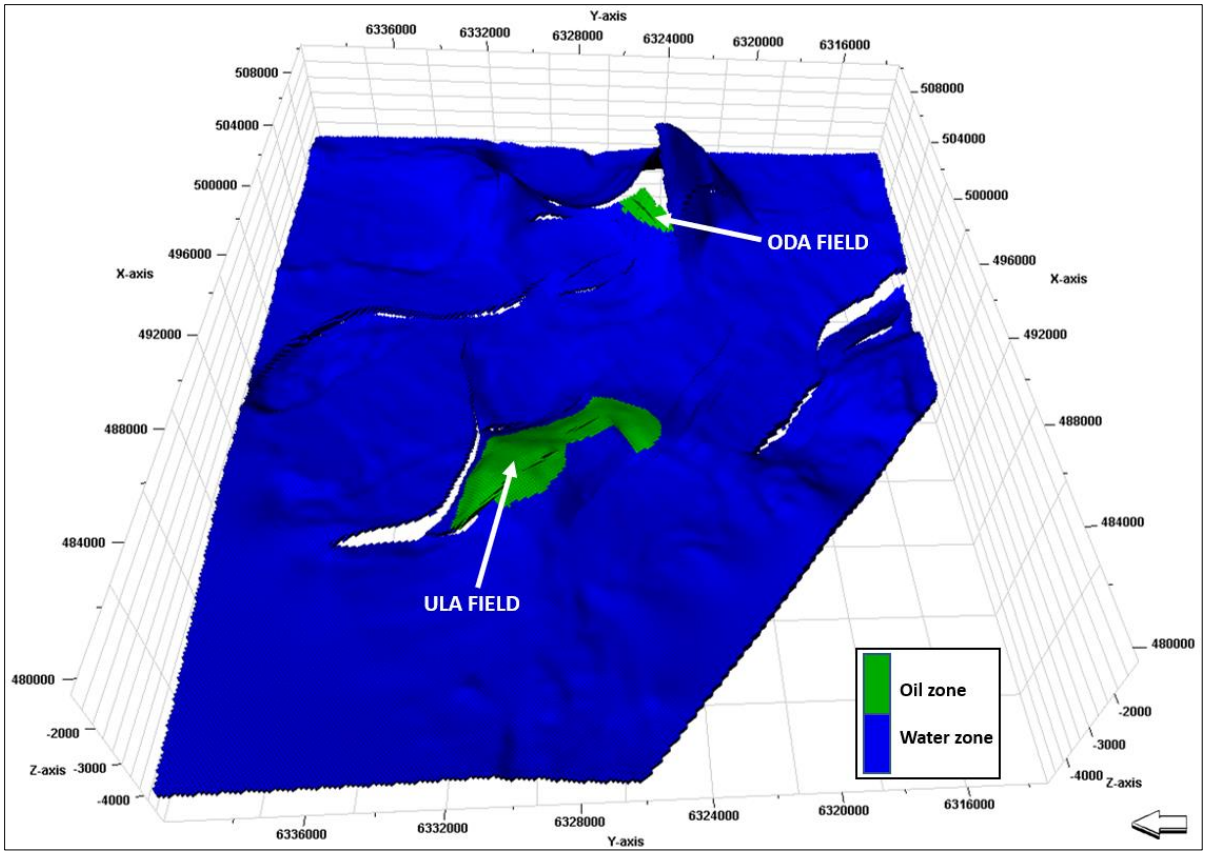

Figure 22. Grid model generated for this study. The model consists of 100 by 100 m grid cells with approximately 100 m thickness divided in 10 layers.

Table 2. QC results of the grid cells geometry. The grid contains a total of 1,256,100 cells.

Characteristic	Mean	Sum	Description
Corners with negative thickness	-	0	No corners with negative thickness.
Corners with zero thickness	-	1499	<0.15% of corners with zero thickness.
Large dip	-	345263	~25% of the cells have large dip (when I or J average direction vectors have a larger Z component than the K average direction vector) due to salt structures influence.
Large twist	-	0	No cells with large twist.
Lateral aspect ratio	1	-	Ratio between lateral cell edges, J-direction vs. I-direction. 1 means no irregularities in the shape of the cell.

Lateral concavity	-	0	No cells with lateral concavity.
Max angle from vertical	0°	-	No angular variation from the vertical in the cells.
Twist angle	0°	-	No twist angle in the cells.
Positive volumes	93801	-	Bulk volume in m^3, the outliers (cells with bulk volumes above 10^6 m^3) were disactivated (ACTNUM = 0).

4.1.4. Fluid Contacts

The fluid contacts in the Oda and Ula fields are at different depths. To assign these differences in the OWC depth for each field, contact regions were created from polygons of the Oda area and of the eastern and western parts of the Ula field (Figure 23). Table 3 shows the OWC depths defined for each region based on Heum (1996) and on the Plan for Development and Operation of the Oda field (Oda Subsurface Team, 2016).

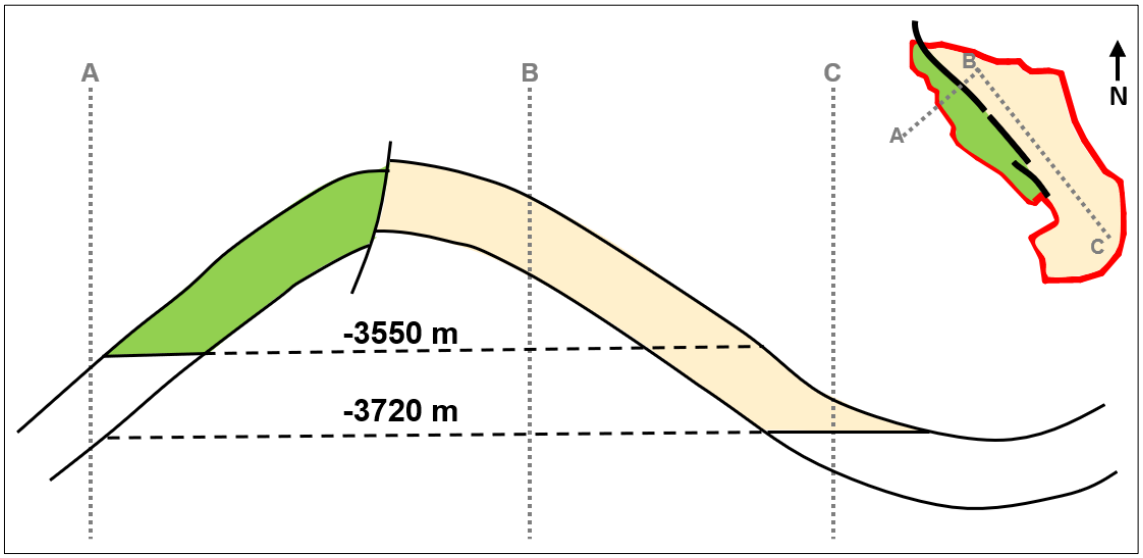

Figure 23. Cross section of the Ula field structure showing its western (green, smaller) and eastern (beige, bigger area) zones divided by a faults' barrier. Modified after Heum (1996).

Table 3. OWC depths defined for each region.

Contact Region	OWC (m)
Oda field	-2985
East Ula field	-3720
West Ula field	-3550

The Ula field was divided in two zones (east and west), and in each zone a horizontal OWC with different depth (Figure 23, Table 3) was used to simulate the large OWC depth change described by many authors as a hydrodynamic flow effect (Dennis et al., 2005; Green et al., 2014; Heum, 1996; O'Connor et al., 2011). Figure 23 shows how the Ula field was divided into western (green) and eastern (beige) zones separated by a faults' barrier. A sealing fault (low permeability barrier) causes pressure decrease in the aquifer across this fault and results in the step down of the OWC. However, in the Ula field, pressure measurements in the hydrocarbon zone on both sides of the fault show no difference (Dennis et al., 2000), which means that the reservoir is not compartmentalized and the large OWC depth difference is a consequence of hydrodynamic effects. The static model does not incorporate these hydrodynamic effects, which is a limitation of the work.

4.1.5. Property Modelling

The grid model was populated with net to gross, porosity, permeability, water saturation and fault transmissibility properties. These properties are related to the heterogeneity of the reservoir, but a facies model is not necessary to run the dynamic model. Therefore, in order to simplify the workflow, three rock types were associated to the depositional lithofacies of the Ula Fm using property calculation. The rock types are transition zone (TZ), lower shoreface

(LSF) and upper shoreface (USF) sediments. USF represents the highest quality reservoir, LSF is the lower quality reservoir and TZ is the poorest quality reservoir.

The rock types (lithofacies) were defined based on petrophysical and core analysis results. The analysis used core data from wells in the Oda, Ula and Tambar fields. Porosity and permeability measured from core data were used to divide the Ula Fm sandstones in the three lithofacies TZ, LSF and USF. Histograms with the porosity data frequency of each lithofacies (Figure 24) were used to define porosity ranges for the rock types in the model. Thus, in the static model, porosities below 15% were associated to TZ, porosities between 15-23% to LSF, and porosities above 23% to USF (Table 4).

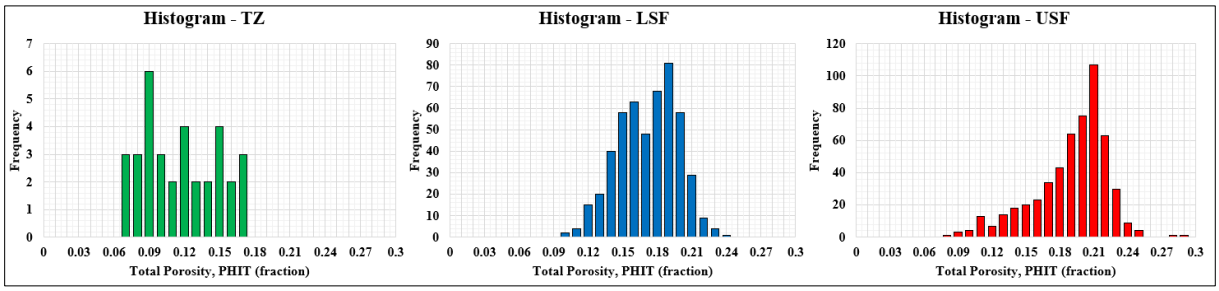

Figure 24. Histograms of porosity for the three rock types TZ, LSF and USF in the Ula Fm.

Table 4. Porosity ranges of the three rock types defined from the histograms in Figure 24.

Facies	Porosity range (fraction)
TZ	$\Phi < 0.15$
LSF	$0.15 < \Phi < 0.23$
USF	$\Phi > 0.23$

The porosity data used for this study was the total porosity (PHIT). Table 1 shows that for the Ula field, CPI well logs are missing. Therefore, a neural network training estimator cross correlating GR, CPOR (overburden corrected), DTCO (compressional sonic log) and DEN logs was used to generate the missing PHIT logs. Figure 25 shows some of the final PHIT logs of the reservoir interval. The porosity data ranges between 0 and 0.3. For the Oda field, PHIT well

logs created with the neural network estimator were compared to the actual PHIT well data to QC this process.

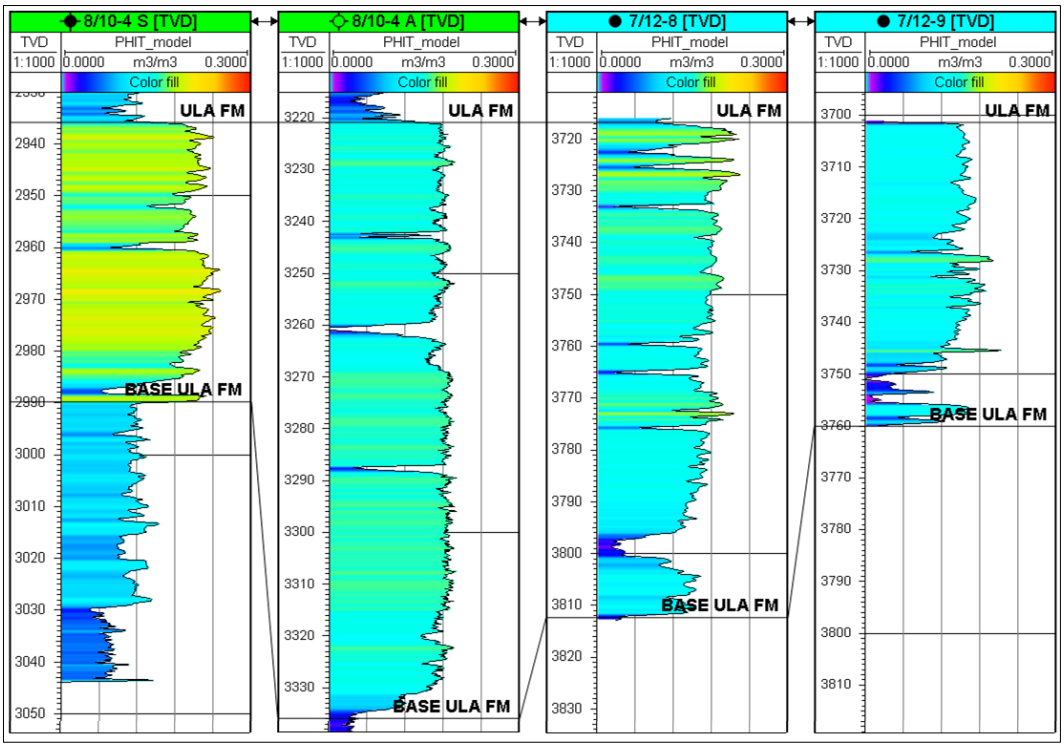

Figure 25. PHIT logs from the reservoir interval of wells 8/10-4 S and 8/10-4 A in the Oda field and wells 7/12-8 and 7/12-9 in the Ula field. The location of the wells is in Figures 2 and 4.

The PHIT logs from the Oda and Ula wells were upscaled using the arithmetic average method – the input series of values from the well log are summed and divided by the total count of the series numbers to be upscaled in the grid cell (Schlumberger, 2020) – and applied to populate the model by Sequential Gaussian Simulation (SGS). SGS is a geostatistical stochastic method of interpolation based on kriging. This sequential algorithm honors the well data and the input distribution, variograms and trends. The variogram and distribution are used to create local variations in the input data to honor the uncertainties in the data (Schlumberger, 2020). For the PHIT property model, a spherical variogram with default values for sill and nugget effect (1 and 0.0001 respectively) was used and the distribution followed the upscaled logs. The depth trend was incorporated into the model using co-kriging since there is a strong relationship

between PHIT and depth in the Ula Fm. Moreover, the well data available for the study area do not cover most of the area outside the Oda and Ula fields, where there are large structural variations.

The PHIT model was checked against the frequency distributions from the well logs and upscaled cells to ensure the PHIT model honored the input data. Figure 26 demonstrates that there is a reasonable match between the modelled PHIT property, the upscaled well logs, and the input well logs.

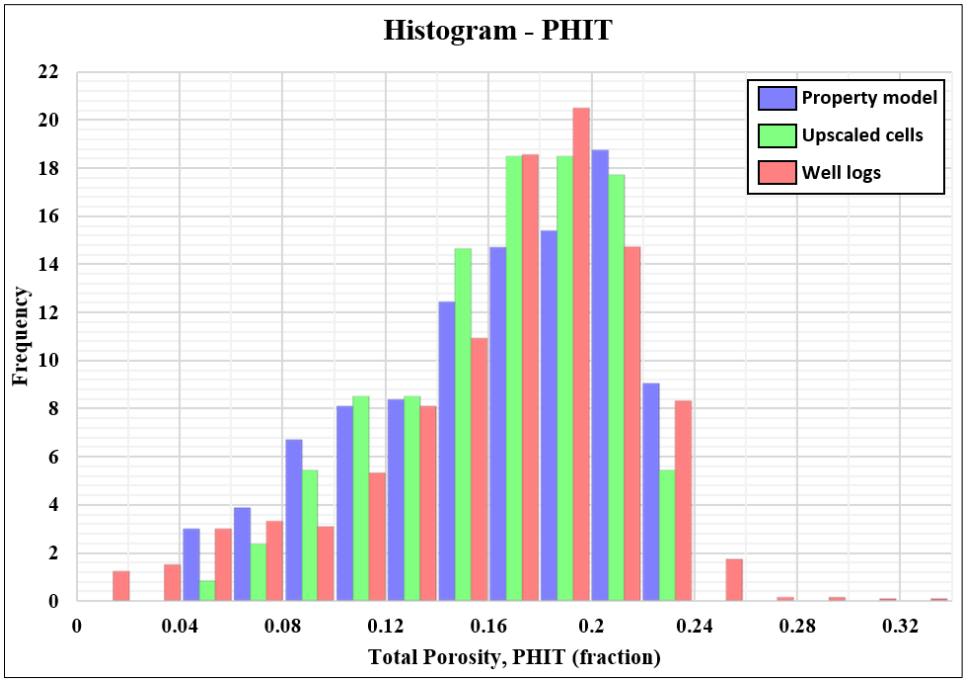

Figure 26. QC of the PHIT model by comparison of the well logs, upscaled logs and the property model.

The horizonal permeability (Kh) was generated as function of porosity-permeability transforms (empirical relations). For each rock type, a transform was calculated from Kh core measurements (Table 5). Kh logs were calculated for all wells in the Oda and Ula fields and compared with core data averages available from petrophysical measurements. Figure 27 shows some of the Kh logs of the reservoir interval. The Kh well data ranges between 0.005 mD to 500000 mD.

Table 5. Transforms used to calculate Kh for each rock type facies.

Facies	Transform
TZ	Kh = Pow(10, 14.7653 * Φ – 2.395668)
LSF	Kh = Pow(10, 17.9798 * Φ – 1.59767)
USF	Kh = Pow(10, 21.5886 * Φ – 2.00355)

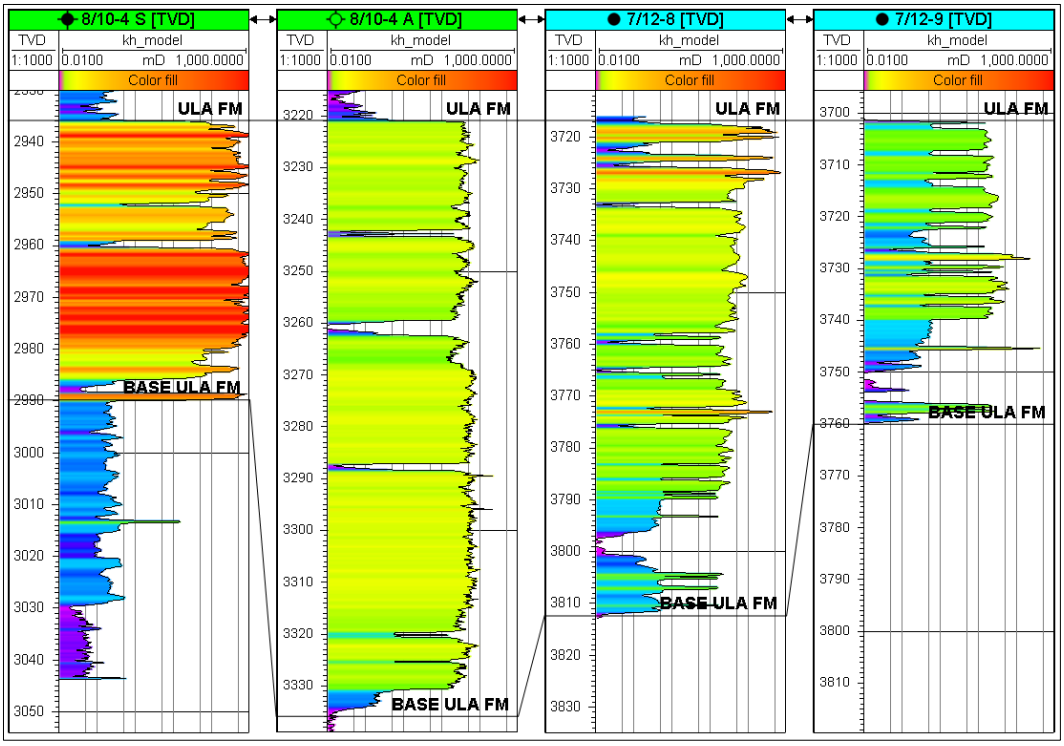

Figure 27. Kh logs from the reservoir interval of wells 8/10-4 S and 8/10-4 A from the Oda field and wells 7/12-8 and 7/12-9 from the Ula field. The location of the wells is in Figures 2 and 4.

The Kh logs were upscaled using the median average method – the input values from the well log are sorted and the center value is selected to be upscaled in the grid cell (Schlumberger, 2020) – and applied to populate the model by Gaussian Random Function Simulation (GRFS). GRFS is a geostatistical stochastic method of interpolation based on kriging that uses a different kriging algorithm than SGS. This non-sequential algorithm also honors the well data and input distribution, variograms and trends (Schlumberger, 2020). For the Kh property model a spherical variogram with default values for sill and nugget effect (1 and 0.0001 respectively) was used and the distribution followed a lognormal function with 100

mD, 70 mD, 10 mD and 500 mD as mean, standard deviation, minimum and maximum values respectively. The values for the lognormal function were selected to fit the average reservoir permeabilities in the Ula (300 mD, air) and Oda (1200 mD, Klinkenberg corrected) fields. Since Kh is a function of PHIT, a depth trend was also incorporated into the model using co-kriging to model the relationship between permeability and depth in the Ula Fm. The Kh model was checked against the well logs and upscaled cells to ensure the property model fits the porosity-permeability transforms. Figure 28 displays the comparison between the modelled property, upscaled well logs and raw well logs. As expected, there is a match between the upscaled well logs and raw well logs, but the modelled property follows the lognormal distribution applied, with larger frequencies at 40-80 mD. The vertical permeability (Kv) property was generated assuming that Kv is 10% of Kh (according to well log data analysis).

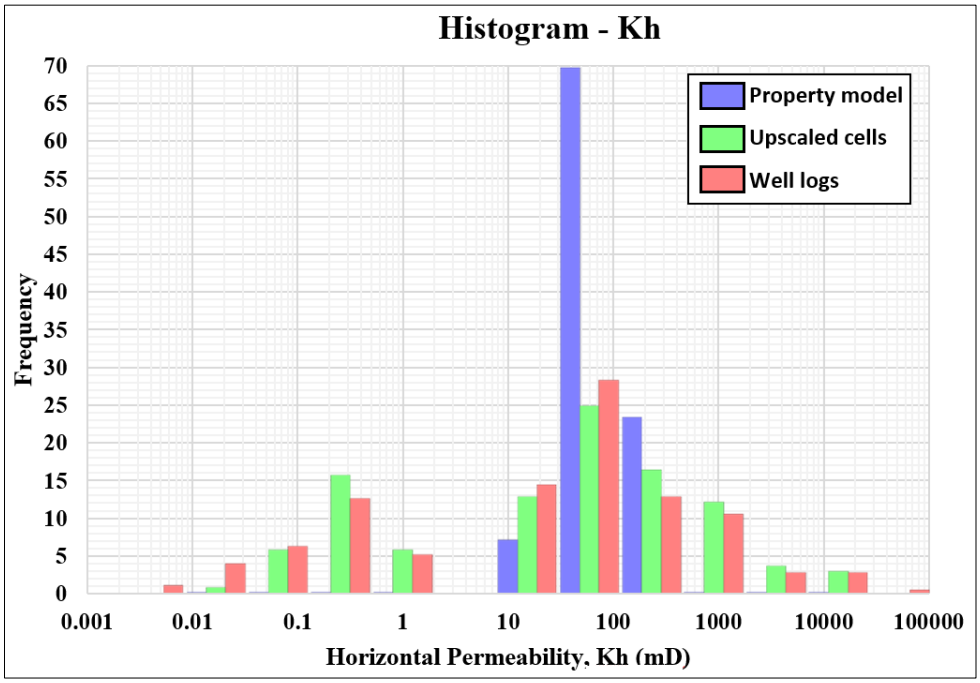

Figure 28. QC of the Kh model by comparison of the well logs, upscaled logs and the property model.

The Ula Fm is characterized by good quality reservoirs. The Ula field presents an average NTG of 93% (DAKS database), while in the Oda field, the NTG average is 86% (Oda Subsurface Team, 2016). Table 1 shows that NTG CPI's were not available for the wells of the

Ula field. From the Plan for Development and Operation of the Oda field (Oda Subsurface Team, 2016), the NTG in the Oda field is equal to 1.0 if the volume of shale (VSH) ≤ 40% and PHIT ≥ 10%, otherwise it is 0. For the Ula field, NTG logs were calculated using the log calculator as equal to 1.0 if the PHIT ≥ 10% and Kh ≥ 1 mD, otherwise equal to 0. In both cases 1.0 means net and 0 non-net.

The NTG logs were upscaled using the mid-point pick average method – the input log value in the middle of the grid cell is used to be upscaled (Schlumberger, 2020) – and applied for model population by SGS. For the NTG property model a spherical variogram with default values for sill and nugget effect (1 and 0.0001 respectively) was used and the distribution followed the upscaled logs. A depth trend was also incorporated into the model through co-kriging. The NTG model was checked against the frequency distributions from well logs and upscaled cells to ensure the property model honored the property calculated in the logs. Figure 29 shows that there is a good match between the modelled property, upscaled well logs and input well logs.

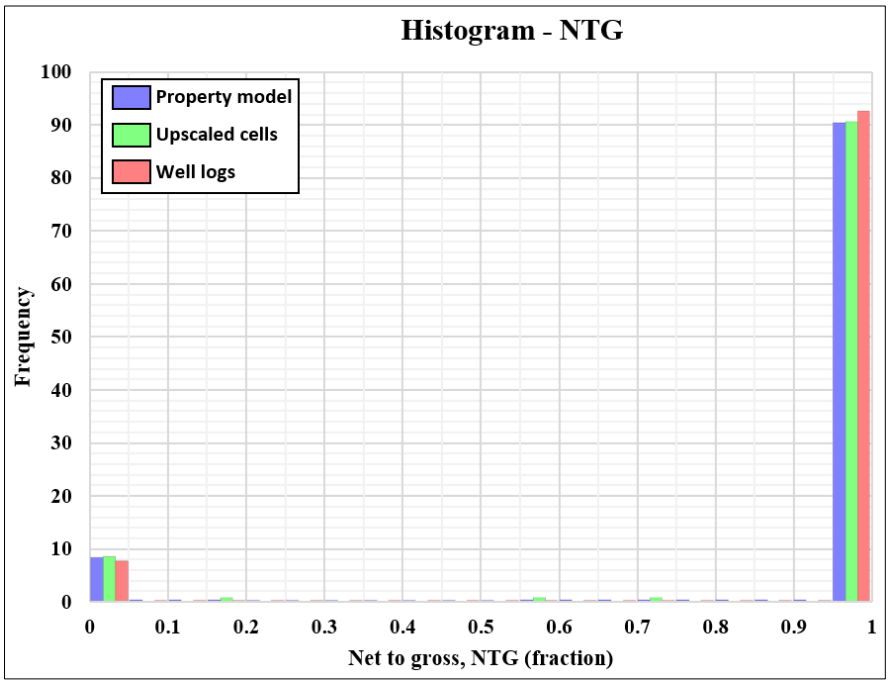

Figure 29. QC of NTG model by comparison of well logs, upscaled logs and the property model.

The water saturation (Sw) property was generated using J-functions for each rock type. The J-functions are dimensionless functions of Sw used as a tool to correlate the capillary pressure of a fluid in the porous medium with the rock properties. The J-functions are derived from Equation 1 (Leverett et al., 1942; Rose and Bruce, 1949).

$$J(S_w) = \frac{AP_c}{\sigma \cos\theta}\sqrt{\left(\frac{k}{\Phi}\right)} \qquad \text{Equation 1}$$

Where A is a constant (3.1415335 $s^2/mD^{0.5}$), P_c is the capillary pressure, σ is the Interfacial Tension (IFT, mN/m), θ is the contact angle (degree), k is the permeability (mD) and Φ is the porosity (fraction).

For each rock type a J-function was fitted to porosity and permeability core data. Figure 30 shows the J-functions for the three lithofacies USF, LSF and TZ.

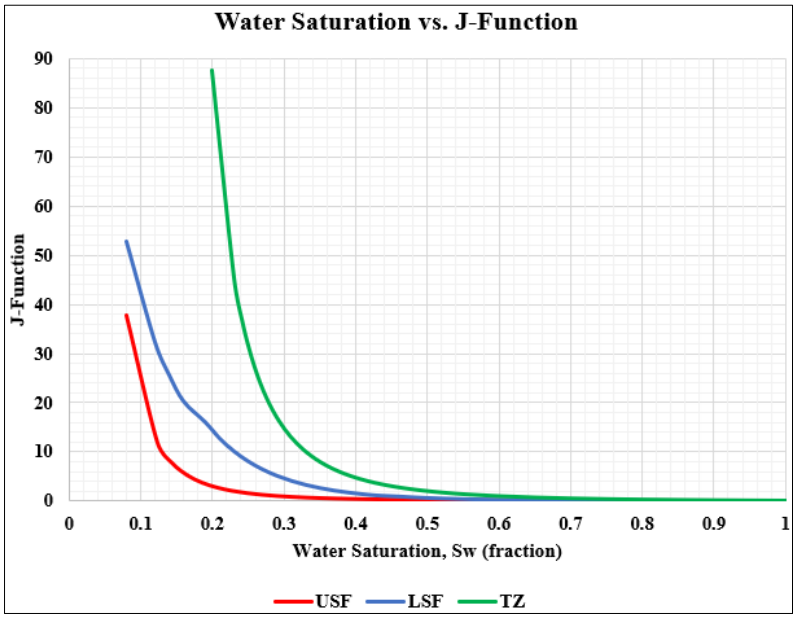

Figure 30. J-functions for the USF, LSF and TZ lithofacies.

The defined J-functions for each rock type were used to calculate Sw using a property calculator. Sw was computed above OWC for each contact region (Oda Field, and E and W of

the Ula Field) using Equation 2 and varying only k and Φ. Equation 2 is a variation of Equation 1, in which $P_c = (\rho_w - \rho_{wn})gh$.

$$J(S_w) = \frac{A(\rho_w - \rho_{wn})gh}{\sigma \cos\theta}\sqrt{\frac{k}{\Phi}} \qquad \text{Equation 2}$$

Where ρ_w and ρ_{wn} are the wetting phase (water, 1125 kg/m^3) and non-wetting phase (oil, 721 kg/m^3) densities respectively, g is gravity (9.81 m/s^2) and h is the height above OWC (m).

The transmissibility multiplier (TM) is a fault property that defines the flow communication across the faults. TM varies between 0 which means the fault is sealing completely, to 1 which corresponds to open communication across the fault. Faults with no juxtaposition of the reservoir interval were defined as sealing (TM = 0). Faults juxtaposing the reservoir interval were evaluated using sensibility analysis during the history matching step. For the initial base case, the TM of the faults juxtaposing the reservoir was assigned as 0 (sealing).

4.1.6. Scaling

Since the grid cells are originally coarse, no grid upscaling was necessary. The simulations were performed on the original grid.

4.1.7. In-place Volumes

The original oil in place (STOIIP) volumes published in the NPD webpage (public access) were compared to the in-place volumes estimated from the contact regions assigned for

each field and the properties modelled. From NPD, the Ula Field STOIIP is 179 MSm^3 and the Oda Field STOIIP is 9 MSm^3. The results from the volume calculation of the final grid using the modelled properties are shown in Table 6. The differences between the published values and the calculated ones are ~2% for the STOIIP in the Ula field and ~5% for the Oda field. These low percentage differences confirm the validity of the static model and the properties modelled.

Table 6. STOIIP from each contact region used as parameter in the grid model QC.

Contact Region	STOIIP (MSm^3)
Oda field	9.454
East Ula field	146.097
West Ula field	35.926

4.1.8. Assumptions and Uncertainties

Dynamic models and simulations are highly dependent on the geological model uncertainties and the assumptions and simplifications applied on the properties modelling. In order to facilitate the understanding and interpretation of the results generated from this study, the main assumptions and uncertainties related to the static model are listed below:

Assumptions:

- Geological model includes only the Ula Fm;
- Ula field has 170 m depth difference in the OWC from the west to the east;
- Faults transmissibility – almost all faults are sealing;
- Grid orientation rotated to 129° to follow the NWSE shoreline trend;
- Rock types associated to the total porosity: transition zone (TZ < 15%), lower shoreface (15% ≤ LSF ≤ 23%) and upper shoreface (23% < USF) sediments;

- USF represents the highest quality reservoir, LSF is the lower quality reservoir and TZ is the poorest quality reservoir;
- Horizontal permeability is equal in I and J directions ($k_x=k_y$);
- Vertical permeability is 10% of the horizontal permeability;
- No grid upscaling was necessary.

Uncertainties:

- Reservoir thickness has uncertainties related to the seismic interpretation of the Ula Fm top and base horizons;
- Coarse grid cells of 100 by 100 m prevent refinement of the model;
- Uncertainties related to the well logs upscaling increase as the distance from the Ula and Oda fields increase and the number of wells decrease;
- Only main faults with large displacement were included in the model;
- OWC depth difference in the Ula field.

4.2. **CONCEPTUAL MODEL OF THE ULA Fm FAIRWAY**

The published studies described in Chapter 2.2. were used as a foundation for the models describing the distribution of the Ula Fm in this thesis. Three scenarios for the Ula Fm fairway were established. These incorporate a possible communication between the Ula and Oda fields through an aquifer in the Ula Fm. A static model was built for each case scenario varying the size of the aquifer due to the different hypothesis about the distribution of the Ula Fm in the study area.

Case 1 (Figure 31) assumes a distribution of the Ula Fm based on the Ichron (2015) study (Figure 14). This case is an oversimplification of the Ula Fm distribution, since as

explained in Chapter 2.2, the Ichron (2015) interpretations are not based on regional geology and geological setting of the area. Case 1 is also an overestimation of the reservoir presence, since it assumes the Ula Fm is laterally continuous throughout all the shoreface zone. The shoreface zone (blue area) is delimited by a NW-SE shoreline to the NE extending to a transitional zone to the SW. An isochore map (in depth) of the reservoir interval was generated from the well tops in the area to QC the shoreline proposed in the Ichron (2015) study (Figure 31). In Figure 32, the red area corresponds to zero thickness. The shoreline suggested by the Ichron (2015) study (green line, Figure 32) was compared with the isochore zero in the map to delimit the reservoir boundary used in case 1 (blue line, Figure 32). A polygon was created to define the shoreline area in the static model (Figure 31, active cells in blue). The cells outside this polygon were set as inactive (Figure 31, inactive cells in grey).

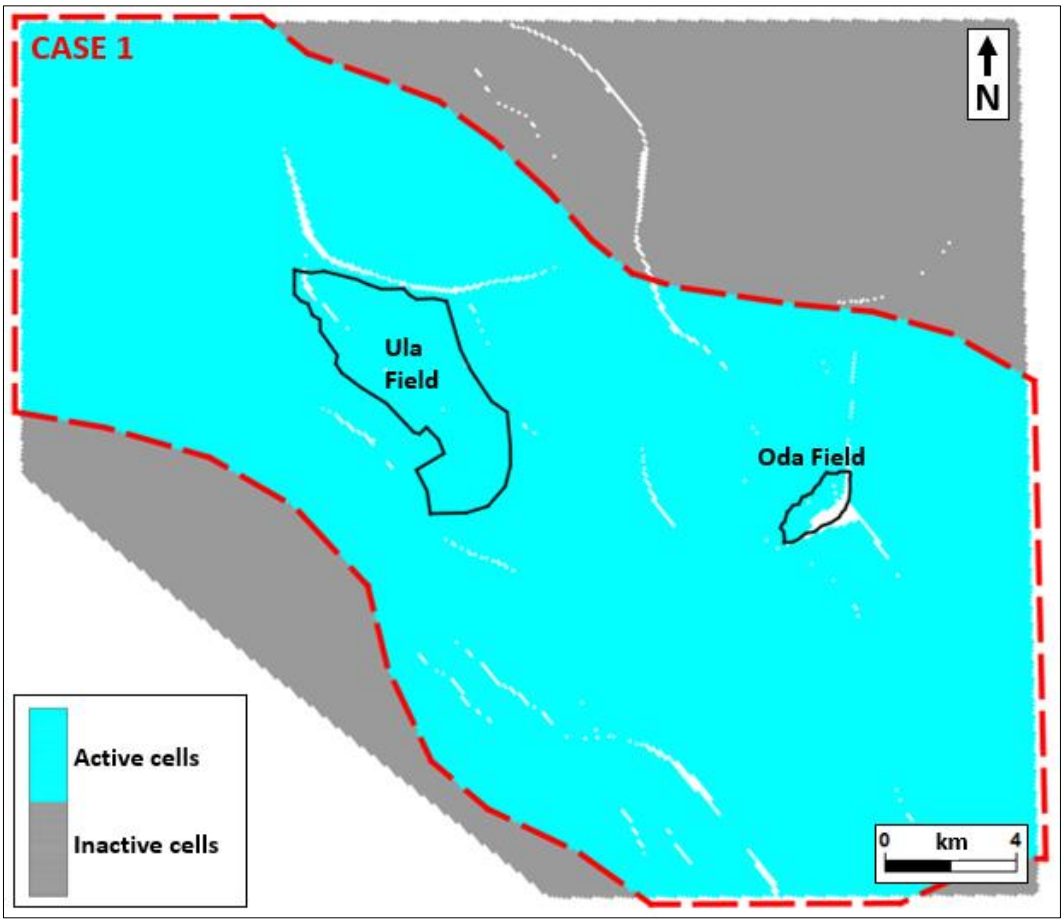

Figure 31. Active and non-active cells used in case 1. The red dashed line indicates the aquifer limits for case 1.

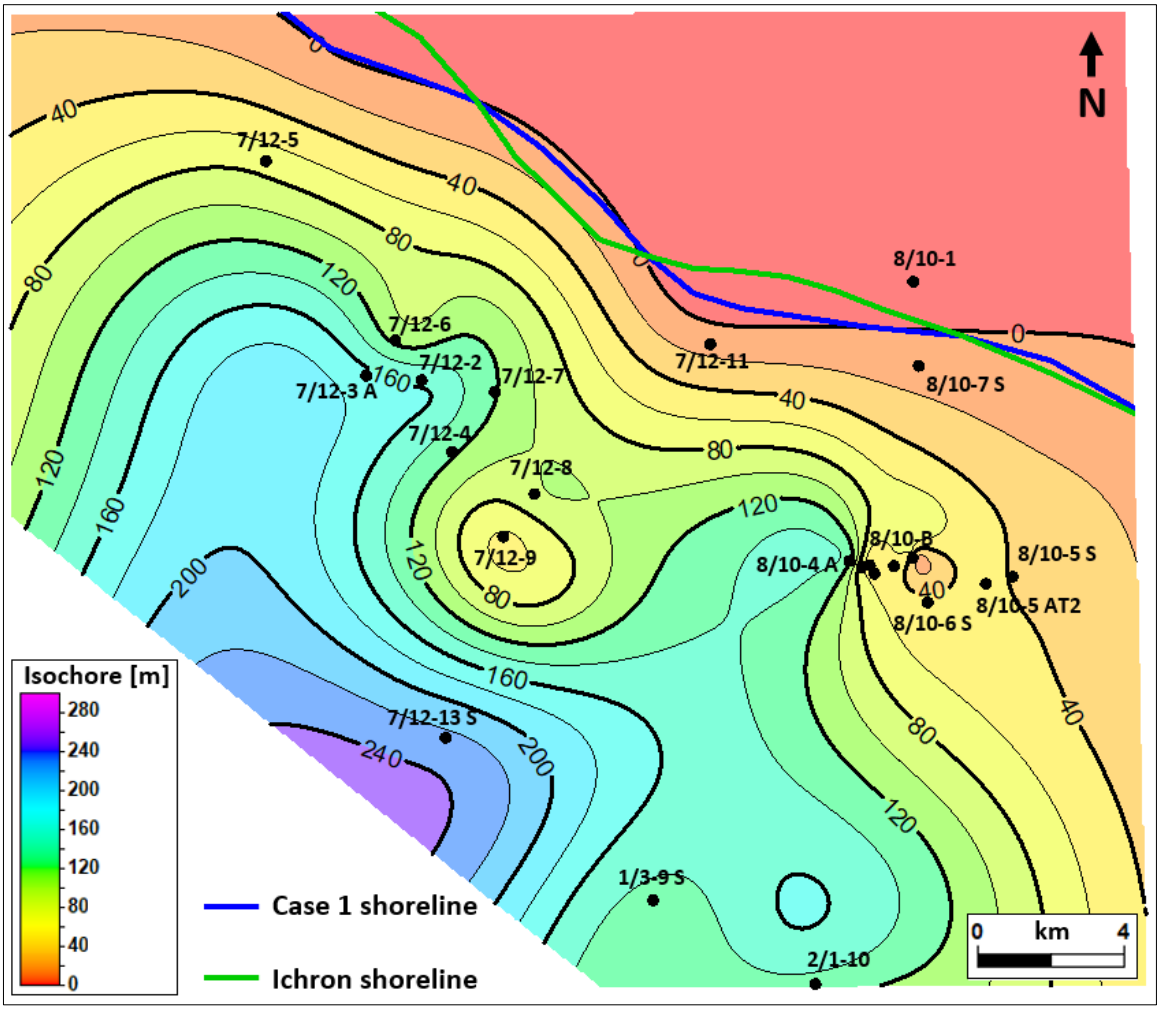

Figure 32. Isochore in depth of the reservoir interval used to QC the shoreline proposed by the Ichron study (green line). The wells used to generate this isochore are shown in the map. The blue line is the shoreline used as the reservoir boundary in case 1.

In case 2, the reservoir presence was limited to the areas above salt walls (Mannie et al., 2014; O'Connor et al., 2011). Therefore, well data and regional structure maps (Figures 16, 17 and 18) were used to delimit the areas above the salt walls and determine the Ula Fm boundaries. An isochore map using the well tops and the surfaces of the top Ula Fm and the top Zechstein Gp was generated to visualize the thickness of this interval (Figure 33). The multicolor, non-purple areas in Figure 33 show the salt wall areas where the thickness of the top Zechstein Gp – top Ula Fm are less than the thickness cutoff and where the Ula Fm is present. From the isochore map, a visual analysis comparing the salt wall areas for different thickness cutoffs was used to select an initial thickness cutoff of 1100 m to delimit the areas

containing the Ula Fm. Figure 34 shows the maximum (1100 m) and minimum (600 m) range of thickness cutoffs analyzed. A maximum thickness cutoff of 1100 m was assumed because higher cutoff values do not show any substantial addition in the Ula Fm areas above salt walls. Cutoff values below 900 m show very narrow communication through the Ula Fm between the Ula and Oda fields (Figure 34 – less than 400 m wide channels in some locations for the 600 m cutoff), and no communication above the salt pillow trap of the Ula field and the other salt structures to the NW and south of the Ula field (Figure 34).

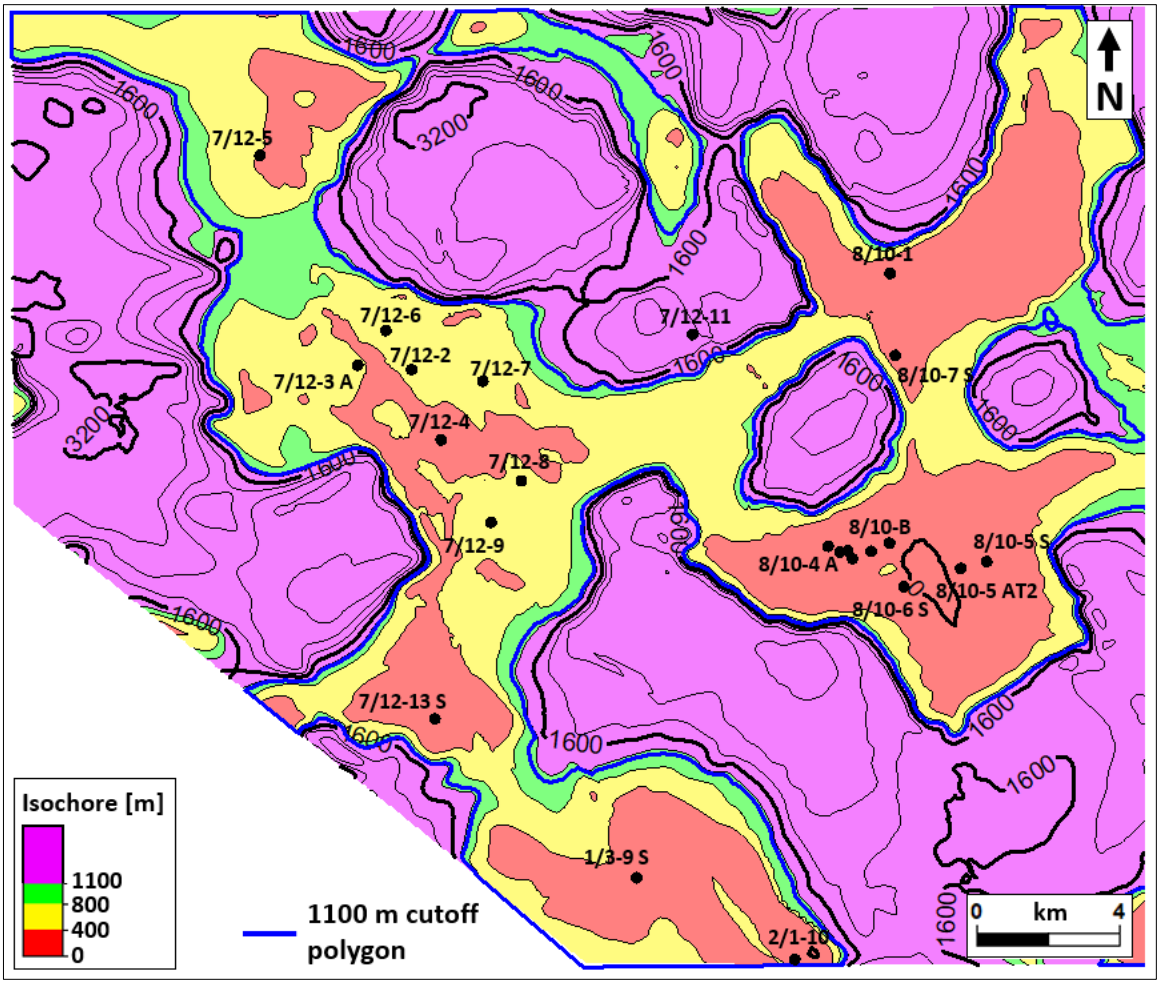

Figure 33. Isochore in depth between the top Zechstein Gp and the top Ula Fm. In case 2, a maximum thickness of ~1100 m is used to define the salt wall areas which are also the areas where the Ula Fm is present. The dark blue polygons delimit these areas.

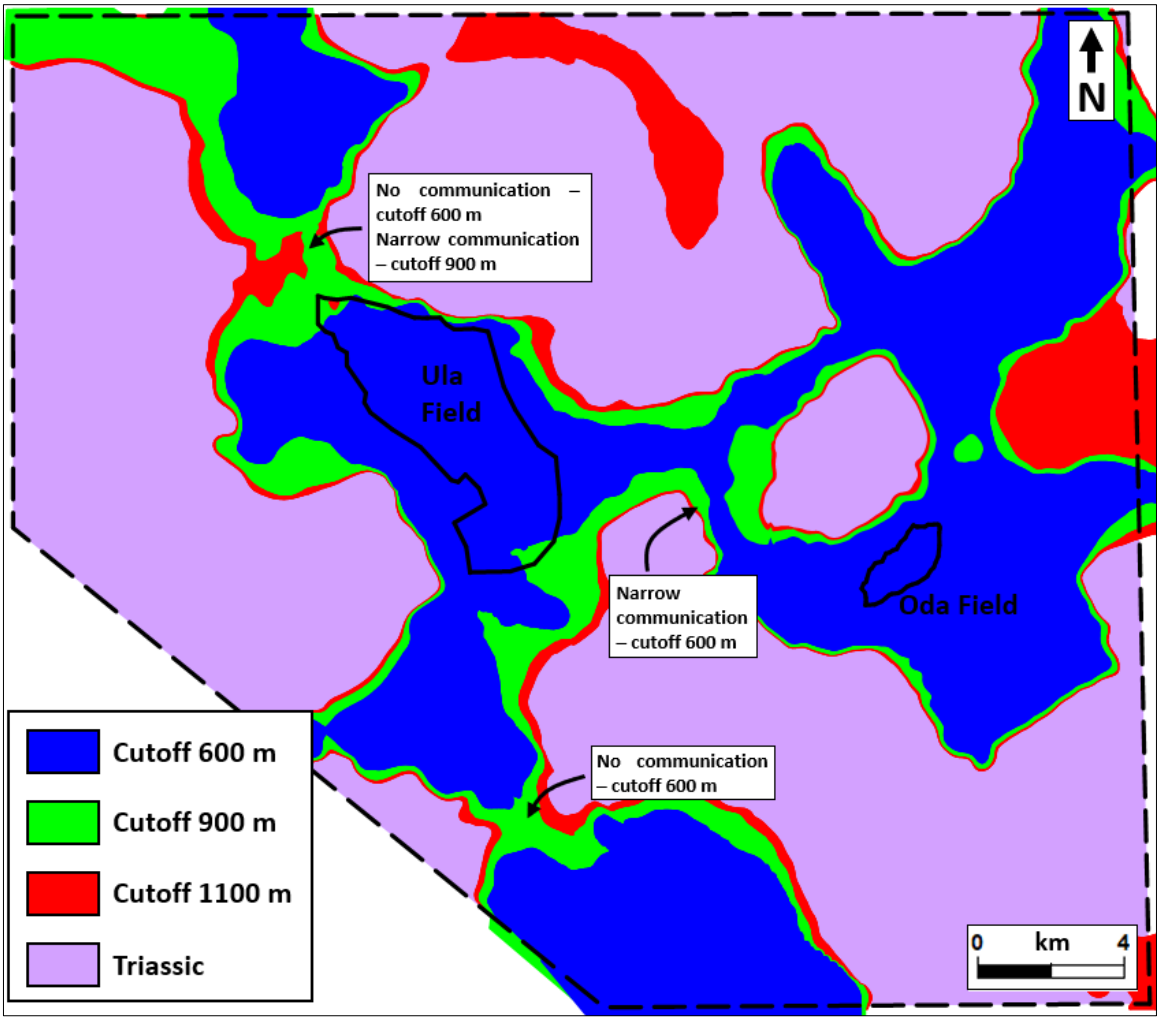

Figure 34. Map comparing the salt wall areas for different thickness cutoffs used to delimit the areas containing the Ula Fm above the salt walls. The area in red is the maximum thickness cutoff (1100 m) and the area in blue is the minimum thickness cutoff (600 m). Cutoff values below 900 m show very narrow communication through the Ula Fm between the Ula and Oda fields and no communication above the salt pillow trap of the Ula field and the other salt structures to the NW and south of the Ula field.

During the history matching step, the thickness cutoff in case 2 was considered as an uncertainty property and it was submitted to adjustments. A polygon was used to delimit the areas above salt walls (Figure 35, active cells in blue). The cells outside this polygon were set as non-active (Figure 35, inactive cells in grey) as they do not contain the reservoir.

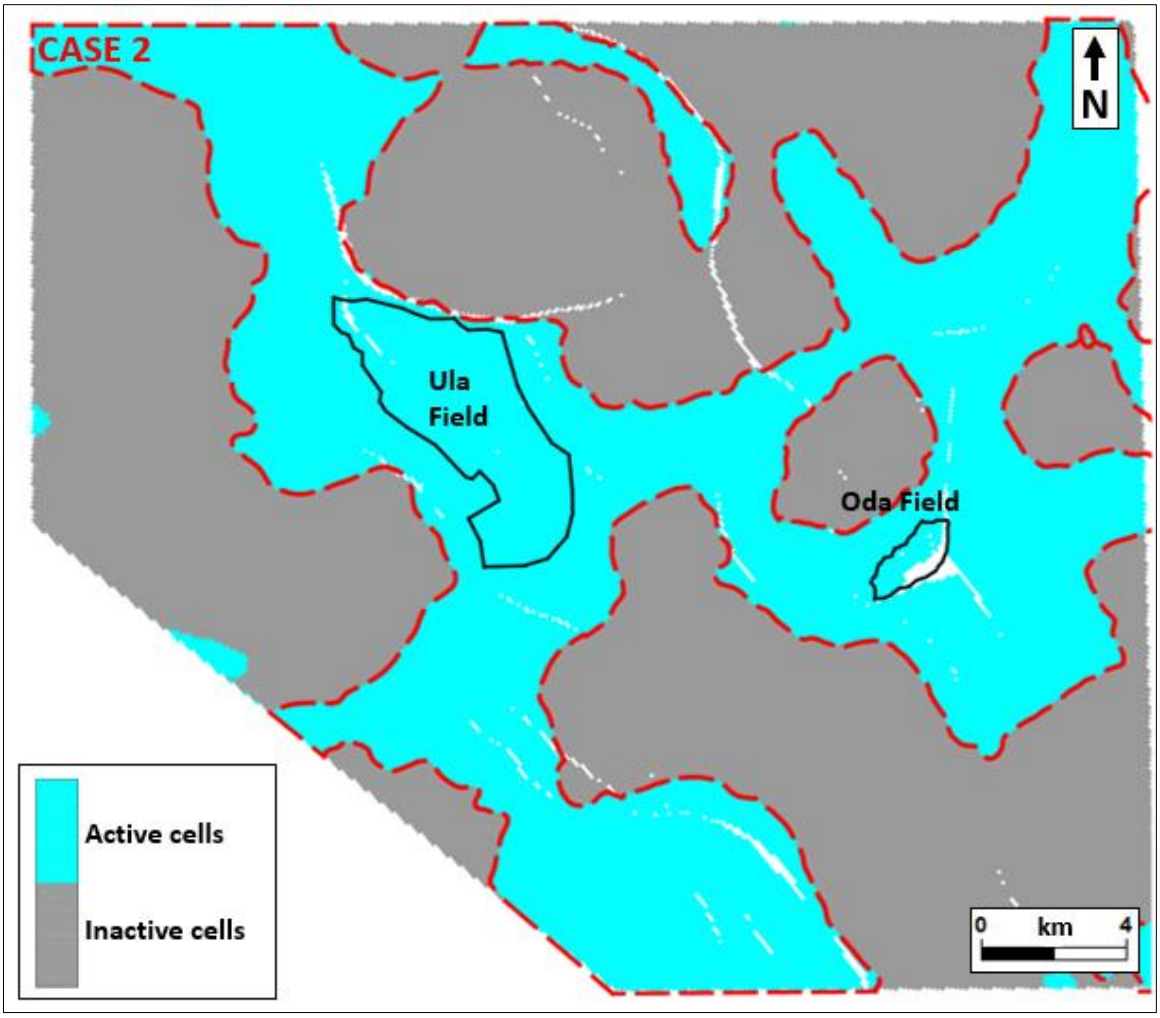

Figure 35. Active and non-active cells used in case 2. The red dashed line indicates the aquifer (Ula Fm) limits for case 2.

An additional case was performed combining the most important assumptions from cases 1 and 2. In case 3 (Figure 36), the reservoir presence was limited to the areas above salt walls (case 2) and within a shoreface zone delimited by the same NW-SE shoreline from case 1. This scenario is important since it incorporates the regional geology and geological setting of the area into the well data study of the Ula Fm presence.

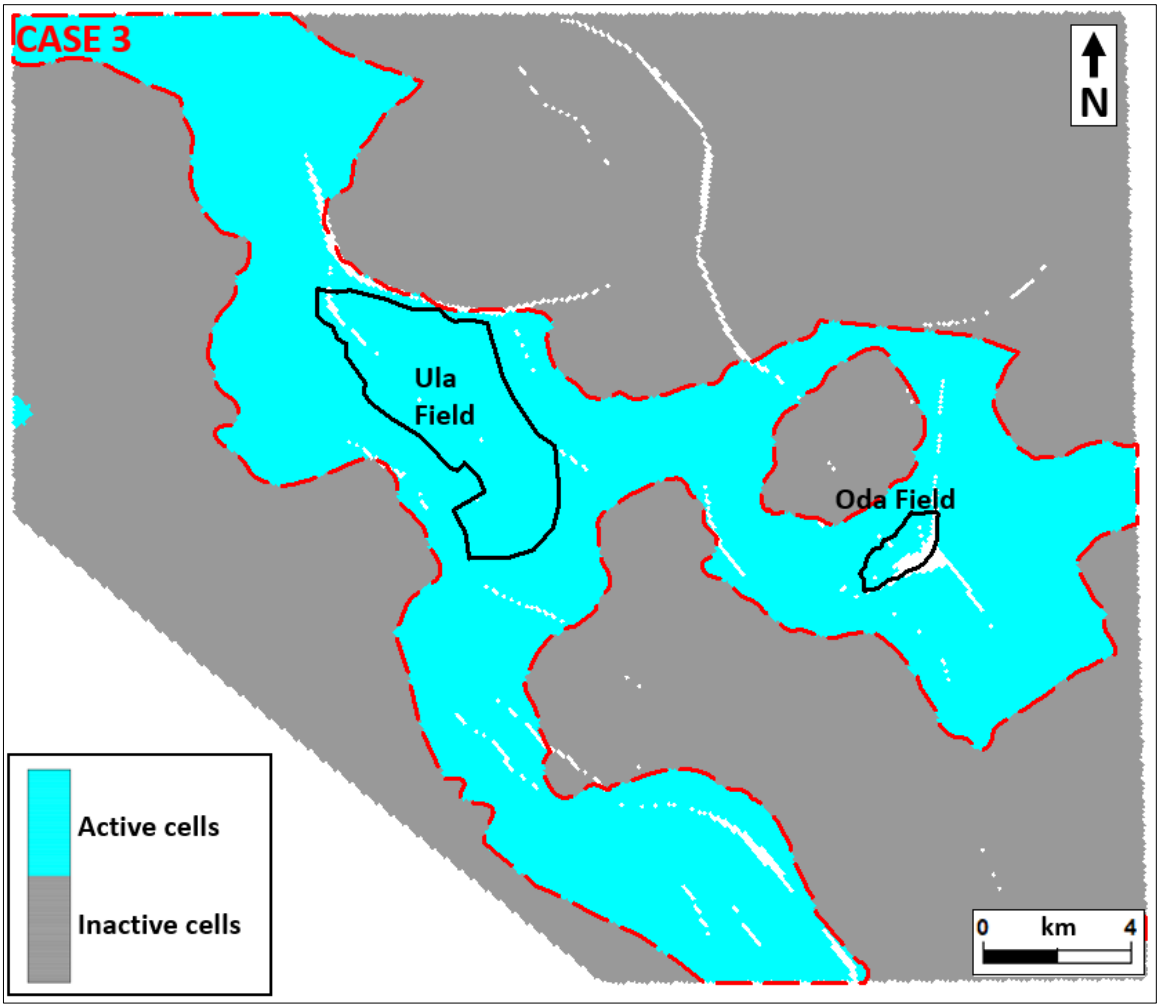

Figure 36. Active and non-active cells used in case 3. The red dashed line indicates the aquifer (Ula Fm) limits.

4.2.1. Assumptions and Uncertainties

The main assumptions related to each conceptual model for the Ula Fm fairway are listed below:

Case 1:

- Distribution based only on well data analysis (does not consider regional geology and geological setting of the area);
- NW-SE shoreline;
- Ula Fm is laterally continuous throughout all the shoreface zone.

Case 2:

- Distribution based on well data and seismic analysis, regional geology and geological setting of the area;
- Reservoir presence was limited to the areas above salt walls;
- The absence of the Ula Fm to the NE of the study area observed from the well data analysis was not included in this case.

Case 3:

- Distribution based on well data and seismic analysis, regional geology and geological setting of the area;
- NW-SE shoreline;
- Reservoir presence was limited to the areas above salt walls and inside the shoreface zone delimited by the shoreline based on analysis of well data.

The uncertainties of the conceptual models are mainly associated to the reservoir interval thickness and the Ula Fm depositional extension. The major uncertainties of each conceptual model are listed below:

- Case 1: Oversimplification and overestimation of the Ula Fm distribution.
- Case 2: Limits of the areas above the salt walls and the absence of the Ula Fm to the NE of the study area.
- Case 3: Limits of the areas above the salt walls.

4.3. **DYNAMIC MODEL**

The main purpose of a dynamic flow simulation is to estimate field performance under different producing strategies (Batycky et al., 2007). The basic principle for reservoir simulation models is the conservation of mass (Kleppe and Andersen, 2019).

For this part of the study, all processes were performed using the commercial software Petrel (Schlumberger) and Eclipse (Schlumberger). The reservoir was simulated using a black oil model with three phases and three components (oil, gas and water). From the observed history data, the simulation cases were defined to start in October 1984 and end in March 2020, allowing two years at the beginning of the simulation for the system to achieve equilibrium. Due to the long duration of time, the reporting frequency from the simulation was specified every quarter of a year. The simulations for each case scenario took about 2 hours to complete.

4.3.1. Reservoir Fluids

The reservoir fluids in the Ula and Oda fields have very similar characteristics. The oils are light with densities (ρ_o) varying between 38 and 41 °API, average viscosities (υ_o) of 0.34 and 0.39 cP, and gas oil ratio (GOR) averages of 82 and 90 sm^3/sm^3. The oils are undersaturated in the whole reservoir interval in both fields, so they do not present gas cap. The PVT average values used as input for the fluid models are summarized in Table 7.

Table 7. PVT average properties of the Oda and Ula fields.

Contact Region	Reservoir depth (mTVDSS)	Reference pressure (bar)	GOR (sm^3/sm^3)	Pb (bar)	ρ_o (°API)	υ_o (cP)	FVF_o (rm^3/rm^3)
Oda Field	2950 - 2985	414	82	132	40.7	0.39	1.59
Ula Field	3350 - 3800	490	90	159	39	0.34	1.33

4.3.2. Rock Physics

The main reservoir for the Ula and Oda fields is the Ula Fm. Thus, the same rock physics functions were used in both reservoir intervals. Water saturation versus relative permeability functions for water-oil and gas-oil were generated based on SCAL studies. Different Kro, Krg and Krw curves were assigned for each rock type (USF, LSF and TZ). The initial water saturation (Swi) defined for USF and LSF was 0.08 and for TZ it was 0.2. The capillary pressure (Pc) at WOC was assigned as 0 bar.

4.3.3. Numerical Aquifer

The history matching results showed that it is necessary to include a numerical aquifer at the NW corner of the model to provide additional pressure effects from the aquifer. The numerical aquifer was connected to the model by a row of cells in the northwestern edges with a NW-SW inflow, as illustrated in Figure 37.

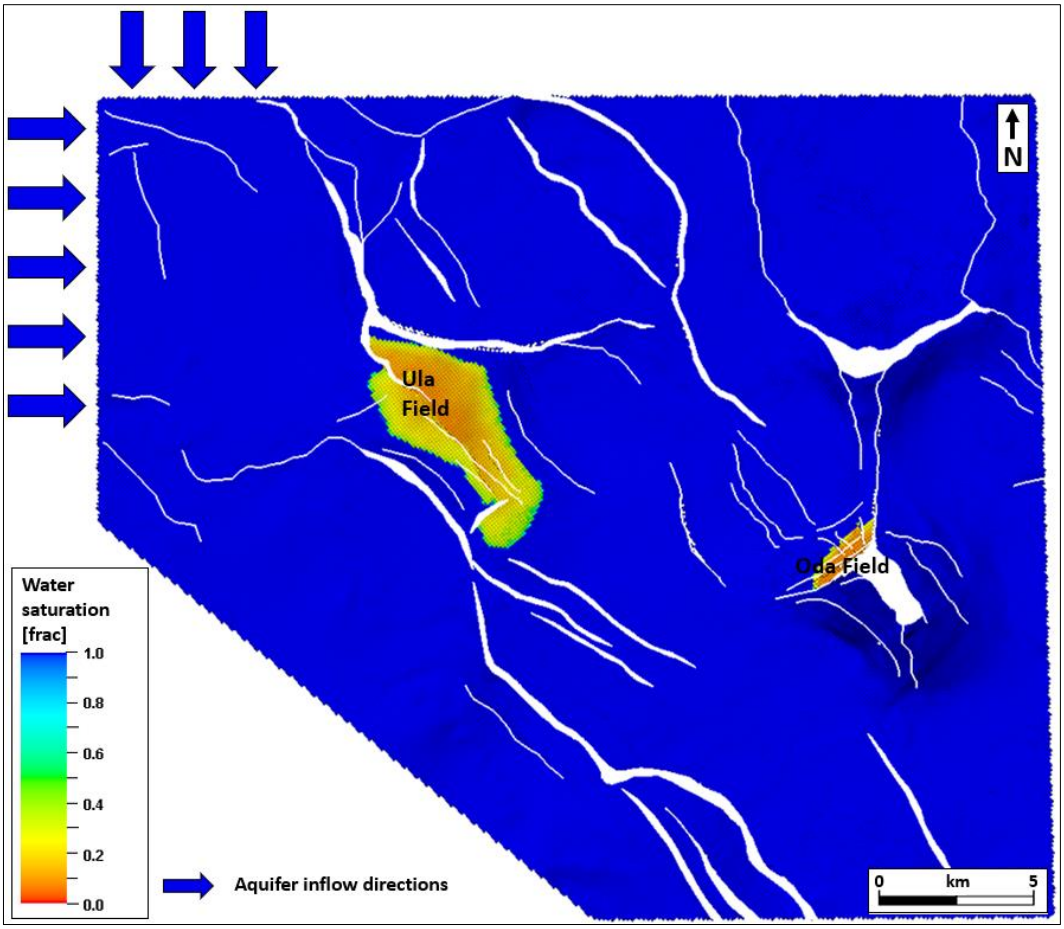

Figure 37. Water saturation property model indicating the numerical aquifer inflow directions (blue arrow).

4.3.1. Assumptions and Uncertainties

The history matching objectives and the parameters to be adjusted during this process are highly influenced by the reservoir characterization properties and simplifications. The main assumptions and uncertainties related to the dynamic model are listed below:

Assumptions:

- Black Oil model;
- Similar fluid properties in the Ula and Oda fields;
- Same rock physics functions used in the Ula and Oda fields;

- No flux boundaries in the model except for the NW corner of the model where a numerical aquifer is connected to the grid.

Uncertainties:

- Bubble point pressure and initial gas-oil ratio tables from the Oda field fluid measurements can lead to uncertainties in the Ula field;
- Wells completion interval not available.

4.4. **HISTORY MATCHING**

A dynamic model can forecast the performance of a new reservoir, or it can be adjusted to reproduce the historical behavior of an existing reservoir (Batycky et al., 2007). History matching is the adjustment process to fit the numerical data to the historical field data, in order to validate the numerical model and to reduce the prediction uncertainties. These adjustments must be geologically consistent.

Figure 38 shows the workflow used for the history matching process applied in this thesis. The first step after generating the dynamic model, is to define the objectives and criteria for history matching, including the parameters to be adjusted, the data to be matched and the acceptable matching uncertainty (Baker et al., 2006). The second step is to input the available historical data. Afterwards, the process consists of performing a set of simulation runs using the historical data from the field as control mode for the production and injection wells and comparing the results with the stated matching criteria. If the results are not eligible, a series of parameters are adjusted. The process stops once the matching criteria is achieved (successful match). It is important to highlight that history matching is a non-unique inverse problem. The models will never provide a unique and right answer, since the output (historical data) is the

known variable, but the input parameters are unknown. Consequently, the history matched models will be the most plausible results and they are highly dependent on the geological model uncertainties and the assumptions applied on the reservoir characterization.

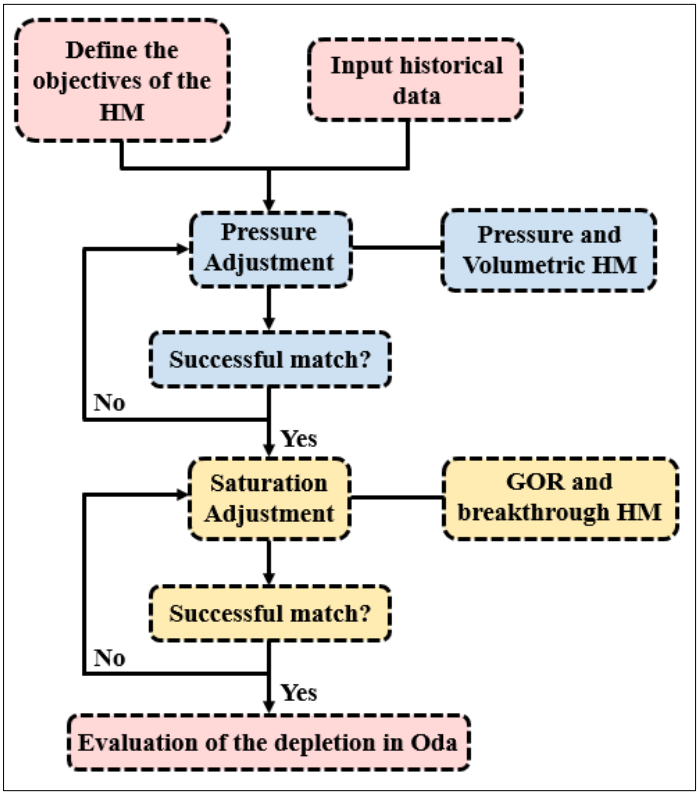

Figure 38. History matching workflow with the main steps of the process. HM = History matching. Based on Baker et al. (2006).

According to Baker et al. (2006), a model is properly history matched if it achieves the defined matching criteria for each adjusted parameter. In order to reach these criteria, the first step is to match the trend of the reservoir performance, so that the recovery drive mechanism and the main properties of the reservoir are correctly characterized. Then, each parameter adjusted must match a determined uncertainty range. Baker et al. (2006) proposed standard matching criteria that were used as a guideline in this work for the reservoir average pressure and cumulative production curves (Table 8).

Table 8. Matching criteria assigned for the objective parameter curves based on Baker et al. (2006).

Parameter	Matching Criteria
Average reservoir pressure	± 10%
Cumulative production (oil, gas and water)	± 10%

For the purposes of this study, the history matching process was divided in two steps: pressure adjustment (step 1) and saturation adjustment (step 2) (Figure 38). Step 1 consisted of history matching the reservoir average pressure, liquid production (oil and water) and injection volumes (gas and water) in the Ula field. The parameters adjusted to reach the match criteria were aquifer properties (volume), absolute permeability and faults transmissibility. The saturation adjustment is a more detailed step in which the fluids movement is inferred from the matching of the "time of breakthrough" (water and gas) and gas production curves. The control modes of the wells with higher influence on the reservoir performance were adjusted in the development strategy of the Ula field in order to achieve the matching criteria. The key factors for steps 1 and 2 are shown in Tables 9 and 10, respectively.

Table 9. Summary of the parameters to be adjusted and the data to be matched in the pressure adjustment step (Step 1).

Pressure Adjustment	
Adjust	Match
• Aquifer properties • Absolut permeability • Faults	• Reservoir average pressure • Oil cumulative production • Water cumulative production

Table 10. Summary of the parameters to be adjusted and the data to be matched in the saturation adjustment step (Step 2).

Saturation Adjustment	
Adjust	Match
• Ula field development strategy	• Reservoir average pressure • Water breakthrough

The history matching process was applied to each conceptual model of the Ula Fm fairway. The historical data of the simulated cases were observed, including production (oil, gas and water), injection (gas and water) rates, and average reservoir pressure.

The evaluation of the possible communication between the Ula and Oda fields through an aquifer in the Ula Fm was performed using the history matched models for each conceptual model of the Ula Fm fairway. A dummy well measuring the pressure behavior in the Oda field since the beginning of the Ula field production (Figure 2 – same location as well 8/10-B-3 AH) was used to test a correlation between the historical pressure data from the Ula field with the depletion observed in the Oda field between 2011 and 2018.

4.4.1. Historical Data

In order to reproduce the historical behavior of more than 30 years of production in the Ula field using the dynamic model, it is necessary to understand the input historical data.

The Ula field started production in October 1986 driven by waterflood from the aquifer and solution-gas mechanisms, i.e. primary recovery (C&C Reservoirs, 2011; NPD, 2019). After less than two years, because of weak aquifer support, peripheral water injection was implemented to improve oil recovery. The water breakthrough happened in the end of 1991 with water production rising steadily until 1997. The increase of water cut lead to a sharp decline in oil production from 1994 on. In 1998, water alternating gas injection (WAG) was

introduced in order to stabilize the oil production curve. After 2000, the oil production rates kept stable between 2000 and 4000 sm^3/d. The water production increased again after 2009. The gas production followed the oil production trend until the gas breakthrough around 2000 due to the gas injection. Between 2009 and 2018, a considerable pressure decrease was observed, probably due to the water production increase and the oil production decrease. The oil (green), gas (red) and water (blue) cumulative production graphs in Figure 39, show a summary of the input history data from the Ula field.

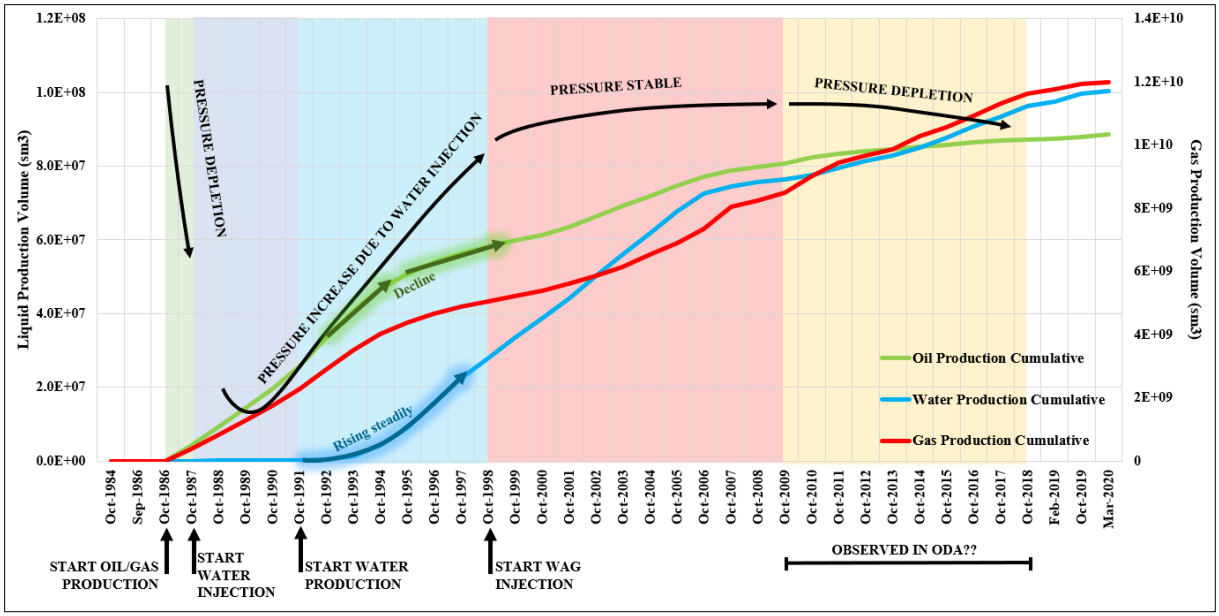

Figure 39. Historical data summary of reservoir performance in the Ula field from 1986 to 2020. The average reservoir pressure trend is represented by black arrows. Important periods are separated by colors to make the analysis easier.

The total volumes of oil, gas and water production, and gas and water injection from 1986 until 2018 in the Ula field are given in Table 11.

Table 11. Summary of the cumulative and average rates values of the historical data in the Ula field.

Parameter	Cumulative (Msm^3)
Oil production	80
Gas production	12000
Water production	100
Water injection	150
Gas injection	6700

4.4.2. Initial Model

The initial model for cases 1, 2 and 3 was used to understand the properties adjusted during the history matching process. The numerical aquifer described in section 4.3.3. was not implemented in this phase, so the true aquifer support derived from the volumes of water in the model could be evaluated. Two development strategies were implemented for each case comparing liquid and oil rates as the production control modes and with surface rate as the control mode for the injectors.

4.4.3. Aquifer Properties

The observations and interpretations from the initial model simulation results lead to the next step in the history matching process in which cases 1, 2 and 3 were performed using liquid as production control mode and a numerical aquifer was implemented.

A sensitivity analysis on the influence of the numerical aquifer properties upon the average reservoir pressure showed that varying the porosity, the absolute permeability, or the length of the numerical aquifer does not affect considerably the reservoir pressure results. On the other hand, the cross-sectional area of the numerical aquifer has high influence on the reservoir pressure values and curve trend. Thus, three scenarios with high range differences

(low, medium and high) were assigned for cases 1, 2 and 3 in order to analyze the effects of the numerical aquifer cross-sectional area on the simulation results. The size and properties of the numerical aquifer cells for each scenario are shown in Table 12.

Table 12. Aquifer cell properties.

Scenario	Cross-sectional area (km^2)	Length (km)	Porosity (fraction)	Permeability (mD)
Low	1	16	0.2	150
Medium	100	16	0.2	150
High	10.000	16	0.2	150

4.4.4. Absolute Permeability

Transmissibility multipliers for three scenarios (high, medium and low) were used to reduce the absolute horizontal permeability (x and y) of areas outside the Ula and Oda fields. This was done in all areas bellow - 3800 m (datum below the reservoir interval in the Ula and Oda fields) and with absolute permeabilities higher than 100 mD (Figure 40). The transmissibility multipliers applied for each scenario are shown in Table 13.

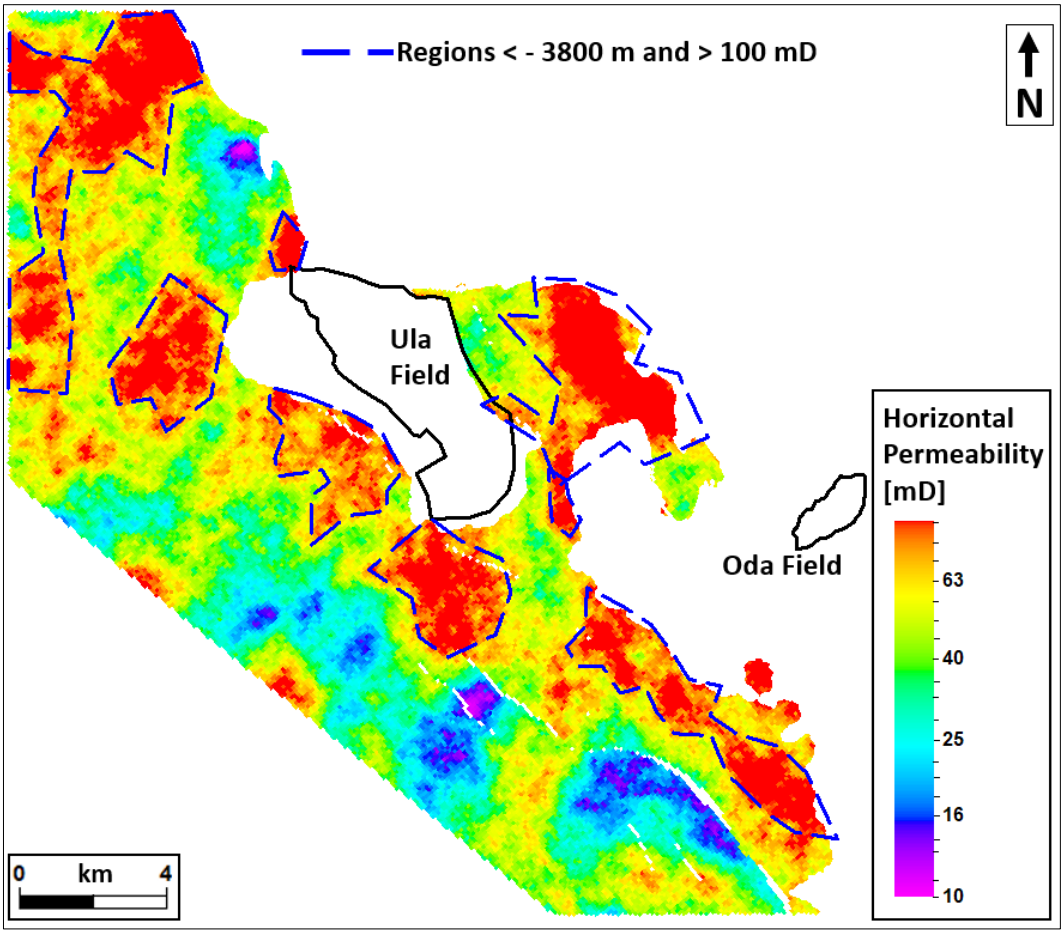

Figure 40. Absolute permeability model of the Ula Fm showing the areas below - 3800 m (datum below the reservoir interval in the Ula and Oda fields). The blue polygons show the areas with absolute permeability higher than 100 mD.

Table 13. Transmissibility multipliers applied for each scenario to reduce the absolute horizontal permeability of the areas outside the Ula and Oda fields.

Scenario	Transmissibility multiplier
Low	0.08
Medium	0.1
High	0.5

4.4.5. Faults Transmissibility

As described in section 4.1.5., the faults transmissibility was set initially to 0 (sealing) for all faults in the geological model. However, the faults juxtaposing the reservoir interval

(Figure 41, light pink) were evaluated using sensibility analysis during the history matching step to understand their influence in the communication between the Ula and Oda fields, specifically their effects on the oil and water cumulative production and average reservoir pressure in the Ula field. Three transmissibility multipliers were tested on these faults: sealing (TM = 0), partially sealing (TM = 0.5) and no sealing (TM = 1).

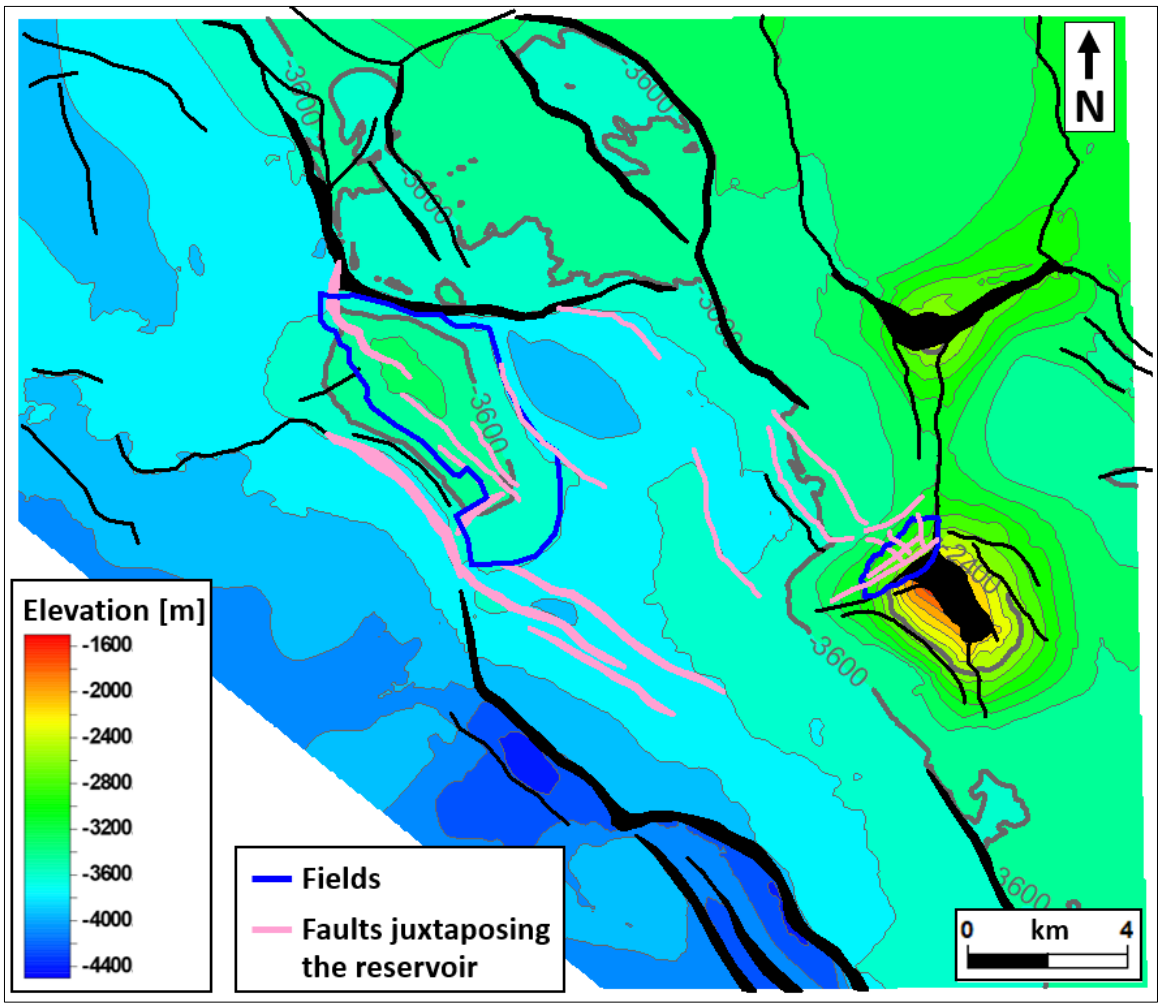

Figure 41. Top Ula Fm structure map in depth showing the faults juxtaposing the reservoir that were analyzed in the pressure adjustment step (light pink polygons). Blue polygons – Oda and Ula fields.

4.4.6. Development Strategy

A general development strategy was implemented for the pressure adjustment step of the history matching, in which the production control mode was specified as the liquid rate and the surface rate was set as the control mode for the injector wells.

For the saturation step, in order to adjust the fluids movement behavior in the reservoir, the wells production of oil and water was history matched individually changing the production control mode for different periods.

A sensibility analysis on the producer wells affecting the most the Ula field performance showed that wells 7/12-A-6, 7/12-A-10, 7/12-A-12, 7/12-A-15, 7/12-A-16 and 7/12-A-18 were the target for the saturation adjustments using the development strategy. Table 14 shows the summary of the development strategy applied after the observations of each well production rates.

Table 14. Development strategy applied for each well after history matching. All the wells in the Ula field started with liquid production control mode from 1986.

Well	Period	Production rate control
7/12-6	2015 – 2019	Water
7/12-10	2015 – 2019	Water
7/12-12	2000 – 2011	Oil
7/12-12	2011 – 2019	Water
7/12-15	1988 – 2000	Oil
7/12-15	2000 – 2015	Liquid
7/12-15	2015 – 2019	Water
7/12-16	2015 – 2019	Water
7/12-18	1986 – 1992	Oil
7/12-18	1992 – 2000	Water
7/12-18	2000 – 2015	Liquid
7/12-18	2015 – 2019	Water

4.4.7. Cases 2 and 3: Thickness Cutoff

The thickness cutoff in cases 2 and 3 is an uncertain property which can be subjected to adjustments. The initial thickness cutoff (1100 m) used in the previous stages of the history matching process was selected based on the visual analysis of the isochore (depth) between the top Zechstein Gp and the top Ula Fm (Figure 33). However, this parameter is uncertain and therefore other scenarios were tested. These scenarios include thickness cutoffs of 900 and 600 m. These values were chosen due to the visual analysis showed in Figure 34.

In addition, the completion report (NPD, 2019) of the exploration well 7/12-11, located about 7 km east of the Ula field (Figure 42), states that a very thin (12.5 m) Ula Fm sandstone with low reservoir quality was encountered in the area outside the salt wall limits and above the Triassic pods. Therefore, a thickness cutoff of 2100 m, which includes this well (Figure 42) was also tested in cases 2 and 3.

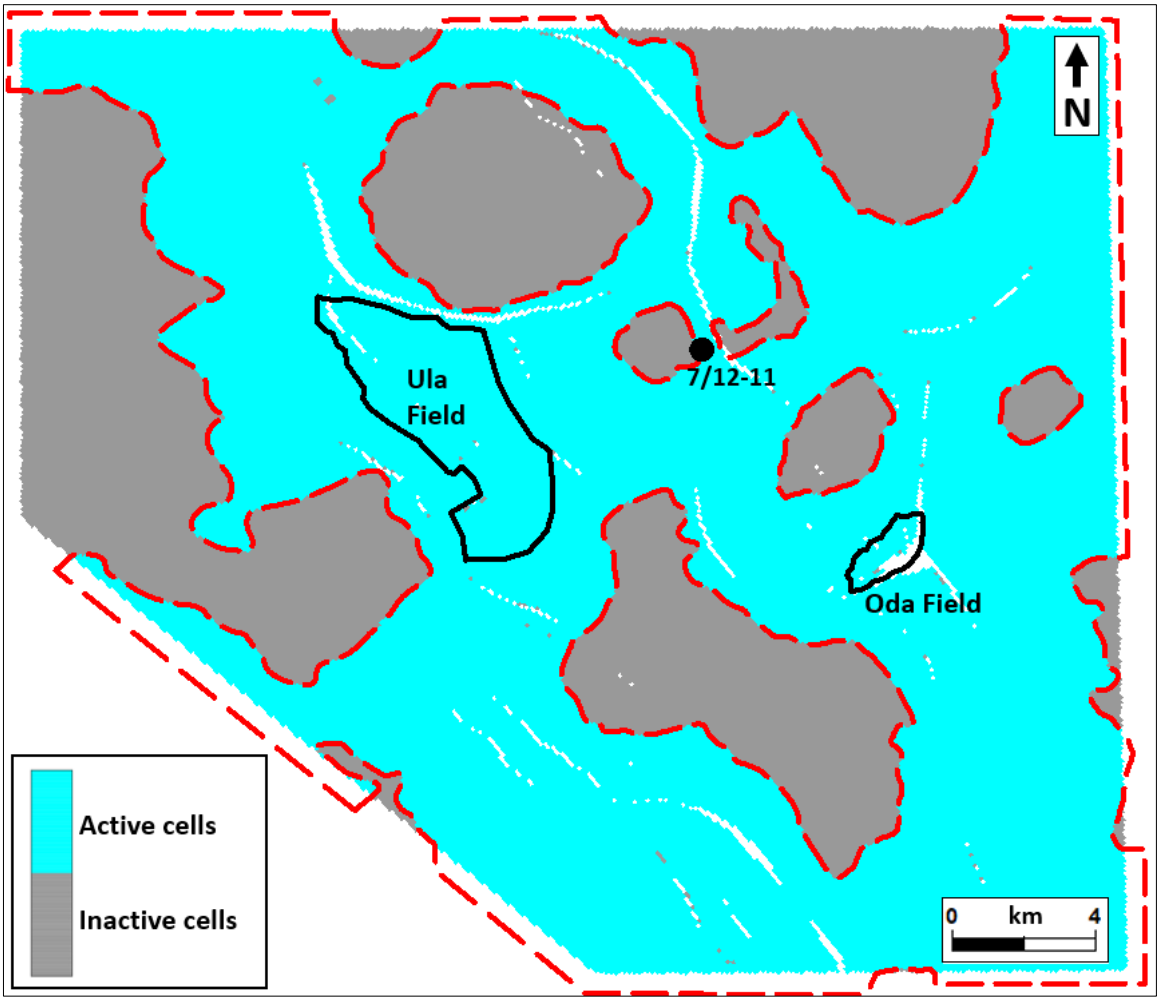

Figure 42. Active and non-active cells for a thickness cutoff of 2100 m. The red dashed line indicates the aquifer limits for case 1.

4.4.8. Assumptions and Uncertainties

The main assumptions and uncertainties related to the history matching process are listed below:

Assumptions:

- Period of two years before start of production for the system to achieve equilibrium;
- Surface rate as injector control mode;
- Wells shut at surface, allowing crossflow.

Uncertainties:

- Reservoir average pressure;
- Water and gas breakthrough;
- Numerical aquifer volume;
- Absolut permeability between the Ula and Oda fields;
- Fluid contacts in the Ula field;
- Thickness cutoff and limits of the Ula Fm. areas above the salt walls for cases 2 and 3.

5. RESULTS

5.1. History Matching: Pressure Adjustment

The pressure adjustment step comprised a global history match of the dynamic model and properties to the historical data of the reservoir. The main results were the reservoir average pressure and the liquid cumulative production (oil and water) in the Ula field. The matching criteria for this step was the overall trend of these curves. The parameters adjusted were numerical aquifer cross-sectional area (Table 12), absolute permeability (Table 13) and faults transmissibility (TM = 0, 0.5 and 1).

5.1.1. Initial Model

The graphs of oil cumulative production for cases 1, 2 and 3 (Figure 43 A) show exact match with the historical data curve (black dots) for the cases in which oil is the production control mode, and less than 10% uncertainty in the periods of higher discrepancy (1992 – 1998 and 2004 – 2012) for the cases in which liquid is the production control mode.

Similarly, the graphs of liquid (oil and water) cumulative production for cases 1, 2 and 3 (Figure 43 B) show exact match with the historical data curve for the cases with liquid production control mode, as expected. However, for the cases in which oil is the production control mode, there is an increase in the liquid production rate after 1991. In this case, the liquid cumulative production curves do not have the same trend as the historical data, and there is 20% - 25% uncertainty in the results for cases 1, 2 and 3. This behavior is due to the higher water production rates in the oil production control mode when compared to the liquid production control mode and the historical data (Figure 43 C).

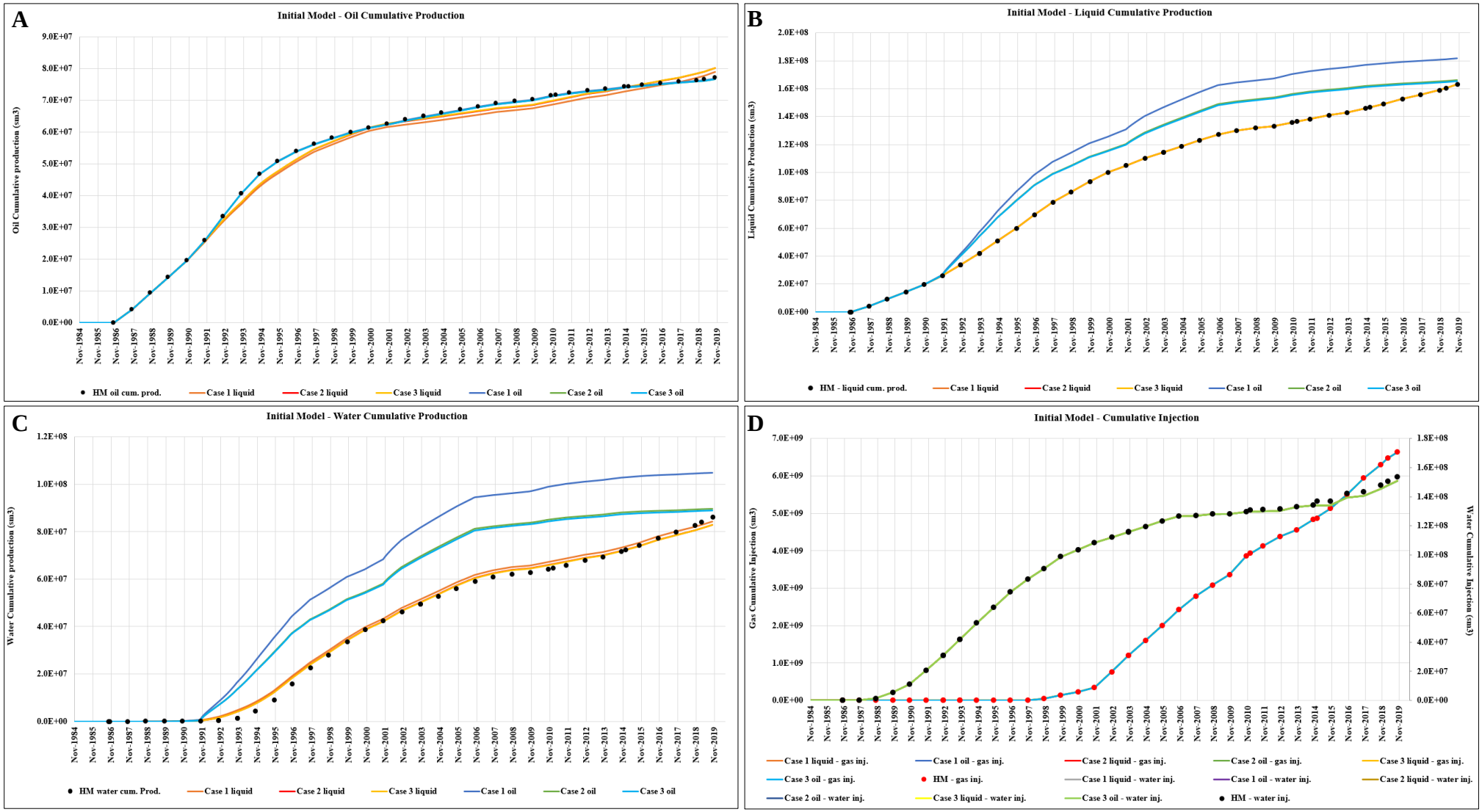

Figure 43. Initial model results in the Ula field through time for cases 1, 2 and 3. Comparison of the scenarios with oil and liquid production control modes. The dots are the historical data for the Ula field. A) Oil cumulative production (sm3) B) Liquid (oil and water) cumulative production (sm^3) C) Water cumulative production (sm^3) D) Water cumulative injection (sm^3) and gas cumulative injection (sm^3).

The water cumulative production curves (Figure 43 C) also show that for all the cases independent of the production control mode, the water breakthrough happens one year earlier than the historical data. In the historical data, the water production starts at a low rate by the end of 1992 and rise steadily until 1997. In the cases with liquid as the production control mode, the water production starts at the end of 1991 and the trend of the curves match the historical data. For the cases with oil as the production control mode, there is a much steeper increase in water production after the water breakthrough.

In order to verify if the injector wells were matching the Ula field historical data during the whole production period for any simulated case, the gas and water cumulative injection curves were plotted (Figure 43 D). These curves show an identical match to the historical data regardless of the case analyzed.

The most prominent differences between each conceptual model and both production control modes (oil and liquid) was observed in the average reservoir pressure (Figure 44). Comparing with the historical data, none of the cases controlled by oil production show a similar trend to the historical data, and the cases controlled by liquid production have a similar trend but a poor match to the historical data (differences higher than 40% in some periods), especially during the first year of pressure depletion and afterwards during the beginning of water injection.

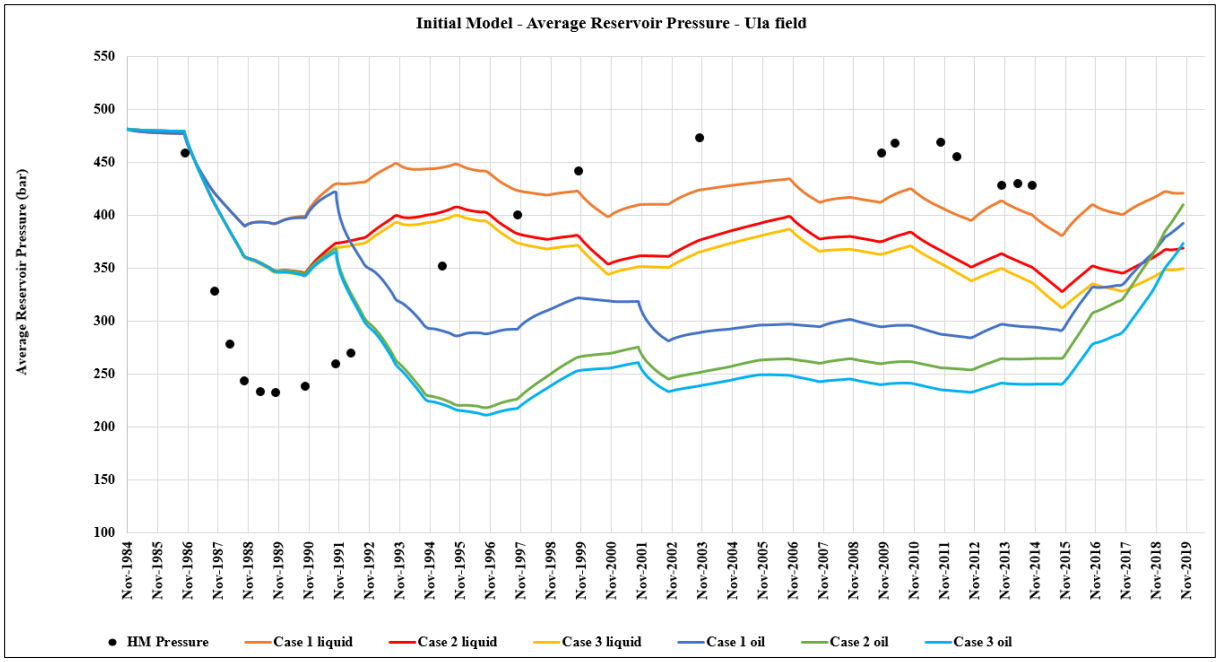

Figure 44. Average reservoir pressure (bar) in the Ula field through time for cases 1, 2 and 3 of the initial model. Comparison of the scenarios with oil and liquid production control modes. The black dots are the historical data from the Ula field.

In the cases with liquid control mode (Figure 44), the initial pressure depletion of the reservoir is less steep than in the historical data, dropping the initial reservoir pressure ~20% (case 1) and ~30% (cases 2 and 3), while the historical data show more than 45% pressure decrease. The successive pressure buildup occurs in the same period, but at a lower rate, since the pressure increases less than in the historical data. After 1996, whilst the historical pressure keeps increasing, the simulated pressure shows another significant depletion until 2001. From 1997 until 2018, the simulated pressure is 10% lower than the historical data. The considerable pressure decrease observed between 2009 and 2018 in the historical data, can also be noticed in the simulations, however, for a shorter period, since there is a sudden increase in the simulated reservoir pressure after 2016.

In the cases with oil control mode (Figure 44), the simulated reservoir pressure follows the same trend as the cases with liquid production control until October, 1991, when the pressure abruptly decreases to ~290 bar for case 1 and ~220 bar for cases 2 and 3, showing an opposite behavior to the historical pressure data. After 1996, the simulated cases show a low

rate pressure increase until 2001, when there is another rapid depletion until the end of 2002. Between 2002 and 2015, the simulated reservoir pressure is stable, but it is more than 30% lower than the historical data. There is also a sharp increase in the simulated reservoir pressure after 2016. Clearly the oil control mode does a worse job in simulating the average reservoir pressure through time than the liquid control mode.

5.1.2. Numerical Aquifer Cross-sectional Area

The initial model cases with liquid production control showed that the oil and water cumulative production match the trend of the historical data (Figure 43 A and B), but the models need additional aquifer support to adjust the pressure curve (Figure 44). Therefore, the next steps were intended to adjust only the average reservoir pressure curves without changing the matches already obtained.

The graphs of oil and water cumulative production for cases 1, 2 and 3 in Figure 45 (A and B), shows that the cross-sectional area of the numerical aquifer implemented in the dynamic model does not change the matches already obtained for these parameters. Figure 45 B also includes the aquifer influx for each scenario (dashed lines). In comparison to the volumes of water production, the aquifer influx variations due to different cross-sectional areas (Table 12) are small.

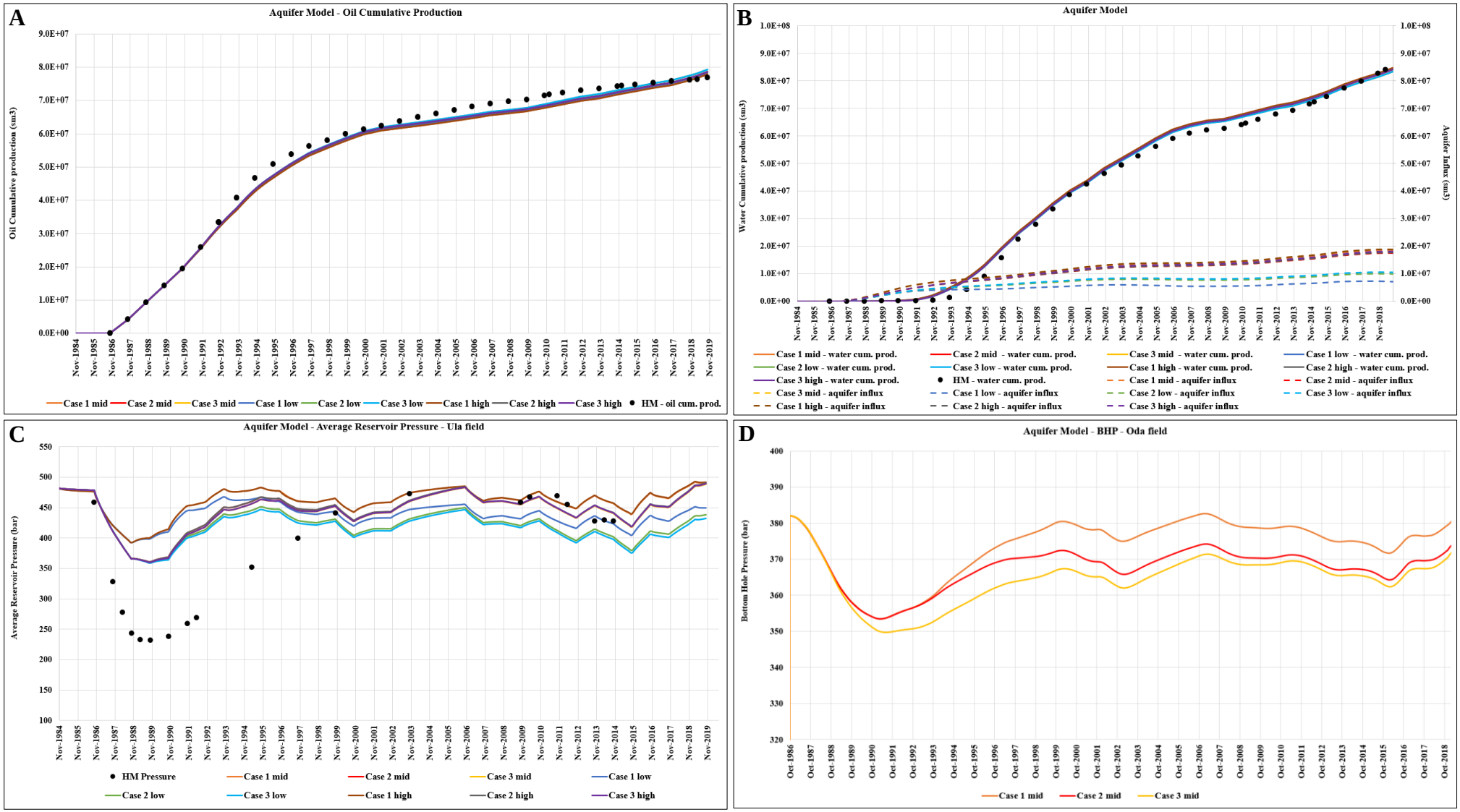

Figure 45. Numerical aquifer cross-sectional area results for cases 1, 2 and 3. Comparison of the low, medium and high cross-sectional area scenarios. The dots are the historical data for the Ula field. A) Oil cumulative production (sm^3) B) Water cumulative production (sm^3) and aquifer influx (sm^3) C) Average reservoir pressure (bar) D) Bottom hole pressure (bar) from the dummy well in the Oda field.

The average reservoir pressure results for all cross-sectional area scenarios (Figure 45 C) have the same trend as in the initial model cases with liquid production as the control mode. However, the mid to high cross-sectional aquifer areas produce higher average reservoir pressures, closer to the historical data, especially during the period from 1997 until 2018. The variation of the cross-sectional area in the numerical aquifer has this effect in all cases 1, 2 and 3. The medium and high cross-sectional area scenarios present similar results, while the low cross-sectional area scenario shows lower average reservoir pressures, though higher than in the initial model without the numerical aquifer.

Figure 45 D shows the bottom hole pressure results from the dummy well in the Oda field measured during the production period of the Ula field for cases 1, 2 and 3 with the medium cross-sectional area scenario of the numerical aquifer. From these results, the bottom hole pressure in the Oda field, years before its production, is highly variable and it ranges between 350 and 390 bar.

5.1.3. Absolute Permeability

In this section, the effect of absolute permeability in areas outside the Ula and Oda reservoir interval (Table 13) is evaluated. The starting point or reference model for this analysis is the numerical aquifer with medium cross-sectional area, which fits well the historical data (Figure 45).

The graphs of oil and water cumulative production for cases 1, 2 and 3 and the low, middle, and high scenarios of absolute permeability, show that this property does not change significantly the matches already obtained for these parameters (Figure 46).

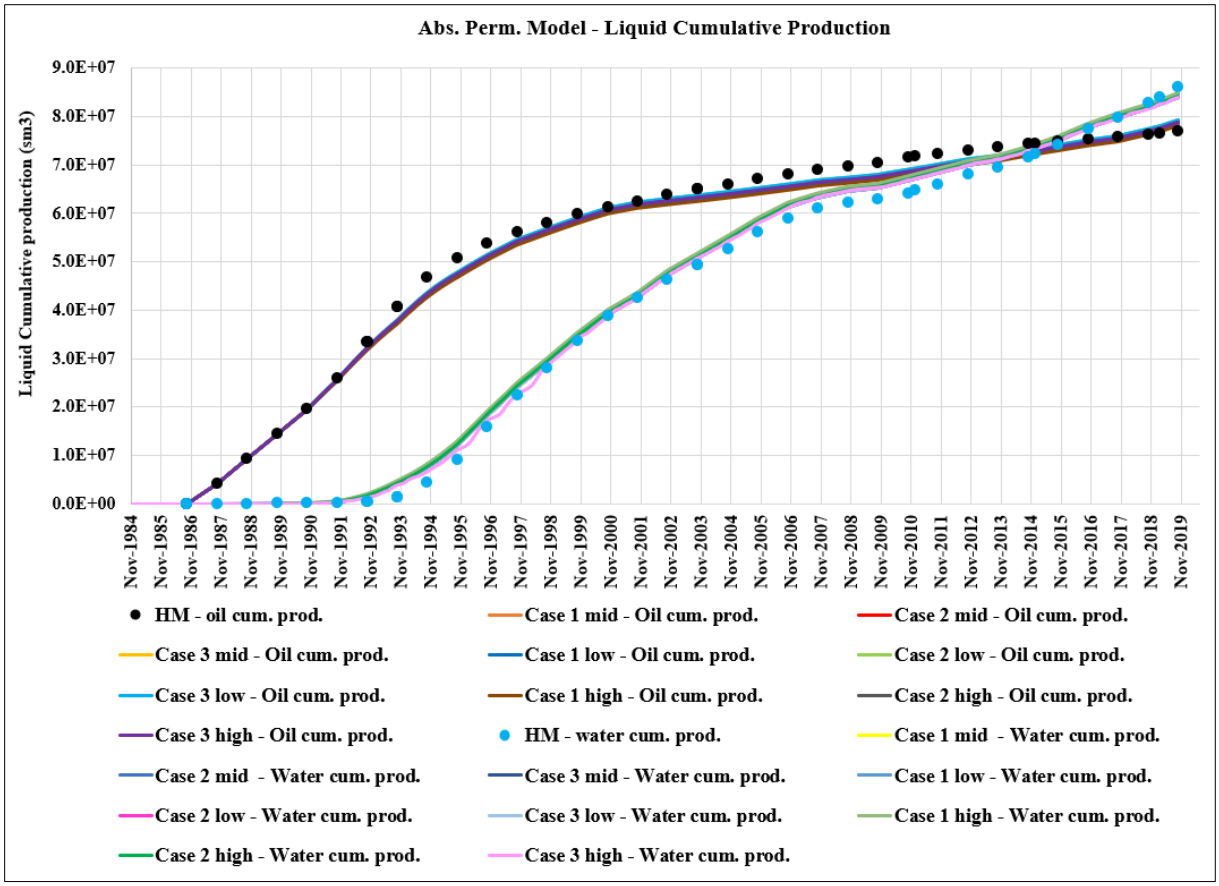

Figure 46. Oil and water cumulative production (sm^3) in the Ula field through time for cases 1, 2 and 3 of the low, medium and high absolute permeability scenarios. The dots are the historical data from the Ula field.

The average reservoir pressure results for the absolute permeability scenarios and for cases 1, 2 and 3 have the same overall trend and order of magnitude as in the reference model (numerical aquifer with middle cross-sectional area) during 1997 to 2018 (Figure 47). Absolute permeability influences the average reservoir pressure in a similar way in all three cases. The most affected period is from 1986 until 1997, with the low absolute permeability scenario resulting in more reservoir depletion until 1990, and a lower rate of average reservoir pressure increase afterwards (Figure 47).

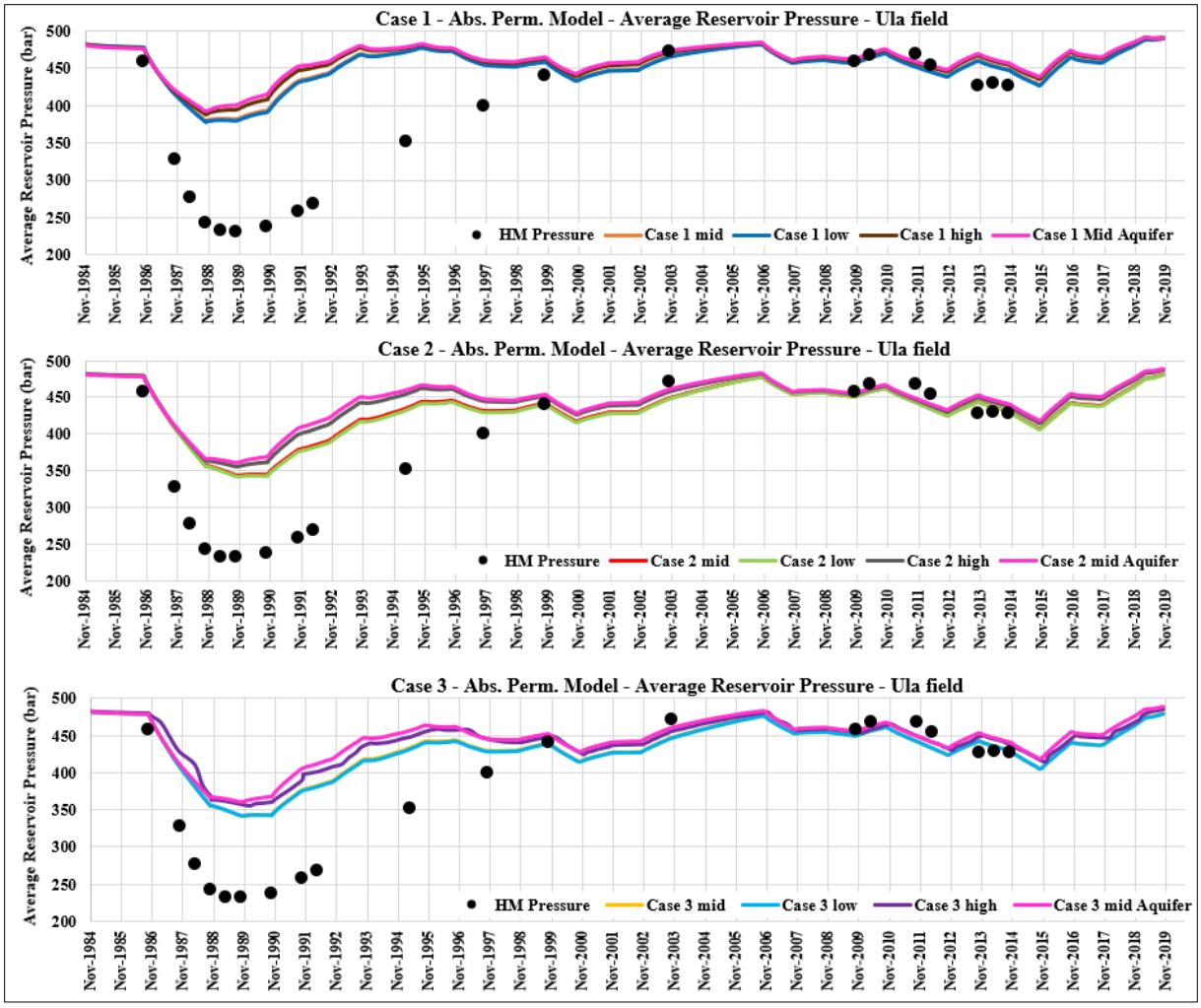

Figure 47. Average reservoir pressure (bar) in the Ula field through time for cases 1, 2 and 3 of the low, medium and high absolute permeability scenarios. The reference model or medium cross-sectional area aquifer scenario is included for comparison. The black dots are the historical data from the Ula field.

The bottom hole pressure results from the dummy well in the Oda field for the absolute permeability scenarios when compared to the medium numerical aquifer scenario show that the pressure in the Oda field is much less variable and more stable for the low and medium absolute permeability scenarios (Figure 48). The high absolute permeability scenario on the other hand shows similar results to the mid-aquifer model.

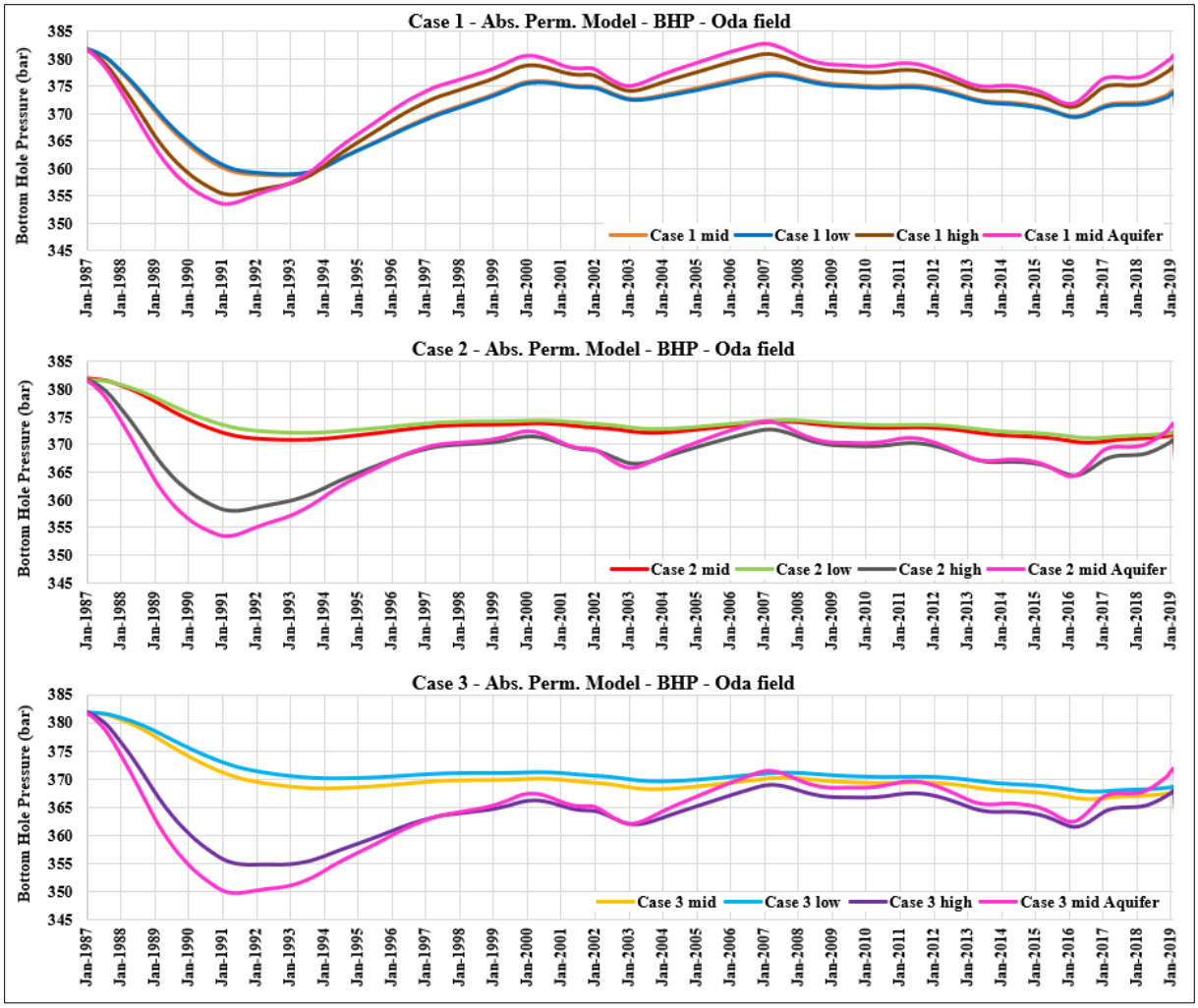

Figure 48. Bottom hole pressure (bar) from the dummy observation well in the Oda field through time for cases 1, 2 and 3 of the low, medium and high absolute permeability scenarios. The medium cross-sectional area aquifer scenario is included for comparison.

5.1.4. Faults Transmissibility

The results from the sensibility analysis of the faults juxtaposing the reservoir using the three transmissibility multipliers (sealing, partially sealing and not sealing) showed that the faults numbered in Figure 48 were the ones affecting the most the oil and water cumulative production and average reservoir pressure in the Ula field. The results for cases 1, 2 and 3 have the same overall trend and order of magnitude for all the three fault transmissibility scenarios.

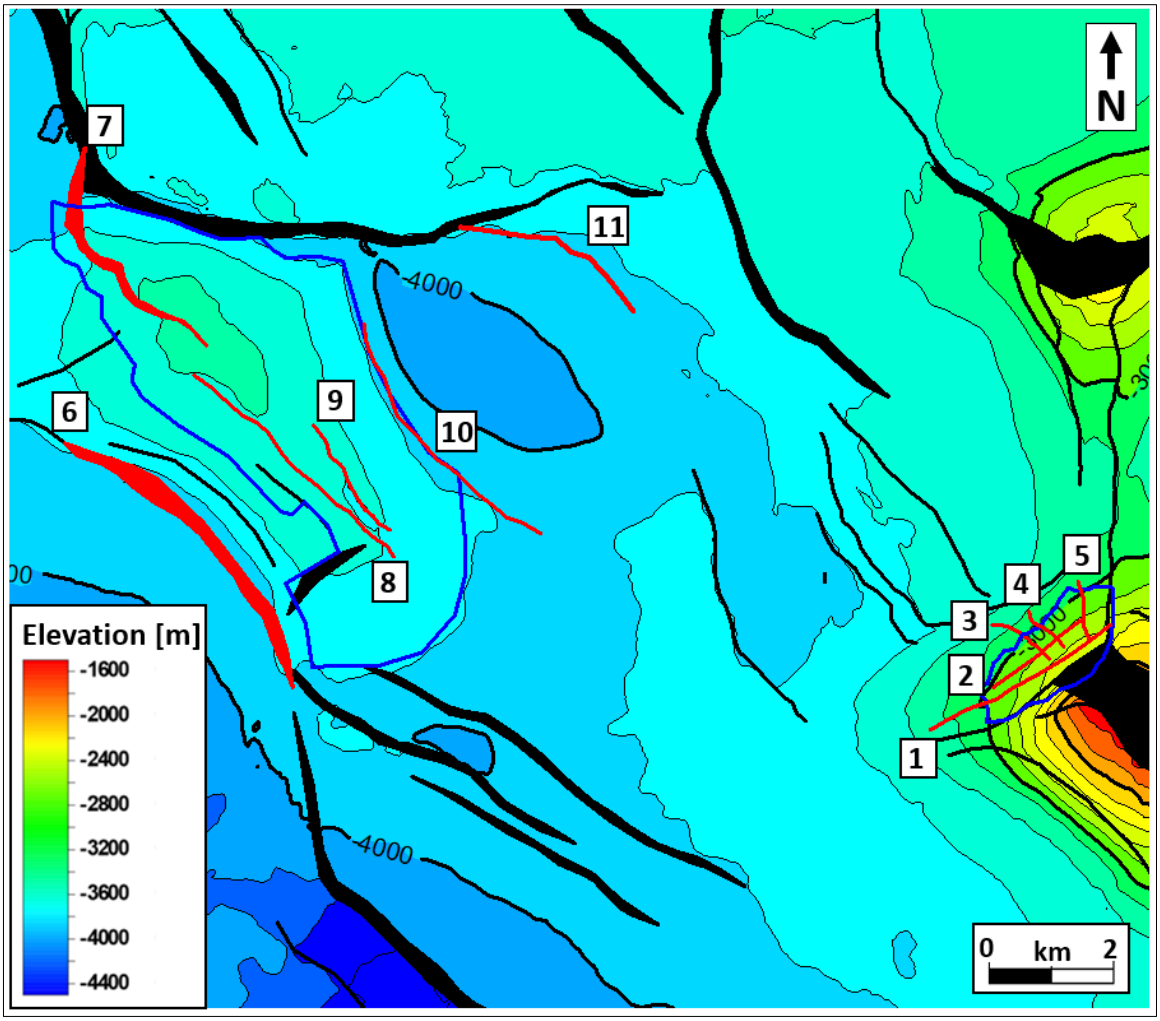

Figure 49. Top Ula Fm structure map in depth showing the faults juxtaposing the reservoir that affect the most the oil and water cumulative production and average reservoir pressure curves in the Ula field (red polygons). Blue polygons – Oda and Ula fields.

Many attempts to adjust the transmissibility of the faults in Figure 49 were simulated. The scenario in which faults 6, 8, 10 and 11 are sealing (TM = 0), and faults 7 and 9 are partially sealing (TM = 0.5) generated the best history matching results for the oil and water cumulative production (Figures 50 and 51, respectively) and for the average reservoir pressure (Figure 52).

Significant differences in the oil and water cumulative production were observed during the period between 1991 and 2019 when comparing the different faults transmissibility scenarios (Figures 50 and 51, respectively). In some cases, the water cumulative production was ~5% higher than the historical data, and the opposite happened for the oil cumulative production. For the average reservoir pressure (Figure 52), the faults transmissibility scenarios

affected almost the whole production period (1988 until 2019). This exercise shows that the initial assumption of all the faults in the model sealing is not entirely correct. Adjustments in the transmissibility multiplier of the faults juxtaposing the reservoir can result in better matches.

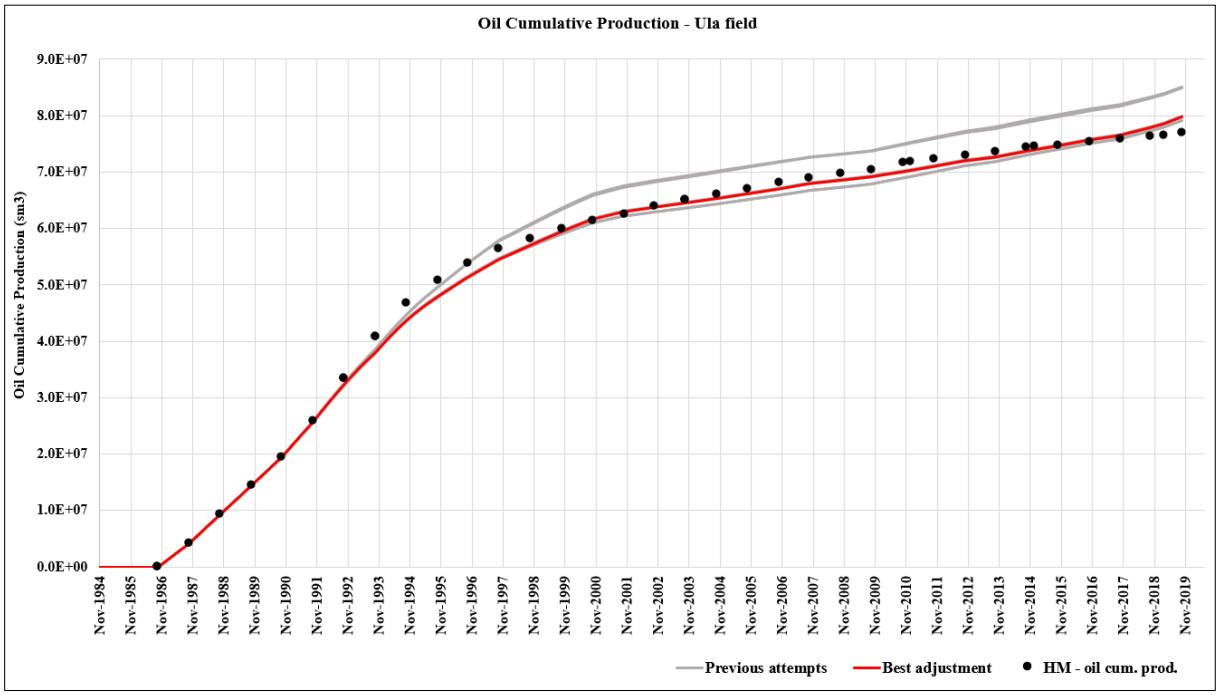

Figure 50. Oil cumulative production (sm^3) in the Ula field through time for case 3 and different fault transmissibility scenarios. The dots are the historical data from the Ula field. The grey lines are different fault transmissibility scenarios. The red line is the best matching scenario which consists of faults 6, 8, 10 and 11 sealing (TM = 0), and faults 7 and 9 partially sealing (TM = 0.5) (Figure 49).

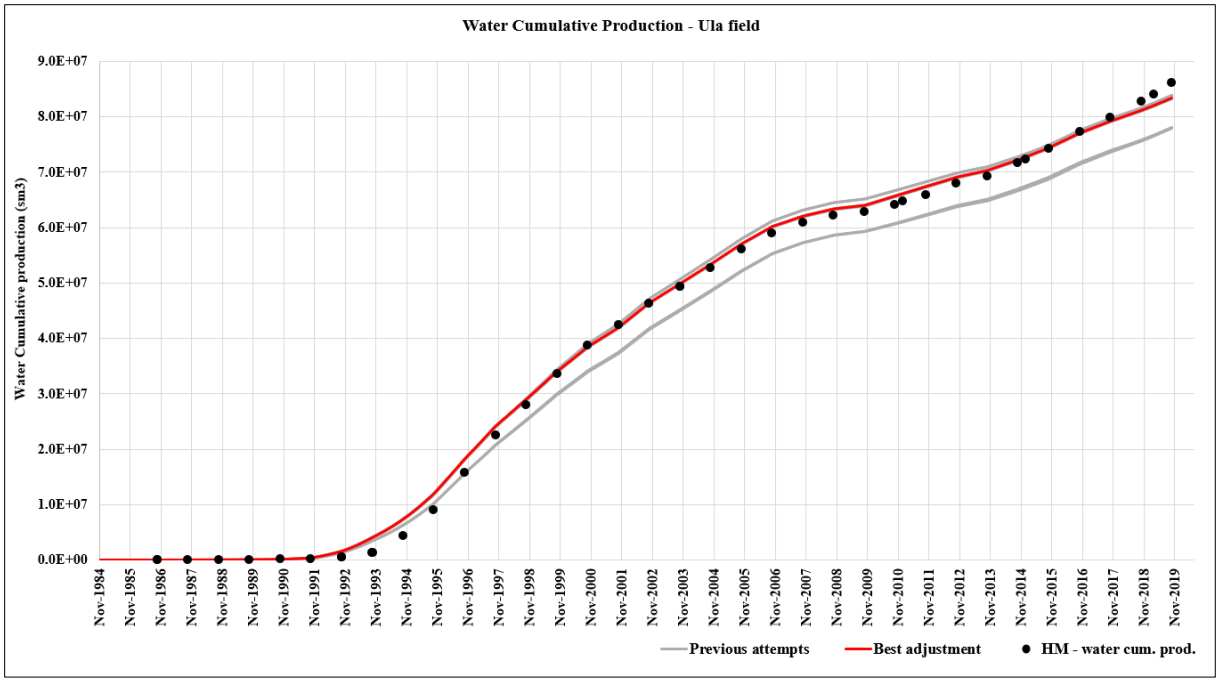

Figure 51. Water cumulative production (sm^3) in the Ula field through time for case 3 and different fault transmissibility scenarios. The dots are the historical data from the Ula field. The grey lines are different fault transmissibility scenarios. The red line is the best matching scenario which consists of faults 6, 8, 10 and 11 sealing (TM = 0), and faults 7 and 9 partially sealing (TM = 0.5) (Figure 49).

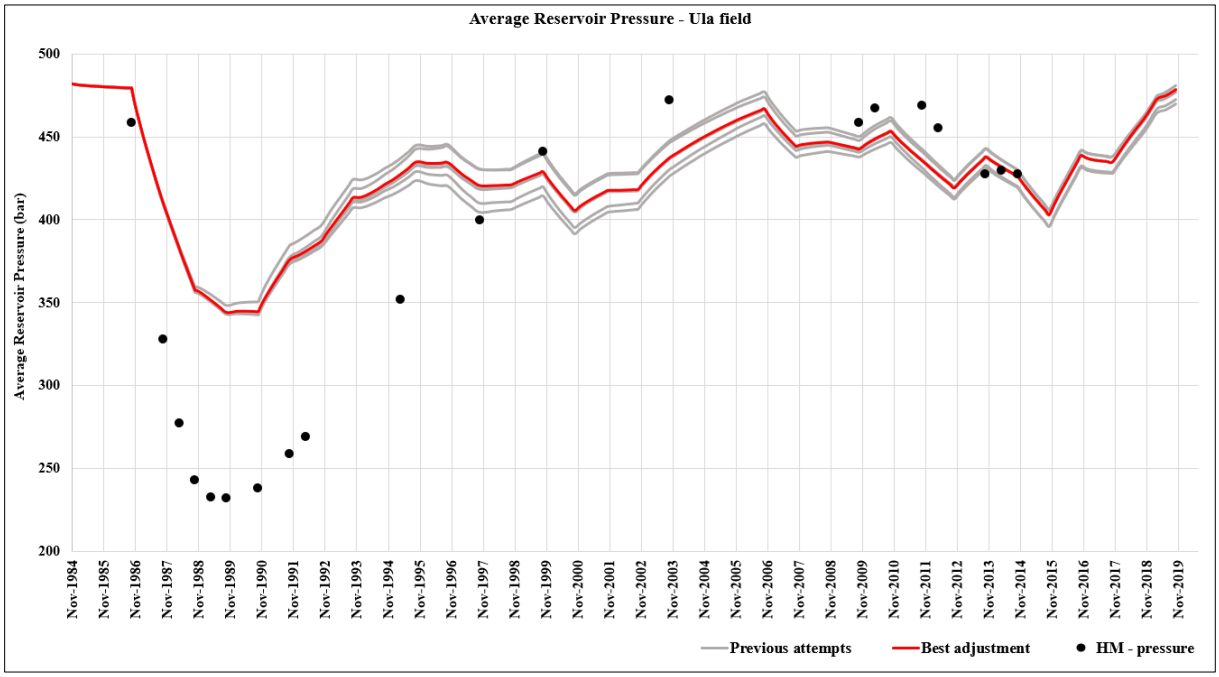

Figure 52. Average reservoir pressure (bar) in the Ula field through time for case 3 and different fault transmissibility scenarios. The dots are the historical data from the Ula field. The grey lines are different fault transmissibility scenarios. The red line is the best matching scenario which consists of faults 6, 8, 10 and 11 sealing (TM = 0), and faults 7 and 9 partially sealing (TM = 0.5) (Figure 49).

5.1.5. Summary: Pressure Adjustment

The best results from the global pressure adjustment can be summarized as follows:

- The trend of the cumulative production curves matches the historical data, i.e. the recovery drive mechanism of the Ula field in the model is correct;
- The uncertainty of the cumulative production curves is ± 10% the historical data;
- The trend of the average reservoir pressure matches the historical data.

In terms of the three parameters adjusted: numerical aquifer cross-sectional area, absolute permeability, and faults transmissibility, the main observations are:

- The reservoir pressure in the Ula field is the parameter with higher uncertainties and most difficult to history match, especially in the early years of production;
- The absolute permeability in the areas outside the Ula and Oda fields reservoir interval is a key property to history match and correlate the depletion in the Ula field, (2009 – 2018) with the depletion in the Oda field (2011 to 2018).
- Fault transmissibility is an uncertain parameter and most probably not all faults in the model are sealing. However, even in the case of all faults sealing, there is communication between the Ula and Oda fields.

The points that need to be adjusted in the next step, detailed saturation history match, are:

- Initial reservoir depletion from 1986 until 1989;
- Pressure build up rate from 1990 until 1999;
- Pressure depletion between 2016 and 2019;
- Water and gas breakthroughs;

5.2. History Matching: Saturation Adjustment

The saturation adjustment step is a more detailed phase in the history matching process. In order to adjust the fluids movement behavior in the reservoir, it is necessary to match the wells production of gas, oil and water individually.

From the results obtained in the pressure adjustment step, the average reservoir pressure, the water and gas breakthroughs and the gas production were the main targets for the saturation adjustment history matching. The matching criteria for this phase was ± 10% of uncertainty in the resulting curves. The wells production was adjusted by varying the production control mode through time in the development strategy of the Ula field (Table 14), and checking the conceptual model cutoff thickness for cases 2 and 3.

5.2.1. Development Strategy

The production wells: 7/12-A-6, 7/12-A-10, 7/12-A-12, 7/12-A-15, 7/12-A-16 and 7/12-A-18 were selected as the target for the saturation adjustments using the development strategy due to their high influence on the performance of the Ula field.

Figure 53 shows the Ula field oil and water production rates (sm^3/day) compared to the average reservoir pressure for the final history match from the pressure adjustment step and the historical data. The overall matches with the historical data for the oil and water production rates are good, but there are several periods in which the differences are higher than ±30% (periods of 1991 – 2003 and 2014 – 2019). The comparison between the average reservoir pressure curve with the production rates shows a possible connection between the pressure mismatch (pressure decrease followed by increase) in the period of 1996 – 2006 with the higher matching uncertainties related to the oil and water production rates in the same period. In

addition, the anomalous increase of the reservoir pressure in the period after 2016 could be associated with higher rates of oil production combined with lower rates of water production.

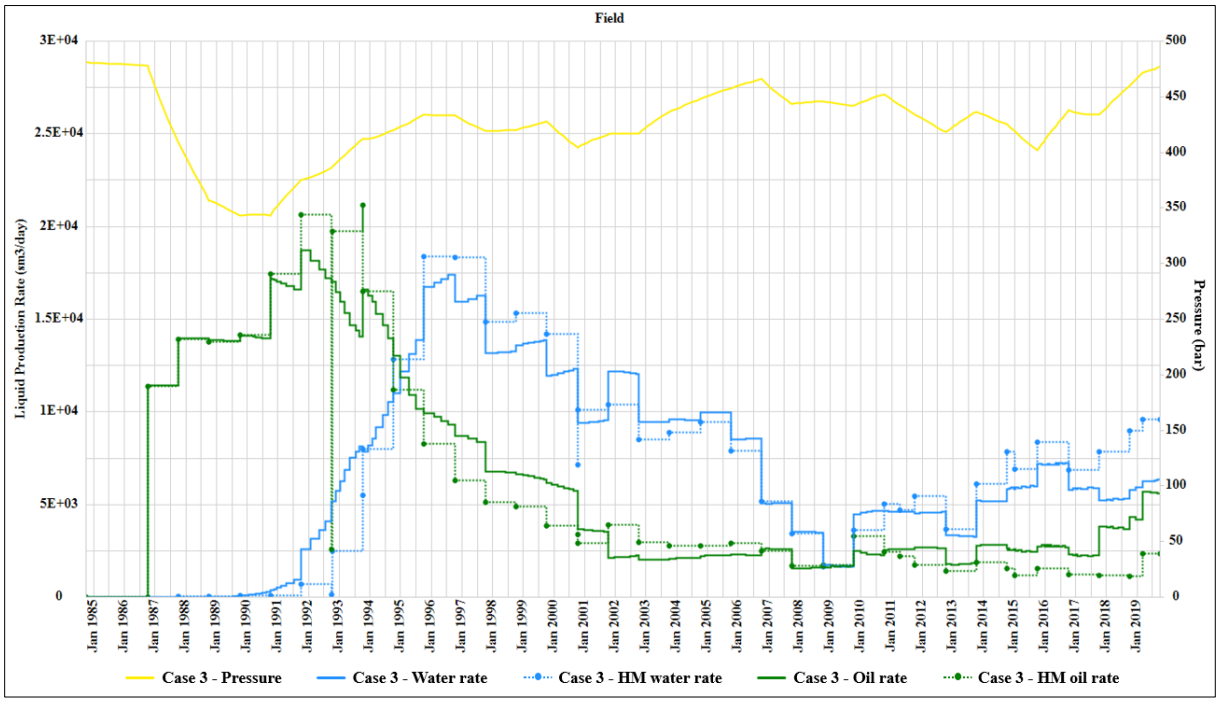

Figure 53. Oil (green) and water (blue) production rates (sm^3/day) and average reservoir pressure (bar) (yellow) in the Ula field through time for case 3 and the final history match from the pressure adjustment step. The dots are the historical data from the Ula field.

Figure 54 compares the average reservoir pressure curves for case 3 using the development strategy before and after the wells adjustment of the liquid production rates. It can be seen that the local well adjustments in the higher rates of oil production and lower rates of water production in the periods of 1996 – 2006 and 2016 – 2019 helped to fit the average reservoir pressure trend to the historical data. Although, the uncertainty criteria (± 10%) in the period of 1988 and 1998 is still not achieved.

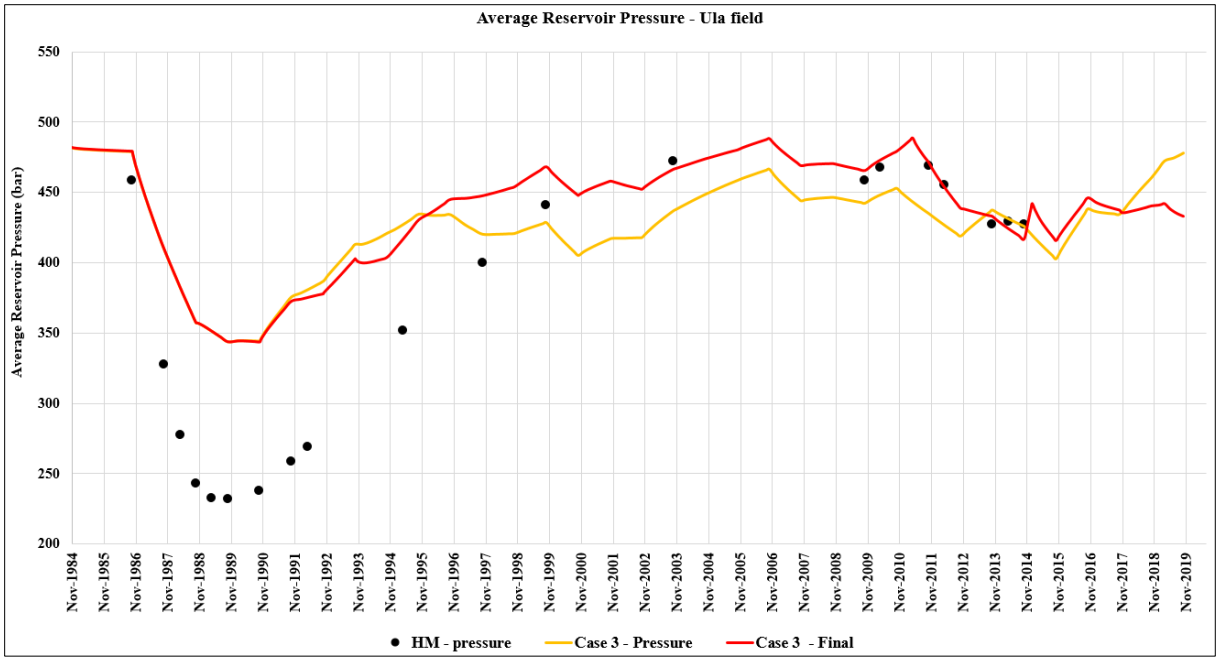

Figure 54. Average reservoir pressure (bar) in the Ula field through time of case 3 comparing the development strategy before and after the wells adjustment of the liquid production rates. The black dots are the historical data from the Ula field.

The average reservoir pressure curves for cases 1, 2 and 3 using the development strategy after the saturation adjustment step show that cases 2 and 3 have the same trend and order of magnitude (Figure 55). However, case 1 presents order of magnitude discrepancies in the period between 1987 – 2000 and after 2012. During 1987 and 1988 the initial pressure depletion in cases 2 and 3 is higher than in case 1. The pressure build-up after 1988 and until 2000 occurs at a similar rate for the three cases. In 2012, the pressure decrease for cases 2 and 3 is higher than for case 1.

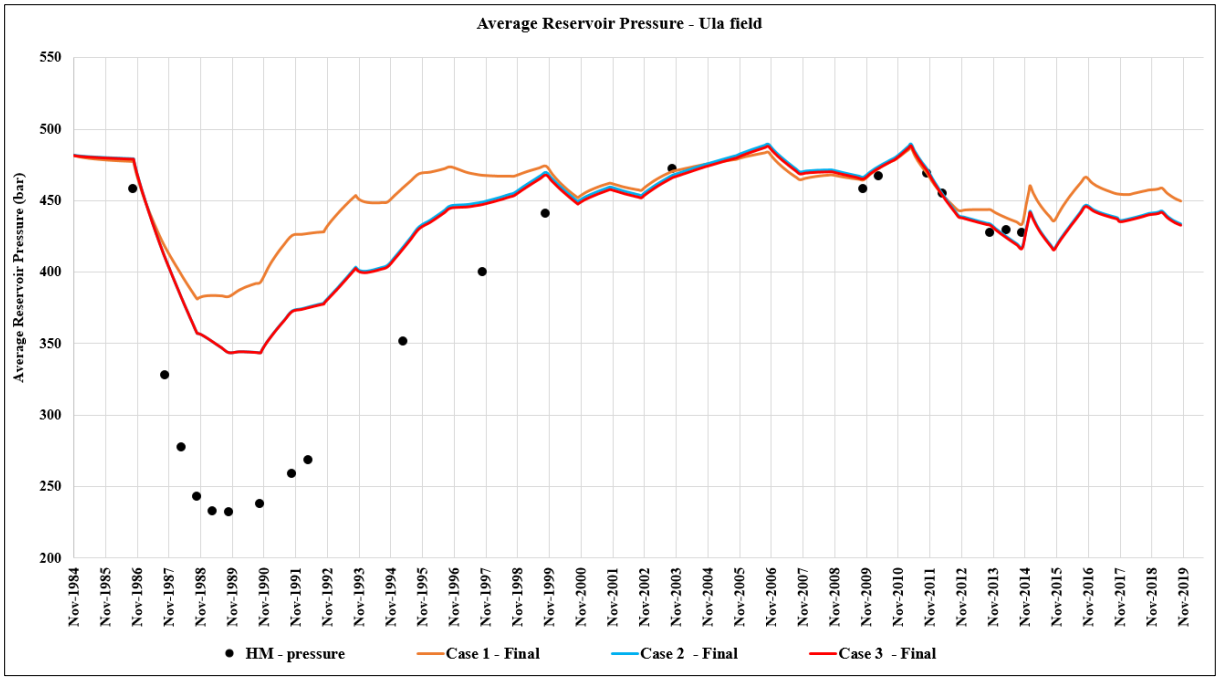

Figure 55. Average reservoir pressure (bar) in the Ula field through time for cases 1, 2 and 3 and the development strategy after the wells adjustment of the liquid production rates. The black dots are the historical data from the Ula field.

5.2.2. Cases 2 and 3: Thickness Cutoff

The graphs of oil and water cumulative production for cases 2 and 3 with different thickness cutoffs (600, 900, 1100 and 2100 m) show that the variation of this property does not influence significantly the matches already obtained for these results (Figures 56 and 57). However, the cumulative water production of the scenarios with the thickness cutoff of 600 m for cases 2 and 3 shows a slightly better match than the other thickness cutoffs.

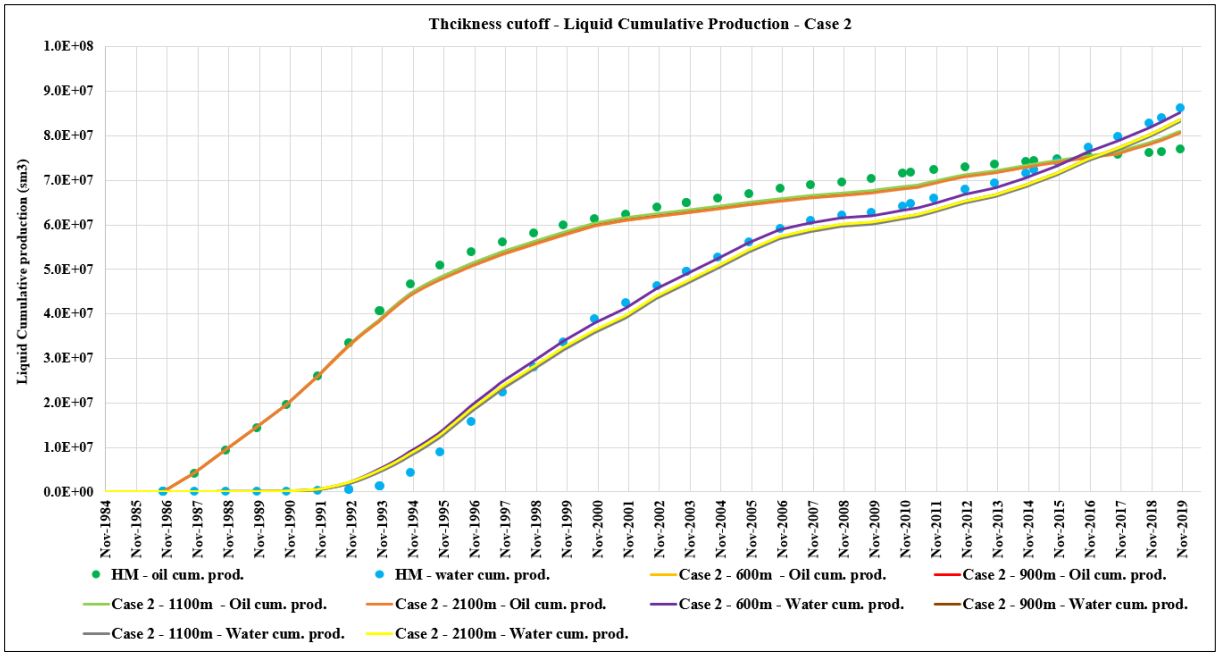

Figure 56. Oil and water cumulative production (sm^3) in the Ula field through time for case 2 with different thickness cutoffs (600, 900, 1100 and 2100 m). The dots are the historical data from the Ula field.

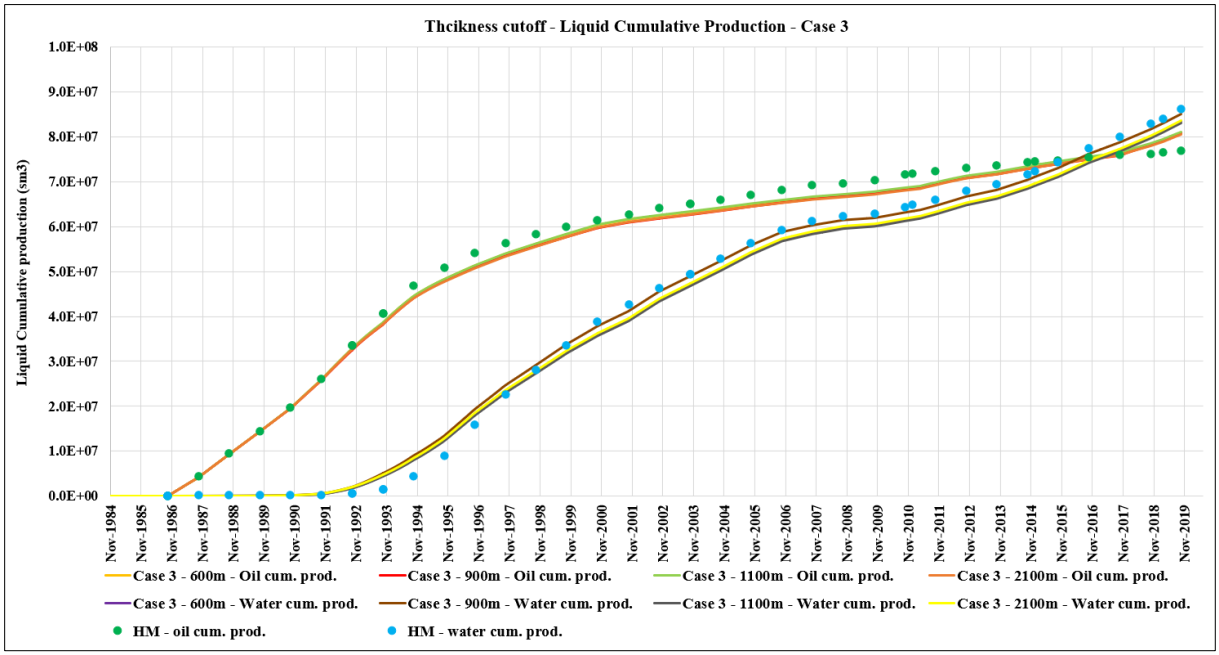

Figure 57. Oil and water cumulative production (sm3) in the Ula field through time for case 3 with different thickness cutoffs (600, 900, 1100 and 2100 m). The dots are the historical data from the Ula field.

The average reservoir pressure curves for cases 2 (Figure 58) and 3 (Figure 59) show similar results for the same thickness cutoffs. The scenarios with 2100, 1100 and 900 m thickness cutoff have the same trend than the historical data and display small variations from

2000 on. The periods with higher uncertainty are the initial pressure depletion of the reservoir, between 1986 and 1989 (initial reservoir pressure dropped ~15% less than the historical data); and the successive pressure build up from 1989 until 2000. The scenario with the thickness cutoff of 600 m shows the worst matching results for the reservoir pressure, with a small depletion between 1986 and 1988, followed by a pressure increase and stabilization ranging between 450 and 500 bar until the end of the production period.

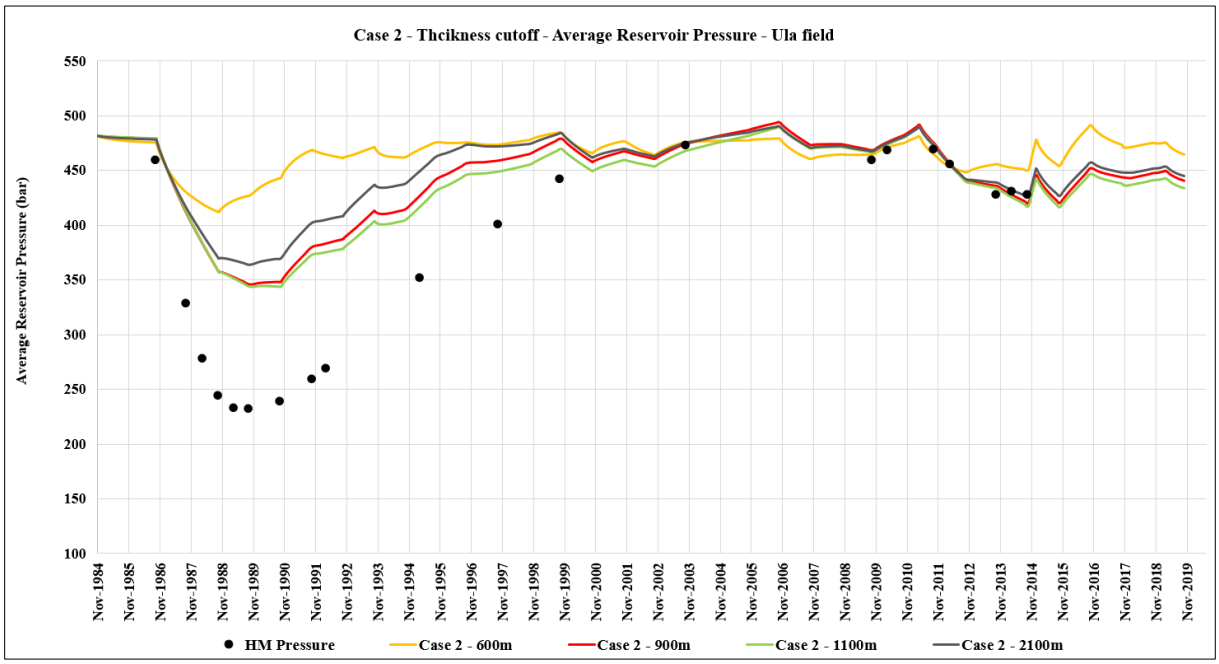

Figure 58. Average reservoir pressure (bar) in the Ula field through time for case 2 with 600, 900, 1100 and 2100 m thickness cutoffs. The black dots are the historical data from the Ula field.

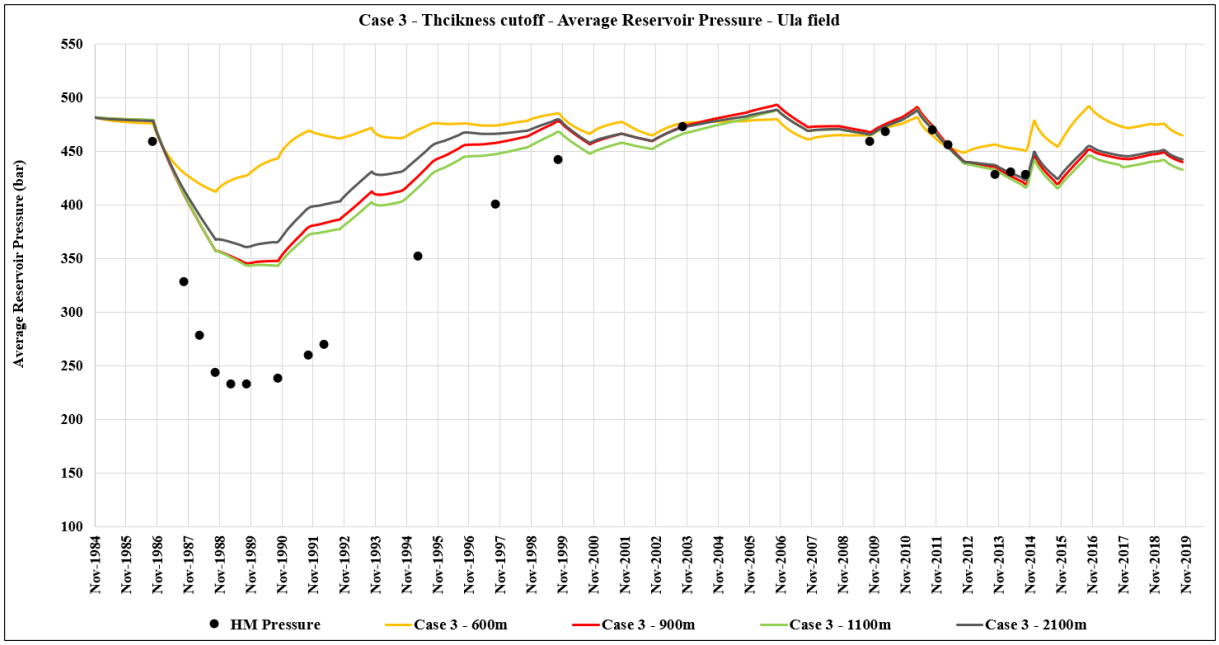

Figure 59. Average reservoir pressure (bar) in the Ula field through time for case 3 with 600, 900, 1100 and 2100 m thickness cutoffs. The black dots are the historical data from the Ula field.

5.2.3. Depletion in the Oda field

Figure 60 shows the bottom hole pressure results from the dummy well in the Oda field measured during the Ula field production period for cases 1, 2 and 3 with the final adjustments applied after the history matching process. These results show that the pressure in the Oda field before beginning of production is highly variable in case 1, ranging from 355 until 385 bar, and has a smother trend in cases 2 and 3. Also, cases 2 and 3 had similar trends, though some differences in the pressure values. Case 2 shows about 375 bar after 2000, and case 3 about 371 bar in the same period.

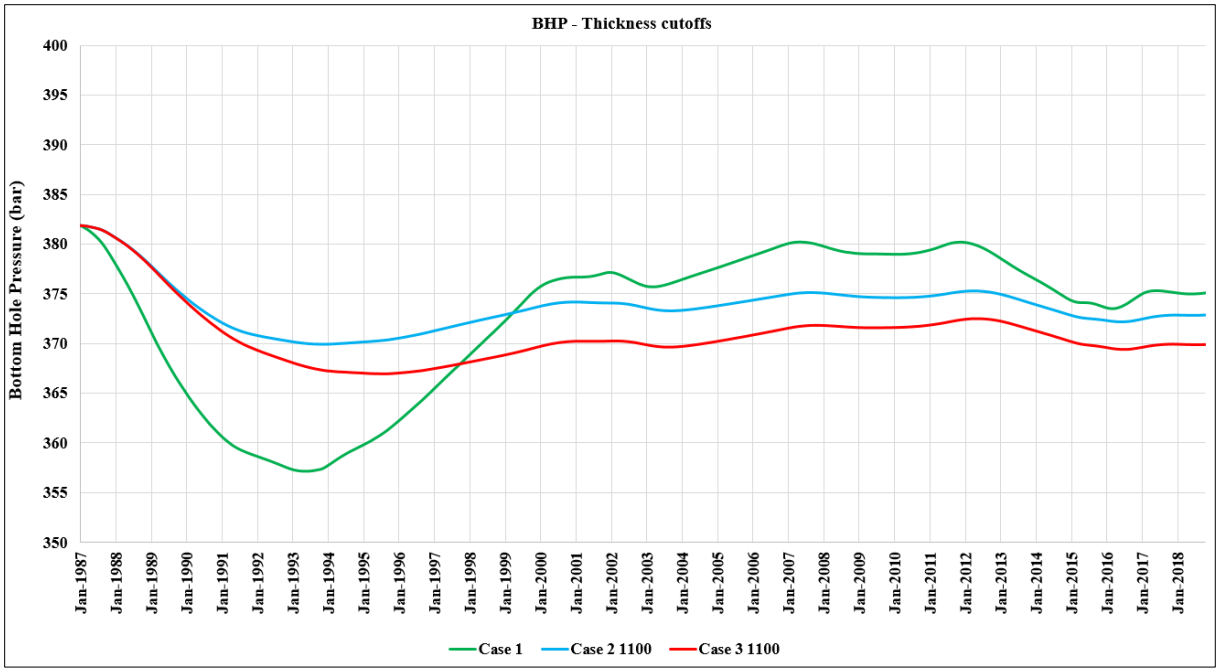

Figure 60. Bottom hole pressure (bar) from the observation well in the Oda field through time for cases 1, 2 and 3 with 1100 m thickness cutoff.

Figure 61 shows the bottom hole pressure results from the dummy well in the Oda field measured during the Ula field production period for case 2 with different thickness cutoffs of 600, 900, 1100 and 2100 m. The pressure curves show different trends and order of magnitude for each thickness cutoff. From these results, it can be seen that the thickness cutoffs 900, 1100 and 2100 m have similar trends after 2000, varying only one order of magnitude due to pressure increase between 1996 and 2000. Case 2 with the thickness cutoff 600 m shows a constant pressure trend with a pressure of about 380 bar.

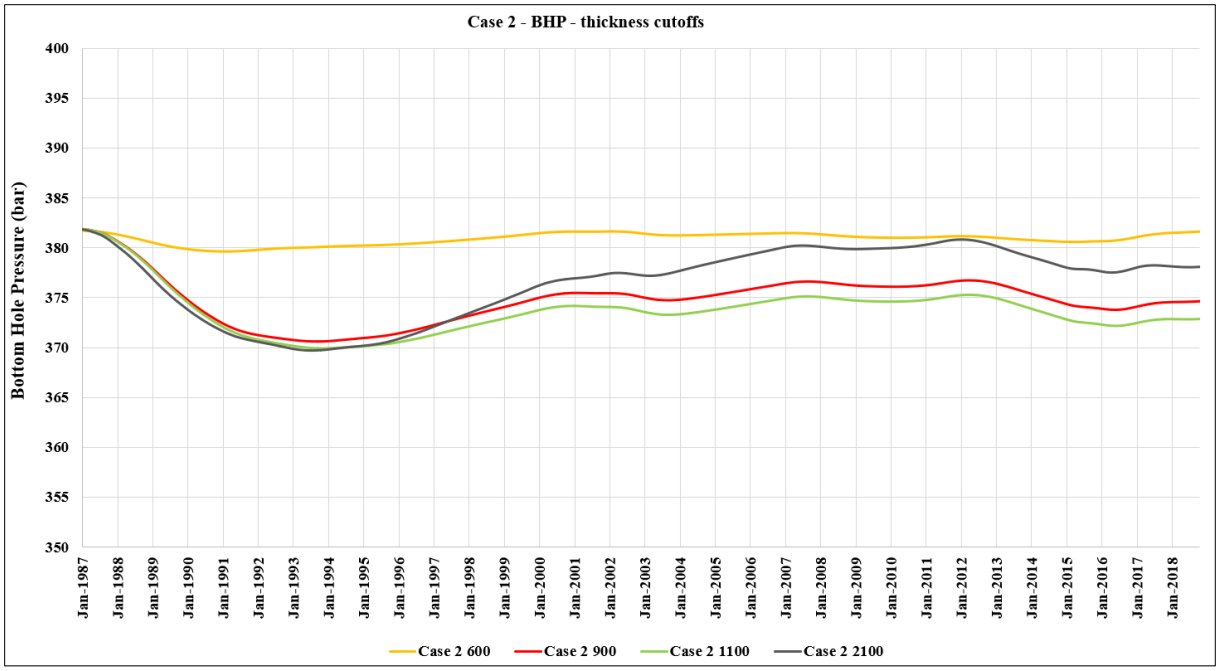

Figure 61. Bottom hole pressure (bar) from the observation well in the Oda field through time for case 2 with 600, 900, 1100 and 2100 m thickness cutoffs.

Figures 62 shows the bottom hole pressure results from the dummy well in the Oda field measured during the Ula field production period for case 3 with 600, 900, 1100 and 2100 m thickness cutoffs. The pressure curves show different trends and magnitudes for each thickness cutoff tested. The thickness cutoffs 900 and 1100 m have similar trends after 2000, varying only one order of magnitude due to differences in the level of pressure decrease in the period of 1991 – 1995 and pressure increase between 1995 and 2000. Case 3 with 600 m thickness shows a constant pressure trend of about 380 bar, very similar to the pressure curve from case 2 with the same thickness cutoff. Finally, case 3 with the 2100 m thickness cutoff shows higher pressure depletion from 1986 and 1995 and higher-pressure build-up from 1995 until 2007, as well as a similar trend and values than the scenario with 900 m thickness cutoff after 2007.

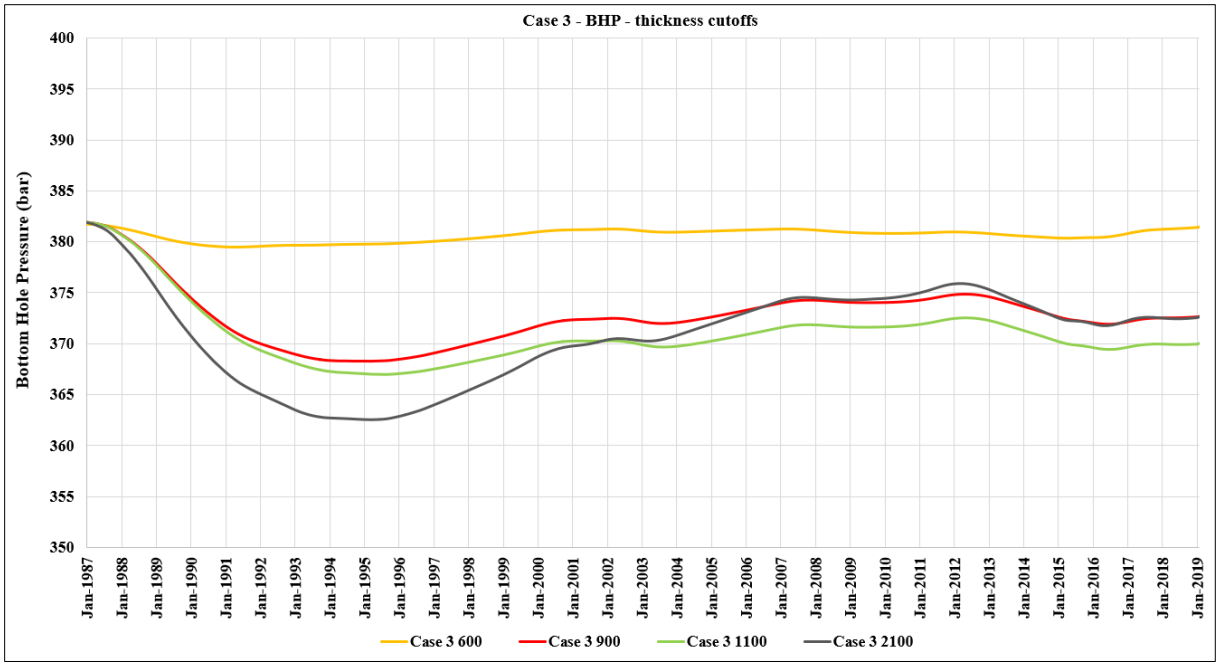

Figure 62. Bottom hole pressure (bar) from the observation well in the Oda field through time for case 3 with 600, 900, 1100 and 2100 m thickness cutoffs.

The pressure difference results for each of the cases and thickness cutoffs tested during the history matching process are included in Table 15. The pressure differences were calculated in the same period as the pressure depletion from well measurements in the Oda field was observed (August 2011 to August 2018). A graph of the thickness cutoff versus the calculated depletion in the Oda field shows a direct correlation between the thickness cutoff and the reservoir depletion (Figure 63). Cases 2 and 3 with thickness cutoff of 900-1100 m are within the uncertainty range (± 1 bar) of the original depletion measured in the Oda field between 2011 and 2018.

Table 15. Table of the average pressure and pressure differences between August 2011 and August 2018 in the Oda field for each of the cases and thickness cutoffs tested.

Case	Depletion (bar)	Average pressure (bar)
Original data	1.5 ± 1	380
Case 1	5.05	376.2
Case 2 (2100 m)	2.62	378.8
Case 2 (1100 m)	2.21	373.4
Case 2 (900 m)	1.9	375
Case 2 (600 m)	-0.47	381
Case 3 (2100 m)	3.17	373.4
Case 3 (1100 m)	2.35	370.6
Case 3 (900 m)	2.02	373.2
Case 3 (600 m)	-0.39	380.8

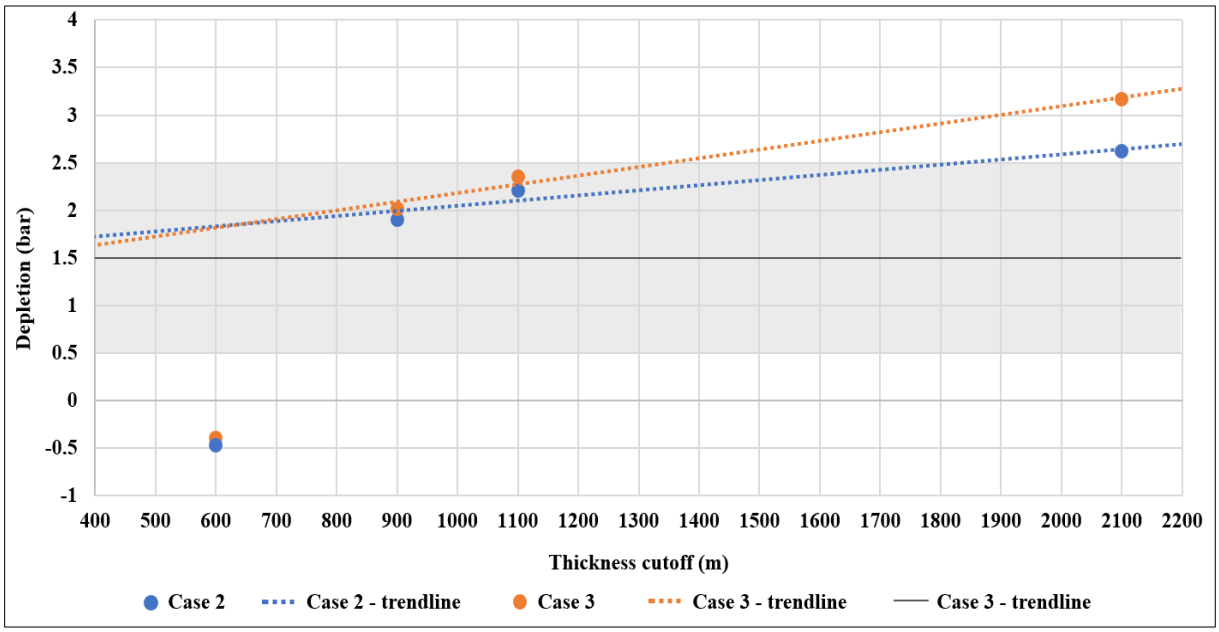

Figure 63. Graph of the thickness cutoffs from cases 2 and 3 versus the calculated depletion in the Oda field in the period between 2011 and 2018. The gray line is the original depletion ± 1 bar uncertainty (gray area) measured in the Oda field between 2011 and 2018. Cases 2 and 3 with thickness cutoff of 900-1100 m are within the uncertainty range.

6. DISCUSSION

The Ula and Oda fields are in contact with large volumes of water towards the north and west. The production history data from the Ula field shows more than 75 Msm^3 of water cumulative production from 1992 to 2019 (section 4.4.1). As the area of the dynamic model is very wide (to include both fields and surrounding areas) and the thickness is low (since the model includes only the Ula Fm), the volume of water in the model is limited and is not enough to reproduce the historical water production rates and keep the average reservoir pressure in any of the conceptual cases simulated (Figures 43 C and 44). Therefore, it is necessary to include a numerical aquifer in the model to provide additional pressure effects (section 5.1.1).

The initial model results from the cases using oil as the production control mode (Figures 43 A and B and 44), make possible to interpret that the anomalous depletion periods observed after 1991 and 2001 in the Ula field were related to extreme volumes of water production (more than 20 Msm^3/d during a very short period) in wells 7/12-A-16 and 7/12-A-17 B. Both wells were water bearing and well 7/12-A-17 B was converted to an injector well (WAG) in 2015 due to its peripheral location (Figure 4).

The implementation of a numerical aquifer in the model (section 5.1.2) was an effective way to provide additional pressure support to the average pressures of the Ula field without affecting the aquifer influx, i. e. there was no extra water production due to the numerical aquifer (Figure 45 B). The three tested aquifer cross-sectional areas (Table 12) kept the average reservoir pressure in all the cases simulated (Figure 45 C). Cross-sectional area values higher than the medium scenario no longer affected the results, and cross-sectional area values lower than the medium scenario were not enough to match the average reservoir pressure of the historical data. This means that the dynamic model needs at least an extra 1.000 km^3 volume of water to assure the required pressure support in the Ula field. These results are in accordance

with previous studies describing the Ula field as part of a giant hydrodynamic aquifer. As stated by Dennis et al. (2005) and Heum (1996), the hydrodynamic aquifer in the Ula field is part of a major system that extends along the North Sea basin and which is formed by dewatering of the deep Central Graben in a section more than 400 km wide. Groundwater is expelled from the Central Graben by overpressure and the water escapes in a NW-SE direction through permeable aquifers in the Paleocene/Lower Cretaceous/Jurassic sands, Upper Cretaceous chalk, or vertically routes provided by salt diapirs.

The aim of this thesis was to evaluate the possible communication between the Ula and Oda fields through the Ula Fm aquifer using dynamic models. Therefore, a dummy well measuring the pressure behavior in the Oda field (well 8/10-B-3 AH, Figure 2) since the beginning of the Ula field production was used to evaluate a correlation between the historical pressure data from the Ula field with the depletion observed in the Oda field between 2011 and 2018 (Figure 3). Since cases 1, 2 and 3 assume communication between the Ula and Oda fields (section 4.2.), it was already expected that the Oda field average pressure would be affected by the fluids production in the Ula field (Figure 45 D). However, both fields are separated by more than 10 km distance, so the influence in the average pressure of the Oda field in the initial model and numerical aquifer step was expected to be lower.

The property that most affected the reservoir flow communication is the absolute permeability. The absolute permeability model was quality controlled in the areas where there was well data (Figure 28). From section 4.1.8, one of the main uncertainties related to the property modelling was the well logs upscaling, since as the distance from the Ula and Oda fields increases, the number of wells decreases, and consequently, there are fewer well data available.

The absolute permeability of areas deeper than the reservoir interval in the Ula and Oda fields (below -3800 m), and with initial absolute permeabilities higher or equal to the shallower

reservoir zones (Figure 40) was evaluated in the history matching process. The period from 1988 until 1997, in which the reduction of the absolute reservoir pressure in these areas was most sensitive to the changes in the average reservoir pressure (Figure 47), coincides with the turning point in the pressure curve, when water injection was implemented to improve oil recovery and stabilize the reservoir pressure. The areas in which the absolute permeability is low are mainly around the Ula field (Figure 40), which contributed to make the water injection pressure support more effective, especially during the period of less stability. The bottom hole pressure results from the dummy well in the Oda field for the absolute permeability scenarios tested (Table 13) when compared to the medium numerical aquifer scenario (Figure 48) show that the pressure in the Oda field is less variable, more stable and geologically more consistent with the low absolute permeability scenario.

The faults juxtaposing the reservoir in the Oda field (faults 1 to 5, Figure 49) did not influence the pressure results in the Oda field since the target of the study was the ratio of depletion in the reservoir (section 5.1.4.). The study area is wide and none of the main faults included in the dynamic model compartmentalize or obstruct the communication between the Ula and Oda fields through the Ula Fm in any of the proposed conceptual models of the Ula Fm fairway (Figure 49). This can explain why the variation in the transmissibility multiplier of the faults juxtaposing the reservoir caused the same effects in cases 1, 2 and 3, as observed in section 5.1.4. However, fault transmissibility influences the reservoir performance in the Ula field, since in this field the reservoir has many important faults that represent barriers to fluid flow (Figure 52).

Cases 1, 2 and 3 achieved a successful match for the oil and water cumulative production and for the average reservoir pressure in the period after 2000 (Figures 54 and 55). The matching criteria was that the model fit the trend of the reservoir performance and the results were ± 10% from the historical data.

The primary recovery in cases 1, 2 and 3 did not deplete the reservoir pressure with the same magnitude as the historical data in the period from 1986 until 1988, so the trend of the reservoir pressure data was reached, but the uncertainties were +28% (Figure 55). Consequently, the following pressure build-up after the water injection started (1989) also did not achieve the matching criteria until 2000. This poor initial match of the models could be related to the initial hydrocarbon volumes in the system. The STOIIP calculated in the static model is ~2% higher than the original data (section 4.1.7). This could be the cause for the mismatches observed in the Ula field during primary recovery, since the higher volumes of hydrocarbons in the system restrain pressure depletion in the dynamic models.

The target period for the proposed study was the years between 2009 and 2018. Therefore, since the volumes of fluids produced and injected in the Ula field were well calibrated (Figures 50 and 51) by that time, and the average reservoir pressure was matched almost 10 years before this target period (Figure 55), the uncertainty in the reservoir pressure curve between 1986 until 2000 does not affect the main observations for the average pressure in the Oda field. On the other hand, the effects of the initial depletion of the Ula field, although of a smaller magnitude when compared to the historical data, are well observed in the Oda field reservoir pressure for all conceptual model cases (Figure 60), which confirms the hypothesis of communication between the fields through the Ula Fm.

Another issue that was not solved although improved with the adjustments during the history matching process was the early water breakthrough. The simulated water production started almost one year earlier than the historical data (end of 1991) in all scenarios (with or without numerical aquifer, with all main faults sealing or not) (Figures 43 C, 45 B, 46 and 51). The reason for the difficulties in history matching the water breakthrough could be related to the coarse grid size used in the dynamic model, the simplifications assumed for the properties modelling, and the lack of well data available in the areas outside the Ula field. However, for

the same reason as the initial mismatch in reservoir pressure, the uncertainty related to the water breakthrough in the Ula field does not affect the results for the much latter average pressure in the Oda field.

6.1. **Geological evidence for communication between the Ula and Oda fields**

The communication between the Ula and Oda fields through an aquifer in the Ula Fm cannot be proved entirely based on stratigraphic correlation. As explained previously, many studies confirm that the distribution of the Ula Fm is complex since the deposition of this unit was controlled by halokinesis and extensional faulting (Bailey et al., 1981; Bjørnseth and Gluyas, 1995; Mannie et al., 2014; O'Connor et al., 2011; Spencer et al., 1986; Stewart, 1993). Also, the communication between the fields could not be verified using well data correlation, since there are no wells drilled in the area between the fields. Neither using seismic data since the Ula Fm in some areas is thinner than the vertical seismic resolution at the reservoir depth and the seismic definition of the Ula reservoir is also affected by tuning effects. Therefore, it is necessary to explore conceptual models based on geological evidence, and to perform dynamic simulations on these conceptual models to validate the hypothesis of communication between the Ula and Oda fields.

According to section 2.2, to prove a connection between the Ula and Oda fields, it is necessary to understand the deposition of the Ula Fm and the geological setting of the study area. Hodgson et al. (1992), Mannie et al. (2014) and O'Connor et al. (2011) proposed different models for the generation of accommodation space and the deposition of the shallow marine sediments of the Upper Jurassic Ula Fm. All these studies conclude that the Ula Fm sands were deposited in pod-shaped minibasins located above salt walls.

The assumption that the shallow-marine units of the Ula Fm were deposited in supra-diapir depocenters help us to understand the distribution of this unit in the study area. The top Zechstein Gp is a well-known easily interpreted reflector, characterized by a strong peak. Thus, the combination of the top Zechstein Gp structure map (Figure 16) with the available well data was important to delimit the reservoir presence in the study area and to confirm that the Ula Fm is present between the Ula and Oda fields. From Figure 34, comparing the Ula Fm areas above the salt walls for different thickness cutoffs (1100, 900 and 600 m), it is clear that even in the worst case scenario (600 m thickness cutoff), there is still a narrow Ula Fm channel connecting the Ula and Oda fields.

6.2. **Reservoir modelling evidence for communication between the Ula and Oda fields**

Since there are geological evidences of an Ula Fm pathway connecting the Ula and Oda fields, the assumption of communication between both fields through an aquifer in the Ula Fm can be tested through dynamic reservoir models. The observations from Figures 60, 61 and 62 show that for all the Ula Fm fairway cases evaluated, the production in the Ula field influences though with different magnitude the reservoir pressure of the Oda field.

In the cases in which there is a high and wide cross-sectional area of communication between the Ula and Oda fields through the Ula Fm (cases 1 and 2 and 3 with 2100 m thickness cutoff), the fluids production/injection in the Ula field causes high variations of the reservoir pressure in the Oda field (Figures 60 to 62). On the other hand, cases 2 and 3 with lower thickness cutoffs of 600, 900 and 1100 m have a narrow aquifer pathway between the Ula and Oda fields. Therefore, in these models, the variations of the reservoir pressure in the Oda field generated by the production of the Ula field are lower (Figures 60 to 62).

These pressure effects can be explained by large-scale groundwater flow principles, based on potential flow laws (Bernoulli's Principle). Since in cases 1 and 2 and 3 with thickness cutoff 2100 m the cross-sectional aquifer area connecting the reservoirs is higher, there is no restraint for the fluid besides the barrier effect caused by sealing and partially sealing faults. Thus, the pressure differences between the Ula and Oda fields will be lower (and the communication higher) than on cases 2 and 3 with lower thickness cutoffs (600, 900 and 1100 m), in which there is a restraint in the cross-sectional area between the fields (narrow channel connecting the fields). According to the potential flow laws, two points at the same depth separated by a restraint in the cross-sectional area will cause the increase of the fluid velocity and the decrease of pressure (and communication) in the restraint zone.

As discussed in section 4.2, case 1 is an overestimation and oversimplification of the Ula Fm fairway, which does not consider halokinesis and extensional faulting. This case was tested to get a first-order understanding of the water flow and pressure behavior within a wider aquifer, and to disprove this conceptual case which is geologically incorrect.

The main difference between cases 2 and 3 is the limit of the shoreface area where the shallow marine sands from the Ula Fm were deposited. Both cases generate very similar results for the oil and water production and reservoir pressure of the Ula field (Figures 46 and 55), and less than 1% differences and similar trends in bottom hole pressures in the Oda field (Figures 60, 61 and 62 and Table 15). Both cases display depletion of the Oda field in the period between August 2011 and August 2018 (Figure 60). The simulation of these two cases was important to understand the influence of the uncertainties related to the shoreline position and the extent of the Ula Fm to the NE of the Sørvestland High. Figures 46, 55 and 60 prove that these parameters do not affect significantly the results. However, case 3 is the best scenario since it combines the geological setting of the study area from well data interpretation.

The salt wall areas in which the Ula Fm was deposited were also investigated through a sensibility analysis of the variation of the thickness cutoff that defines these areas. Four thickness cutoffs were tested in cases 2 and 3: 600, 900, 1100 and 2100 m.

The scenario with the thickness cutoff of 600 m showed the worst matching results for the reservoir pressure in the Ula field (Figure 59) and an increase in the reservoir pressure in the Oda field (negative depletion – Table 15, Figure 63). The dynamic model for this case is not consistent with the historical data and therefore this case is incorrect. However, it is important to highlight that even in this low thickness cutoff scenario, there is still communication between the Ula and Oda fields.

The scenarios with the thickness cutoffs of 900, 1100 m and 2100 m show a linear relationship between the thickness cutoff and the amount of depletion in the Oda field in the period between August 2011 and August 2018 (Figure 63). Also, for these scenarios, the reservoir pressure depletion in the Ula field in the period of 2009 and 2018 (Figures 58 and 59) can be related to the reservoir pressure depletion in the Oda field from 2012 until 2016.

Thickness cutoffs of 900 to 1100 m (Figure 34) generate successful history matches to the historical data in the Ula field and have the best results for the calculated depletion in the Oda field (Figure 63). The results are within the uncertainty range of the original depletion measured between 2011 and 2018 in the Oda field. Hence, these scenarios validate the hypothesis of communication between the Ula and Oda fields, proving that the depletion observed in the Oda field can be related to the reservoir performance in the Ula field.

The scenario with a thickness cutoff of 2100 m includes the observations of well 7/12-11 (NPD, 2019) in cases 2 and 3. This well encountered a very thin (12.5 m) Ula Fm sandstone with low reservoir quality in the area outside the salt wall limits and above the Triassic pods. This could indicate that the well is located proximal to the shoreline area. However, Figures 62 and 63 show that this thickness cutoff is probably an overestimation, since the effects of the

Ula field production in the reservoir pressure from the Oda field are too high when compared to the actual reservoir depletion in the Oda field (Figure 63).

The bottom hole pressure values measured from wells 8/10-4 S and 8/10-B-3 AH in the Oda field showed an average pressure around 380 bar (Figure 3), which is ~3% higher than the values obtained from the simulated models (thickness cutoff scenarios 900 m and 1100 m, Figures 61 and 62). This difference does not invalidate the conceptual models. It just shows that the initial reservoir pressure applied to the Oda field in 1986 in the models is probably lower than the actual one. The initial reservoir pressure applied to the Oda field in the simulations was the value measured in the field during the exploration phase in 2011 (section 4.3.1.) and is a rough estimate.

One important limitation of the static model is that it does not incorporate the hydrodynamic effects related to tilting of the OWC in the Ula field (Dennis et al., 2005; Green et al., 2014; Heum, 1996; O'Connor et al., 2011). A simpler solution to represent these hydrodynamic effects in the model was to use different OWC depths in western and eastern fault bounded compartments of the Ula field (Figure 23). The impact of this simplification on the results generated by the simulated conceptual cases should not be significant. According to O'Connor et al. (2011) and Dennis et al. (1998), the water flow rate in a hydrodynamic aquifer is small in comparison to the production water drive in the reservoir. The lateral water flow rate in the hydrodynamic aquifer is in the order of centimeters per year, while the production water drive in the Ula field is in the order of meters per day. This means that the main impact of the hydrodynamic effects are the differences in the OWC depth in the Ula and Oda fields, which are represented in the model.

The results of this study are summarized in the geological model of Figure 64. The accommodation space for the deposition of the Ula Fm is based on Hodgson et al. (1992) Mannie et al. (2014) and O'Connor et al. (2011), combined with the shoreface limits of Ichron

(2015). Therefore, the Ula Fm is distributed above the salt walls and only within the shoreface area. An uncertainty zone is applied to the shoreface (shoreline and transition lines). The presence of the Ula Fm above the salt walls is divided in high, medium and low probabilities, according to the thickness cutoff sensibility analysis in case 3 (best scenario). The high and medium probability cases have the same reservoir quality (high) and the main difference is the width of the areas above the salt walls (thickness cutoff range). The high probability case uses the thickness cutoffs of the Ula and Oda fields reservoir limits (600-900 m, orange), while the medium probability case uses cutoff areas that show the best history matching to the Ula field historical data and the depletion in the Oda field (900-1100 m, light orange). The low probability case (1100-2100 m, yellow) extends the Ula Fm to the areas outside the salt structures, above the Triassic pods. For this case, the Ula formation outside the salt structures is characterized by thin layers of poor reservoir quality, since in these areas there was less accommodation space for the deposition of these sediments.

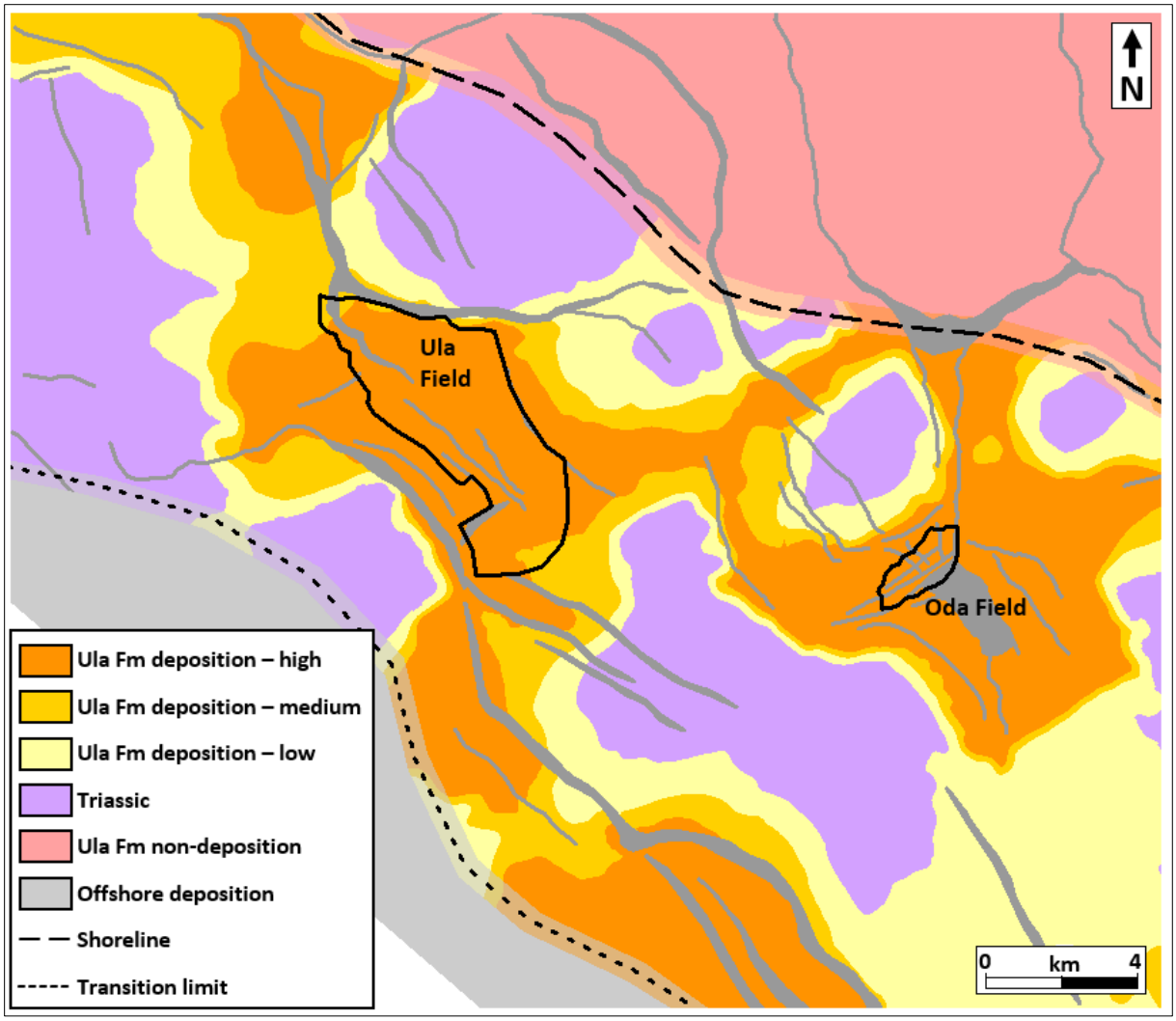

Figure 64. Geological model proposed for the communication between the Ula and Oda fields through the Ula Fm based on the results of this study. In all three cases, there is communication between the Ula and Oda fields. The medium probability case is the one that best matches the historical data from the Ula and Oda fields.

7. CONCLUSIONS

The problem statement of this study was based on well measurements in the Oda field. Pressure data from two wells (8/10-4 S and 8/10-B-3 AH, Figure 2) showed potential depletion of ~1.5 bar in the reservoir pressure between 2011 and 2018 before beginning of production of the field. This anomalous behavior in the pressure curve suggested a possible communication between the Oda field and the nearby Ula field (producing since 1986). Therefore, the aim of this thesis was the dynamic modelling of the Ula Fm aquifer to evaluate the possible communication between the Ula and Oda fields along this formation.

The main conclusions from this study are:

- There are strong geological evidences that prove connection between the Ula and Oda fields through an aquifer in the Ula Fm.
- The main reservoir pressure variations (depletion and build-up) in the Ula field during the production period can be observed, though at a lower magnitude, in the reservoir pressure measured in the Oda field. This validates the hypothesis of a Ula Fm fairway between the Ula and Oda fields.
- Even in the scenario with the smaller Ula Fm areas above the salt walls (thickness cutoff 600 m), there is still a narrow Ula Fm channel connecting the Ula and Oda fields, and the production effects of the Ula field are “felt” by the Oda field.

A geological model for the communication between the Ula and Oda fields through the Ula Fm (Figure 64) is proposed. This model can be expanded to areas outside the study area (NW and SE), used to evaluate the risks related to the Ula Fm presence, and indicate possible new prospects. The high and medium probability cases of the geological model should be used to search for prospects, since these cases are associated with higher reservoir quality sands. The

geological model and the simulation results from the best matching case 3 can be used to improve the understanding of the aquifer size in the vicinities of the Oda field and its pressure support, which can help forecasting the field.

Due to time limitations, the hydrodynamic effects proposed for the Ula field (Dennis et al., 2000) were not fully simulated. Future work could implement this process in an expanded dynamic model based on case 3 and create a non-static aquifer with NW to SE lateral draining as proposed by Dennis et al. (2000) and Heum (1996). This enhanced model could generate more realistic results related to hydrodynamic water flow in the Ula Fm, as well as better constrain new prospects related to hydrodynamic traps in the Upper Jurassic sands.

8. REFERENCES

Armour, A., Bathurst, P., Evans, D., Gammage, J., Hickey, C., 2003. THE MILLENNIUM ATLAS 989.

Bailey, C.C., Price, I., Spencer, A.M., 1981. The Ula Oil Field, block 7/12, Norway. Presented at the Norwegian Symposium on Exploration (NSE-81), Norwegian Petroleum Society, Bergen.

Baker, R.O., Chugh, S., Mcburney, C., McKishnie, R., 2006. History Matching Standards; Quality Control and Risk Analysis for Simulation, in: Canadian International Petroleum Conference. Presented at the Canadian International Petroleum Conference, Petroleum Society of Canada, Calgary, Alberta. https://doi.org/10.2118/2006-129

Baniak, G.M., Gingras, M.K., Burns, B.A., George Pemberton, S., 2014. An example of a highly bioturbated, storm-influenced shoreface deposit: Upper Jurassic Ula Formation, Norwegian North Sea. Sedimentology 61, 1261–1285. https://doi.org/10.1111/sed.12100

Baniak, G.M., Gingras, M.K., Burns, B.A., Pemberton, S.G., 2015. Petrophysical Characterization of Bioturbated Sandstone Reservoir Facies In the Upper Jurassic Ula Formation, Norwegian North Sea, Europe. Journal of Sedimentary Research 85, 62–81. https://doi.org/10.2110/jsr.2015.05

Batycky, R.P., Thiele, M.R., Coats, K.H., Grindheim, A., Ponting, D., Killough, J.E., Settari, T., Thomas, L.K., Wallis, J., Watts, J.W., Whitson, C.H., 2007. Chapter 17 - Reservoir Simulation, in: Petroleum Engineering Handbook: Vol 5: Reservoir Engineering and Petrophysics. Society of Petroleum Engineers, Richardson, Tex.

Bjørnseth, H.M., Gluyas, J., 1995. Petroleum exploration in the Ula Trend, in: Norwegian Petroleum Society Special Publications. Elsevier, pp. 85–96. https://doi.org/10.1016/S0928-8937(06)80038-X

Brown, A., Mitchell, A.W., NIlssen, I.R., Stewart, I.J., Svela, P.T., 1992. Ula Field: relationship between structure and HC distribution?, in: Structural and Tectonic Modelling and Its Application to Petroleum Geology. Elsevier, pp. 409–420.

C&C Reservoirs, 2011. Field evaluation Report - Ula Field. C&C Reservoirs, Norway.

Dennis, H., Baillie, J., Holt, T., Wessel-Berg, D., 2000. Hydrodynamic activity and tilted oil-water contacts in the North Sea. Elsevier 9, 171–185.

Dennis, H., Bergmo, P., Holt, T., 2005. Tilted oil–water contacts: modelling the effects of aquifer heterogeneity. Petroleum Geology Conference series 6, 145–158.

Green, S., Swarbrick, R.E., O'Connor, S.A., 2014. The Importance of Recognizing Hydrodynamics for Understanding Reservoir Volumetrics, Field Development and Well Placement, in: Offshore Technology Conference. Presented at the Offshore Technology Conference, Offshore Technology Conference, Houston, Texas. https://doi.org/10.4043/25150-MS

Heum, O.R., 1996. A fluid dynamic classification of hydrocarbon entrapment. Petroleum Geoscience 2, 145–158. https://doi.org/10.1144/petgeo.2.2.145

Hodgson, N.A., Farnsworth, J., Fraser, A.J., 1992. Salt-related tectonics, sedimentation and hydrocarbon plays in the Central Graben, North Sea, UKCS. Geological Society, London, Special Publications 67, 31–63. https://doi.org/10.1144/GSL.SP.1992.067.01.03

Ichron, 2015. Core description, depositional modelling and gross depositional environment mapping of the Butch Discovery (PL405) and adjacent blocks (No. 13/2284/S). Ichron.

Kleppe, H., Andersen, P.Ø., 2019. PET660 Reservoir Simulation: Introduction.

Leverett, M.C., Lewis, W.B., True, M.E., 1942. Dimensional-model Studies of Oil-field Behavior. Transactions of the AIME 146, 175–193. https://doi.org/10.2118/942175-G

Mannie, A.S., Jackson, C.A.-L., Hampson, G.J., 2014. Shallow-marine reservoir development in extensional diaper-collapse minibasins: An integrated subsurface case study from the Upper Jurassic of the Cod terrace, Norwegian North Sea. Bulletin 98, 2019–2055. https://doi.org/10.1306/03201413161

NPD, 2019. FactPage. URL https://factpages.npd.no/factpages/Default.aspx?culture=en (accessed 11.12.19).

O'Connor, S., Rasmussen, H., Swarbrick, R., Wood, J., 2011. Integrating a hydrodynamically-titled OWC and a salt-withdrawal depositional model to explore the Ula Trend: Hydrodynamics in the Ula Trend. Geofluids 11, 388–400. https://doi.org/10.1111/j.1468-8123.2011.00351.x

Oda Subsurface Team, 2016. PDO Appendix 1 Subsurface Support Document, PL 405 Oda Field Development. Centrica, Stavanger.

Partington, M.A., Copestake, P., Mitchener, B.C., Underhill, J.R., 1993. Biostratigraphic calibration of genetic stratigraphic sequences in the Jurassic–lowermost Cretaceous (Hettangian to Ryazanian) of the North Sea and adjacent areas. Petroleum Geology Conference series 4, 371–386. https://doi.org/10.1144/0040371

Rattey, R.P., Hayward, A.B., 1993. Sequence stratigraphy of a failed rift system: the Middle Jurassic to Early Cretaceous basin evolution of the Central and Northern North Sea. Petroleum Geology Conference series 4, 215–249. https://doi.org/10.1144/0040215

Rose, W., Bruce, W.A., 1949. Evaluation Of Capillary Character In Petroleum Reservoir Rock. Journal of Petroleum Technology 1, 127–142. https://doi.org/10.2118/949127-G

Schlumberger, 2020. Oilfield Glossary. Schlumberger Oilfield Glossary. URL https://www.glossary.oilfield.slb.com/Terms.aspx?filter=s (accessed 7.11.20).

Souche, L., Lepage, F., Iskenova, G., 2013. Volume Based Modeling - Automated Construction of Complex Structural Models. Presented at the 75th EAGE Conference and Exhibition incorporating SPE EUROPEC 2013, London, UK. https://doi.org/10.3997/2214-4609.20130037

Spencer, A.M., Home, P.C., Wiik, V., 1986. Habitat of Hydrocarbons in the Jurassic Ula Trend, Central Graben, Norway. Presented at the Habitat of Hydrocarbons on the Norwegian Continental Shelf, Norwegian Petroleum Society, Stavanger, pp. 111–127.

Standard Lithostratigraphy of Offshore Norway [WWW Document], 2012. . NORLEX. URL www.nhm2.uio.no/norlex (accessed 11.25.19).

Stewart, I.J., 1993. Structural controls on the Late Jurassic age shelf system, Ula Trend, Norwegian North Sea. Petroleum Geology Conference, series 4, 469–483. https://doi.org/10.1144/0040469

Vollset, J., Doré, A.G., 1984. NPD-BULLETIN NO 3 A revised Triassic and Jurassic lithostratigraphic nomenclature for the Norwegian North Sea (No. 3). Oljedirektoratet (Norwegian Petroleum Directorate), Stavanger.

Ziegler, P.A., 1975. Geological Evolution of the North Sea Area and it's Tectonic Framework (No. 7), The American Association of Petroleum Geologists Bulletin.